DALHOUSIE UNIVERSITY

DETERMINING SUBSURFACE SUSPENDED SEDIMENT MECHANISMS THROUGH SURFICIAL REMOTE SENSING TECHNIQUES, SOUTH KOREA

Catherine Evans

SUBMITTED IN PARTIAL FULFILLMENT OF THE REQUIREMENTS FOR
THE DEGREE OF BACHELOR OF SCIENCES, HONOURS
DEPARTMENT OF EARTH SCIENCES
DALHOUSIE UNIVERSITY, HALIFAX, NOVA SCOTIA

April 2019

DALHOUSIE UNIVERSITY

Department of Earth Sciences
Halifax, Nova Scotia
Canada B3H 4R2
(902) 494-2358

DATE: 23 April 2019

AUTHOR: Catherine Evans

TITLE: Determining Subsurface Suspended Sediment Mechanisms Through Surficial Remote Sensing Techniques, South Korea

Degree: B. Sc. Honours Earth Sciences Convocation: October Year: 2019

Permission is herewith granted to Dalhousie University to circulate and to have copied for non-commercial purposes, at its discretion, the above title upon the request of individuals or institutions.

_____
Signature of Author

THE AUTHOR RESERVES OTHER PUBLICATION RIGHTS, AND NEITHER THE THESIS NOR EXTENSIVE EXTRACTS FROM IT MAY BE PRINTED OR OTHERWISE REPRODUCED WITHOUT THE AUTHOR'S WRITTEN PERMISSION.

THE AUTHOR ATTESTS THAT PERMISSION HAS BEEN OBTAINED FOR THE USE OF ANY COPYRIGHTED MATERIAL APPEARING IN THIS THESIS (OTHER THAN BRIEF EXCERPTS REQUIRING ONLY PROPER ACKNOWLEDGEMENT IN SCHOLARLY WRITING) AND THAT ALL SUCH USE IS CLEARLY ACKNOWLEDGED.

Distribution License

DalSpace requires agreement to this non-exclusive distribution license before your item can appear on DalSpace.

NON-EXCLUSIVE DISTRIBUTION LICENSE

You (the author(s) or copyright owner) grant to Dalhousie University the non-exclusive right to reproduce and distribute your submission worldwide in any medium.

You agree that Dalhousie University may, without changing the content, reformat the submission for the purpose of preservation.

You also agree that Dalhousie University may keep more than one copy of this submission for purposes of security, back-up and preservation.

You agree that the submission is your original work, and that you have the right to grant the rights contained in this license. You also agree that your submission does not, to the best of your knowledge, infringe upon anyone's copyright.

If the submission contains material for which you do not hold copyright, you agree that you have obtained the unrestricted permission of the copyright owner to grant Dalhousie University the rights required by this license, and that such third-party owned material is clearly identified and acknowledged within the text or content of the submission.

If the submission is based upon work that has been sponsored or supported by an agency or organization other than Dalhousie University, you assert that you have fulfilled any right of review or other obligations required by such contract or agreement.

Dalhousie University will clearly identify your name(s) as the author(s) or owner(s) of the submission, and will not make any alteration to the content of the files that you have submitted.

If you have questions regarding this license please contact the repository manager at dalspace@dal.ca.

Grant the distribution license by signing and dating below.

_____ _____

Name of signatory Date

Table of Contents

Table of Contents…… i

List of Figures…… iii

List of Tables…… iv

Abstract…….. v

Acknowledgments……... vii

Chapter 1 – Introduction ……... 1

1.1 – Goal……... 1

1.2 – Previous Research…… 1

1.3 – Objectives……. 3

Chapter 2 – Methods ……... 5

2.1 – Site Description…… 5

2.2 – Image Acquisition…… 6

2.3 – Bathymetry……..…. 7

2.4 – Environmental Data……. 8

2.5 – Tidal Model……. 8

2.6 – Statistics…… 9

2.7 – Secondary Locations…….. 10

Chapter 3 – Results……. 11

3.1 – Bathymetry and Reflectance……. 11

3.2 – Other Environmental Variables and Reflectance…….. 13

3.3 – Controls on Reflectance at Secondary Sites…… 15

Chapter 4 – Discussion……..…. 22

4.1 – Surface Reflectance and Stratification…….…… 22

4.2 – Surface Reflectance and Wind…….……. 23

4.3 – Surface Reflectance and Water Level…….…. 23

4.4 – Comparison to Secondary Sites……..…….…. 23

4.5 – Implications…… 24

4.6 – Recommendations for Future Work…… 24

Chapter 5 – Conclusion ……. 26

5.1 – Conclusions……. 26
References…… 27
Appendix A – Data Tables……. 29
Data Table: HMB…… 29
Data Table: GB……... 30
Data Table: GOK…… 31
Appendix B – Atmospherically Corrected Images…….. 32
Satellite Images (Post Correction): HMB……..…… 32
Satellite Images (Post Correction): GB……..…… 36
Satellite Images (Post Correction): GOK……..…… 40
Appendix C – Tidal Graphs……... 63
Tidal Graphs: HMB…… 63
Tidal Graphs: GB...…… 71
Tidal Graphs: GOK…… 79

List of Figures

Figure 1.1: SPM concentration over the HMB…….. 2
Figure 1.2: Example of the banded pattern observed over the HMB…….. 3
Figure 2.1: Landsat 8 image of the study region on October 13, 2017……. 7
Figure 2.2: Series of tidal graphs created in R from the TMD toolbox in MATLAB…… 9
Figure 3.1: Comparison of bathymetry against mean reflectance patterns…….. 11
Figure 3.2: Boxplots of mean reflectance against depth, HMB…….. 11
Figure 3.3: Comparison of bathymetry against standard deviation patterns……...… 12
Figure 3.4: Bar chart comparison of ridge and channel reflectance…….. 13
Figure 3.5: Scatterplot of reflectance against wind speed, HMB….…….. 14
Figure 3.6: Scatterplot of reflectance against sea level, HMB.……... 15
Figure 3.7: Mean and standard deviation patterns, GB……. 16
Figure 3.8: Mean and standard deviation patterns, GOK……. 17
Figure 3.9: Boxplot of mean reflectance against depth, GB……... 17
Figure 3.10: Boxplot of mean reflectance against depth, GOK…….. 18
Figure 3.11: Scatterplot of reflectance against wind speed, GB……. 19
Figure 3.12: Scatterplot of reflectance against precipitation, GB…….. 20
Figure 3.13: Scatterplot of reflectance against sea level, GB…….. 20
Figure 3.14: Scatterplot of reflectance against wind speed, GOK……. 21
Figure 3.15: Scatterplot of reflectance against sea level, GOK…….. 21

List of Tables

Table 2.1: OLI spectral information……...…… 6
Table 3.1: Independent T-Test…….……..… 12
Table 3.2: Comparison of variance……... 12
Table 3.3: Pearson Correlation tests……. 14
Table 3.4: Independent T-Test, GB……..…… 16
Table 3.5: Independent T-Test, GOK……..……. 18
Table 3.6: Pearson Correlation, GB…….. 18
Table 3.7: Pearson Correlation, GOK…….. 19

Abstract

Satellite imagery can provide information on the spatial distribution of surficial suspended sediment over broad scales in coastal environments. An outstanding challenge is to determine the extent to which surficial sediment distributions can be linked to sediment processes occurring near the seabed. Recent research indicates that dense suspended sediment suspensions at the bottom of tidal channels off the southwest coast of South Korea limit upward turbulent mixing of sediment to the sea surface.

The goal of this project is to determine whether this subsurface sediment process is detectable with reflectance at the sea surface measured by the Landsat 8 satellite. The project's hypothesis is that the magnitude and variance of surficial reflectance will be lower over channels than over ridges, due to the presence of dense suspensions in channels that limit vertical mixing. On the ridges this process would not occur, because dense suspensions would flow into adjacent channels under the influence of gravity. As a result, reflectance would be higher and more variable at shallower depths. To assess this hypothesis, Acolite processing software was used to perform atmospheric corrections on Landsat 8 images, and sea surface reflectance at 655 nm and 865 nm were used as proxies for suspended sediment concentration in a total of 15 cloud-free images collected over the years 2013-2018.

Reflectance in both bands was extracted over a tidal channel and over an adjacent tidal ridge using SeaDAS. The reflectance from these two points were assessed for statistical correlation with depth and other environmental variables, including sea level, wind speed, and recent precipitation levels. Results indicate that depth exerts primary control on mean and standard deviation reflectance, consistent with the project's hypothesis. Secondary controls on reflectance are wind speed and sea level. I propose that higher windspeeds are associated with larger reflectance due to resuspension over fringing tidal flats and that the correlation of higher water levels with reduced reflectance is caused by sediment supply limitation.

In order to see if these methods can identify other areas with similar suspended sediment processes, two secondary sites – located in Gyeonngi Bay, South Korea and the Gulf of Khambhat in India have been analyzed. Preliminary results show similar primary and secondary reflectance patterns. While further field work is needed to study the effects of tidally-dependant suspended sediment stratification on surface sediment concentration and associated reflectance,

results indicate that remote sensing may be applicable to detection of subsurface suspended sediment processes.

Key words: South Korea, Heuksan Mud Belt, remote sensing, suspended sediment stratification, tidal seas.

Acknowledgments

I would first like to thank my project supervisor Dr. Paul Hill for his continued support, guidance and enthusiasm of my work both in and beyond this project. I would like to thank Ian Hay for his advice on this project, and for bringing me along to help with his field work this past summer. Thank you to Dr. Chris Greene for the enlightening conversations and for helping me understand the practices and theories behind remote sensing. A large thanks also goes out to the members of the Departments of Earth Sciences and Oceanography for their encouragement over the past year.

I would also like to thank the Office of Naval Research for funding this project, which made this incredible opportunity to learn possible, and to the Dalhousie University Faculty of Science for providing conference funding.

Chapter 1 – Introduction

1.1 – Goal

Stratification of flows by suspended sediment in shallow marine environments can occur in areas with high velocity currents and abundant sediment supply. Macrotidal regions – such as the Heuksan Mud Belt (HMB) off the coast of South Korea – can exhibit suspended sediment stratification that is tidally dependant. This goal of this project is to determine whether subsurface sediment stratification can be identified through the analysis of surficial suspended sediment patterns with remote sensing methods.

Previous work in the HMB shows that sediment resuspended during peak flow can lead to the formation of sharp lutoclines, which are steep vertical gradients of suspended sediment concentration (Hill, 2017). When lutoclines are present during peak flow resuspended sediment is trapped by stratification at the base of the water column, causing lower levels of suspended sediment at the surface (Wolanski, 1988; Trowbridge & Kineke, 1994). As a result, mean reflectance in areas with lutoclines are lower than areas without them. Similarly, by limiting surface concentration of suspended particulate matter (SPM) at peak flow, lutoclines also reduce the variability of reflectance through the tidal cycle. Areas without lutoclines experience higher levels of turbulence throughout the water column during peak flow. Increased turbulence raises the mean surface reflectance due to mixing of suspended sediment to the surface.

Satellite-based remote sensing allows for different wavelengths of reflected light to be analyzed simultaneously over large areas. This project uses images gathered from the Landsat 8 satellite to examine surficial suspended sediment patterns over the HMB.

The hypothesis that lutoclines limit upward turbulent mixing of sediment during peak flow in tidal channels produced two predictions. First, mean reflectance over a tidal ridge should be larger than over a tidal channel, because any dense suspensions that formed over ridges would flow under the influence of gravity into the channels. Second, standard deviation of reflectance should be larger over tidal ridges as well.

1.2 – Previous Research

Over the course of two field excursions in 2016 and 2017, tidal current velocity and suspended sediment concentration (SSC) measurements in a tidal channel in the HMB were

collected. The SSC measurements taken in 2016 only reached approximately 13 m in depth, the 2017 measurements were able to collect data for the entire water column [Figure 1.1]. Data from 2017 indicate that during high slack water SPM levels are fairly homogeneous throughout the water column. At peak flow SPM was lower at the surface, but it increased rapidly to over 600 g/m^3 at 20 m depth. These profiles are consistent with the hypothesis that suspended sediment stratification limits the magnitude and variability of SPM at the sea surface in the tidal channel (Hill, 2017).

Landsat 8 images from the same area have a "banded" pattern at the water surface. Images in the channel where observations were made looked noticeably bluer than the water to either side [Figure 1.2]. This pattern also is consistent with the hypothesis that suspended sediment stratification limits the magnitude of SPM at the sea surface in the tidal channel.

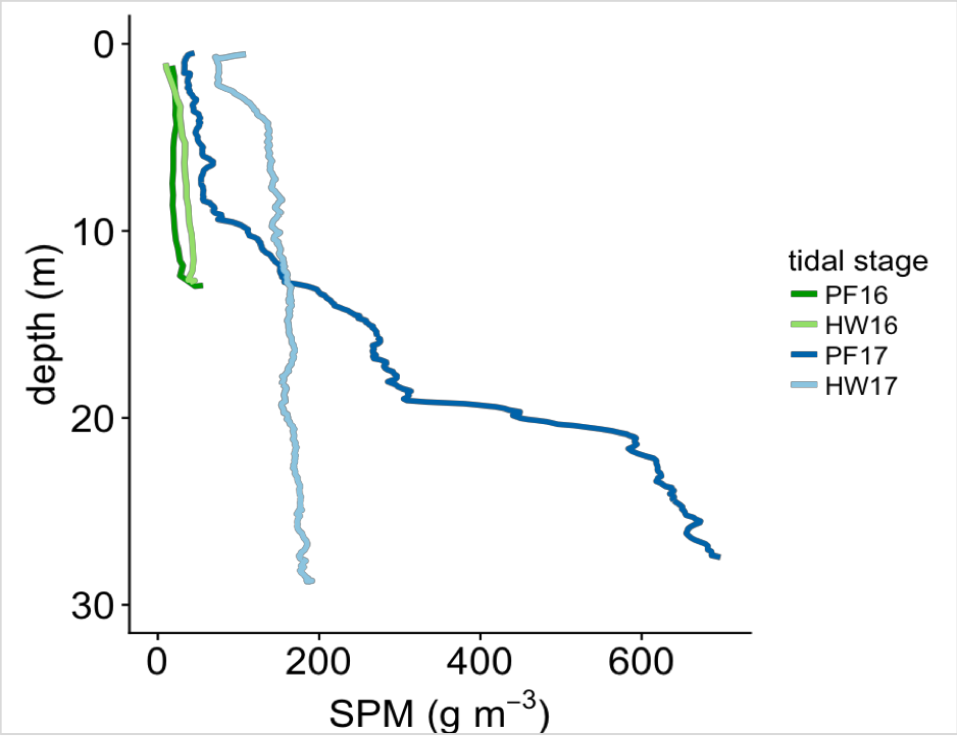

Figure 1.1: SPM concentration over the HMB. Green lines indicate the data gathered in 2016. Blue lines indicate data from 2017. HSW represents high slack water, or when there is no tidal current. PF represents concentration levels gathered at peak flow (Hill, 2017).

Figure 1.2: Example of the banded pattern observed at the water's surface over the HMB at mid tide. Brown streaks on the surface surround "bluer" water at the study site (orange triangle).

1.3 – Objectives

This project has three primary objectives designed to examine the viability of the hypothesis that suspended sediment stratification influence surface reflectance in tidal channels in the HMB:

1. With Landsat 8 imagery, examine whether surface reflectance in the HMB is correlated with depth;
2. Determine whether the mean and standard deviation of reflectance over a point in the channel where observations have been made are statistically smaller than the mean and standard deviation of reflectance over an adjacent ridge;
3. Assess other environmental factors that influence reflectance in the region.

The thesis will first go over the general characteristics of the HMB. It will then walk through the data acquisition and methods used in the project, and the results that were obtained. Comparisons between the results from the HMB and two secondary sites that were analyzed

under the same methods will be made in order to see if remote sensing methods could be expanded to similar sites that have not yet been explored with in situ measurements. Finally, this thesis will outline the implications of the results, and propose future work that can be done to broaden our understanding of the sediment transport processes in tidal seas.

Chapter 2 – Methods

2.1 Site Description

The Heuksan Mud Belt (HMB) is a sedimentary formation composed primarily of mud and silt, located off the southwest coast of South Korea. It has an area of approximately 200 km by 40 km, with a mean thickness of 30 m (Lee & Chu, 2001). The unit has been dated to have begun deposition in the early Holocene, as water levels rose to current levels after the last glacial maximum (Lee, A Review on the Holocene evolution of an Inner-shelf Mud Deposit in the Southeastern Yellow Sea: the Huksan Mud Belt, 2015). Two subunits of the HMB indicate that southward-flowing winter currents have deposited most of the sediment from the Keum River, approximately 140 km north of the HMB (Lee & Chu, 2001).

Tides in the region are dominated by the M2 tidal constituent (Ichikawa, 1997). Tidal amplitude can be over 4 m, with current speeds up to 1.5 m/s (Hill, 2017).The region is classified as a macrotidal environment.

Suspended sediment concentration over the HMB varies both tidally and seasonally. Previous research conducted with the Geostationary Ocean Color Imager hypothesised that the surficial SPM concentration was larger at mid tide (60-75 g/m^3) than at high slack water (25-40 g/m^3). In-situ measurements in October of the same year demonstrated concentrations between 40-180 g/m^3 in turbid surface waters (Choi, 2012). In situ measurements in 2017 actually found that surficial sediment concentrations were lower during peak flow than at high slack water (Hill, 2017). Winter SPM concentrations are much higher than in the summer, primarily due to the winds and waves from the north driving sediment south during the winter (Lee, 2014). Comparisons between the seasonal SPM concentrations found concentrations at the surface to be 2 g/m^3 and nearbed 60 g/m^3 during the summer. Winter concentrations were 100 g/m^3 at surface and 350 g/m^3 at depth (Lee & Chu, 2001).

The region experiences significant rainfall due to its location in the temperate zone. Between 1100 and 1800 mm of rainfall occurs over southwestern Korea annually, primarily in the summer during monsoon season (Korean Meteoroligical Administration, 2009). For areas that have significant input of continental discharge, SPM can be elevated in the days after large precipitation events.

2.2 – Image Acquisition

The Landsat 8 satellite is part of the Landsat remote sensing series run by NASA. It has been running since February 2013 using the Operational Land Imager (OLI) and Thermal Infrared Sensor (Barsi, 2014). The OLI uses nine spectral bands [Table 2.1]. Bands 4 and 5 of the OLI were used to analyze suspended particulate matter load over the HMB.

Images over the southwest tip of Korean Peninsula are captured at 16-day intervals. All L8 images over the study area were accessed at the USGS Earth Explorer site. 27 images without significant cloud cover were downloaded for analysis.

Band	Band Code	Band Wavelength (nm)	Spectral Resolution (m)
1	CA	433 – 453	30
2	Blue	450 – 515	30
3	Green	525 – 600	30
4	Red	630 – 680	30
5	NIR	845 – 885	30
6	SWIR 1	1560 – 1660	30
7	SWIR 2	2100 – 2300	30
8	Panchromatic	500 – 680	15
9	Cirrus	1360 – 1390	30

Table 2.1: OLI spectral band information (Barsi, 2014).

Acolite processing software was used to crop the L8 data to an Area of Interest (AOI) over the study site (Royal Belgian Institute of Natural Sciences, 2019). The bounding coordinates of the AOI are 34.8-35 °N, 125.8-126 °E. Acolite also was used to correct for the effect of the passage of reflected light through the atmosphere with the "dark spectrum fitting" approach (Vanhellemont & Ruddick, 2018). Acolite provided visually useful RGB images of the AOI, as well as top-of-atmosphere and surface reflectances.

The RGB images output by Acolite were useful for identifying clouds that were difficult to resolve in the larger Landsat 8 images. With a much smaller region, any cloud coverage that may have been missed in the original selection process was visible in the AOI. Twelve images were removed from the original 27-image set, leaving 15 cloud-free images for further analysis.

SeaDAS is a software created by NASA for the analysis of ocean colour data. It was used to extract reflectance at two locations in the study area. One point was in a tidal channel where in-water measurements were collected previously (34.888 °N, 125.855 E), and the other was over an adjacent tidal ridge (34.98°N, 125.91 °E). Mean reflectances in bands 4 and 5 were extracted from a 5x5 pixel area in each cloud-free image.

Figure 2.1: Landsat 8 image of the study region on October 13, 2017.

The files processed by Acolite were imported to RStudio for mapping. The mean and standard deviation of reflectance in bands 4 and 5 were calculated and plotted with the PBSMapping toolbox. As these maps cover a relatively small region below 40 °N latitude, simple Lat./Lon. rectangular projections were used.

2.3 – Bathymetry

Using source code similar to that used for plotting the reflectance maps, alterations were made to read and create a map according to the GEBCO's 2014 bathymetry dataset. The data was gathered from the GEBCO website (British Oceanographic Data Centre, 2018), which

composes a global bathymetric and land terrain elevation model at both 30 arc-seconds and one arc-minute increments. 30 arc-second grids for both local and regional maps were created by outlining the latitudinal and longitudinal boundaries for a 2D NetCDF on the GEBCO website, which was downloaded from the British Oceanographic Data Centre's website. Though providing a coarser resolution (30 arc-seconds compared to Landsat 8's 30 m pixel resolution), this global dataset provided consistent data for all study areas.

2.4 – Environmental Data

Wind data were gathered from the National Oceanic and Atmospheric Administration (NOAA) station #22102, which is located at 34.79 °N, 125.78 °E (NDBC, 2018). Precipitation data was gathered on World Weather Online (WWO) for 72 hours before image capture through WWO's online historical database. The location for precipitation levels is located in Mokpo, South Korea. Missing dates from NOAA in wind speed were filled in from WWO.

2.5 – Tidal Model

The OSU Tidal Prediction Software is a tide level model for regions around the world (Egbert & Erofeeva, 2010). The China Seas and Indonesia model predicts tides with a resolution of 1/30° on a 1801x2161 grid. The Tidal Model Driver (TMD) Matlab toolbox was used to run the tidal model (Earth & Space Research, 2019). Water levels relative to mean sea level at lat 34.888° N and lon 125.855° E were calculated at 10-min intervals for each month for which a cloud-free image was available. Monthly mean sea level data from the nearby Heuksando tidal gauging station were gathered from the Permanent Service for Mean Sea Level, from 1977 until the present. Monthly mean sea level was detrended by subtraction of the best-fit linear regression of water level on time. After detrending, the averages of the monthly mean sea levels were calculated for each month. Addition of the linear trend to these average monthly means produced a time series of mean sea level that was added to the TMD output. Finally, monthly mean sea levels are referenced to a Revised Local Reference (RLR) level for the station. This level must be added to the mean levels to calculate actual water level. The RLR for the Heuksando tidal station is 5.132 m (Permenant Service for Mean Sea Level, 2018). The accuracy of the tidal model was assessed by comparison with 3 days of real-time water level data downloaded from the Heuksando tidal station.

The tidal predictions at the study site were used to calculate water level at the time of image capture for each image. They were used to establish where in the spring-neap tidal cycle the image was taken, as well as the relative water level and the amplitude of the tidal range at image capture.

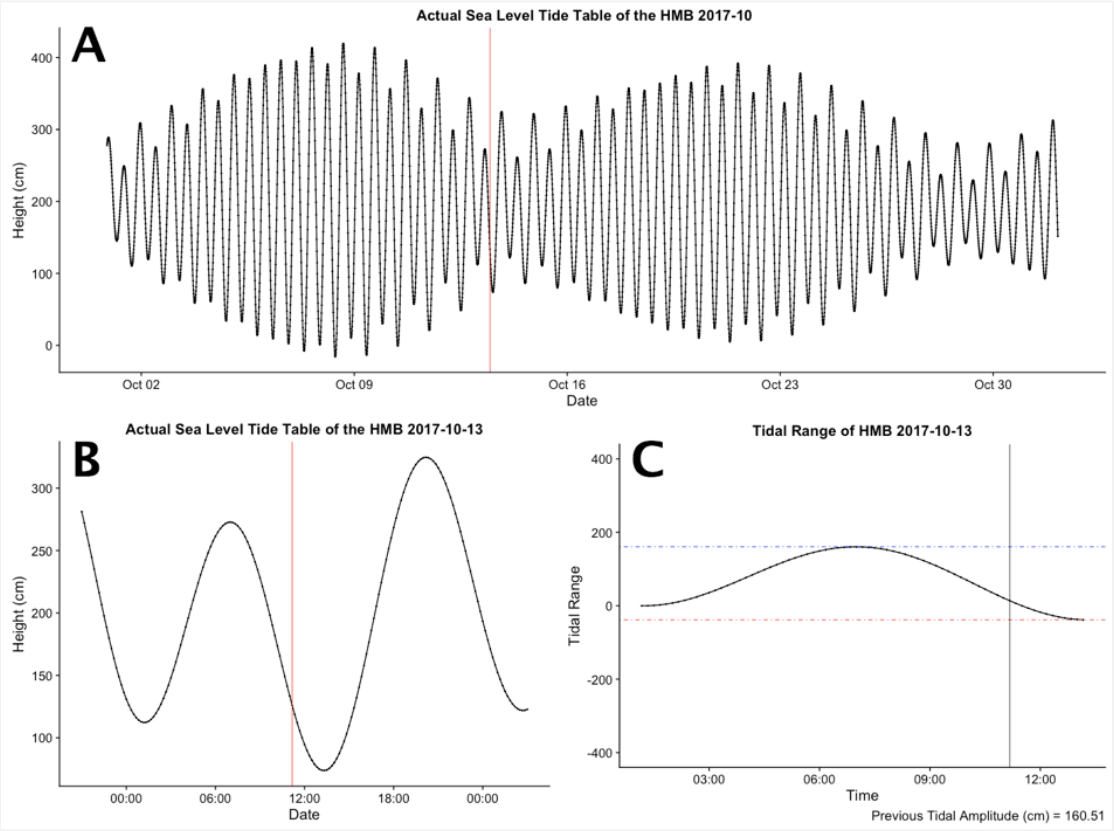

Figure 2.2: Series of tidal graphs created in R from the TMD toolbox in MATLAB. (A) Water levels in October 2017, with a red line marking the time of L8 image capture. (B) Water levels on the day of the image capture, October 13, 2017. (C) Tidal range marked by blue and red lines at the time of image capture.

2.6 – Statistics

Tests run for this project were focused on reflectance behaviour in the channel and ridge, comparing both mean and standard deviation patterns between the two locations. As the sample size was small, robust statistical tests were used to analyze the data.

The Shapiro-Wilkes test was used to resolve levels of normal distribution in the channel and ridge reflectance patterns (Shapiro & Wilk, 1965). Both one and two-sided T-tests were conducted to see which of the two locations had a higher mean reflectance (Student, 1908). The F-test was run to determine the ratio of the variances between the two populations, which would

indicate which location had a higher level of standard deviation in each band. Finally, correlations between the reflectance levels for the ridge and channel in both wavelengths were done against the environmental variables.

2.7 – Secondary Locations

The generalizability of the results from the HMB was assessed by conducting similar analysis of L8 images in other similar environments. Candidate locations of interest had to have a macrotidal range and associated strong tidal currents. Discharge from surrounding rivers could not be a dominant input in order for the tidal currents to be the primary driver of surficial suspended sediment. Finally, candidate locations required similar water depths and channelized morphology.

Two locations were identified that met the above conditions. The first was Gyeonggi Bay, located further north in the West Sea in South Korea. While the tidal amplitudes are greater with an amplitude of 8 m (Kim, 2018), channelized morphology and similar water depths to HMB may produce similar patterns of reflectance in Gyeonggi Bay. The second was the Gulf of Khambhat (GOK) on India's west coast. The GOK is more embayed than the other two sites, but it is also a region with a system of channels and ridges created by strong tides (Ramakrishnan, 2013).

Landsat 8 images were gathered for Gyeonggi Bay at the bounding coordinates of 37.25-37.45 °N, 125.9-126.1 °E. Wind data was taken from a buoy operated by the Korean Meteorological Administration at 37.230 °N, 126.020 °E (NDBC, 2018). Mean water level for the region was taken from National Data Buoy Center station # 956. Missing wind speed information from when the station was out of service was gathered from WWO's database of historical data, which also provided precipitation data for the 72 hours preceding image capture.

The GOK's study area images from Landsat 8 were taken over the bounding coordinates of 21.4-21.6 °N, 72.3-72.5 °E. Wind data was gathered from WWO historical weather reports for Bhavnagar, India. There was not enough precipitation for any meaningful statistics to be analyzed due to nearly all images being taken during the dry season in India.

Chapter 3 – Results

3.1 – Bathymetry and Reflectance

Maps of mean reflectance in Bands 4 and 5 of Landsat 8 (~655 and 865 nm) showed patterns similar to the bathymetric map of the study area [Figure 3.1]. Both bands had higher levels of reflectance over shallow areas than over deep areas [Figure 3.2]. In contrast, maps of standard deviation from mean reflectance showed patterns that had different relationships with bathymetry for the two bands. [Figure 3.3]. Band 4 standard deviation was higher over the channels, while in band 5 the standard deviation was higher over the ridges. The smaller standard deviation of band 4 over the ridge may indicate sensor saturation, which can occur at progressively longer wavelengths as suspended sediment concentrations increase (Novoa, 2017).

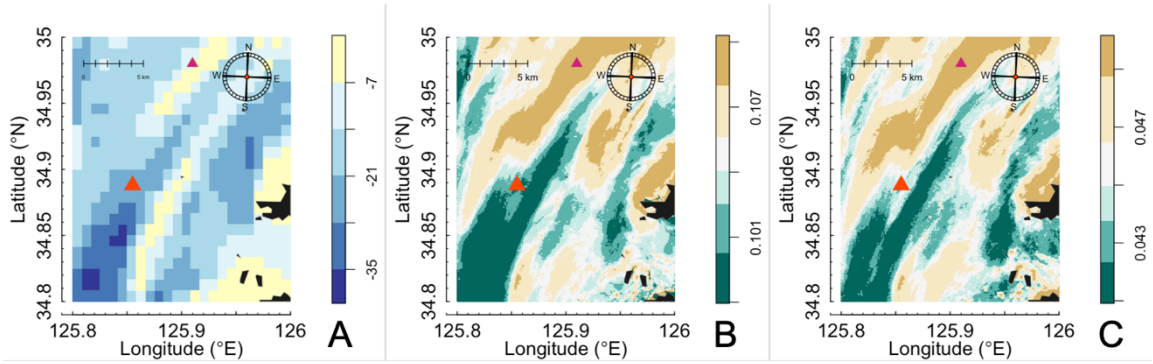

Figure 3.1: A) Bathymetric map of the HMB. B) Mean reflectance in band 4 (655 nm) C) Mean reflectance in band 5 (865 nm).

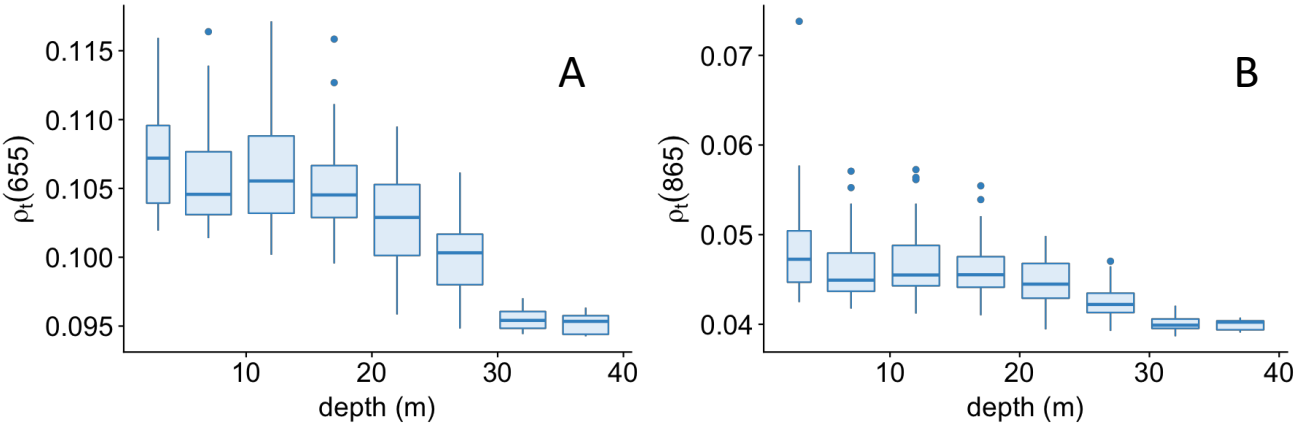

Figure 3.2: Graphs demonstrating reflectance trends in the two Landsat-8 bands. A) Reflectance in band 4 plotted against depth. B) Band 5 reflectance plotted against depth.

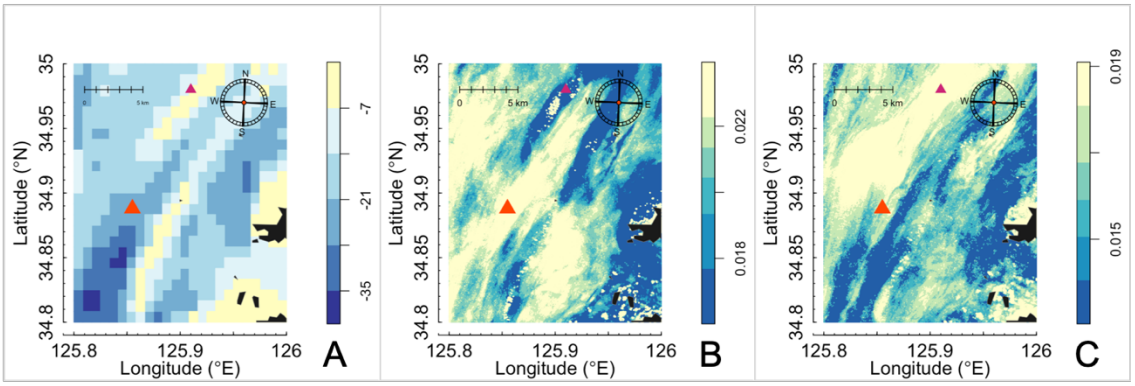

Figure 3.3: Bathymetry and standard deviation in reflectance over the study area. Red triangle indicates the location of in-situ measurements and reflectance levels in the channel. Pink triangle represents reflectance values taken over the ridge. A) bathymetry B) standard deviation in band 4. C) Standard deviation in band 5.

The null hypothesis of the Shapiro-Wilk normality test was unable to be disproven over both the ridge ($p = 0.2018$) and the channel ($p = 0.5016$). Focusing on the reflectance at the established study site, an independent T-Test was performed to compare reflectance in the channel at the study site to reflectance on an adjacent ridge. The test indicated that mean reflectance between the ridge and channel locations was statistically greater than 0 [Table 3.1]. Differences in variance over the channel and ridge were not significantly different in band 4 ($p = 0.196$), but variance was lower over the channel than the ridge in band 5 ($p = 0.045$) [Table 3.2].

Independent T-Test	Band 4	Band 5
t	2.8176	10.263
Difference in Means	0.01988462	0.01747798
p-value	0.009301	6.766e-08

Table 3.1: Independent t-test with the alternative hypothesis that true difference in means is greater than 0.

F-Test	Band 4	Band 5
F	0.49111	2.5546
denom df	14	14
p-value	0.1958	0.04513

Table 3.2: Comparison of variance between bands. In band 4 the null hypothesis that the ratio of the variances is equal to 1 was not rejected at the 95% confidence level. In band 5 the null hypothesis was rejected, while the alternative that the variance over the ridge is greater than over the channel was not.

3.2 – Other Environmental Variables and Reflectance

Though the ridge had consistently higher reflectances than the channel, there also was variability in reflectance among sample images [Figure 3.4]. The underlying causes of the variability in reflectances were explored by comparing reflectance to three environmental variables: wind speed, water level, and precipitation over the 72 hours prior to acquisition of each image.

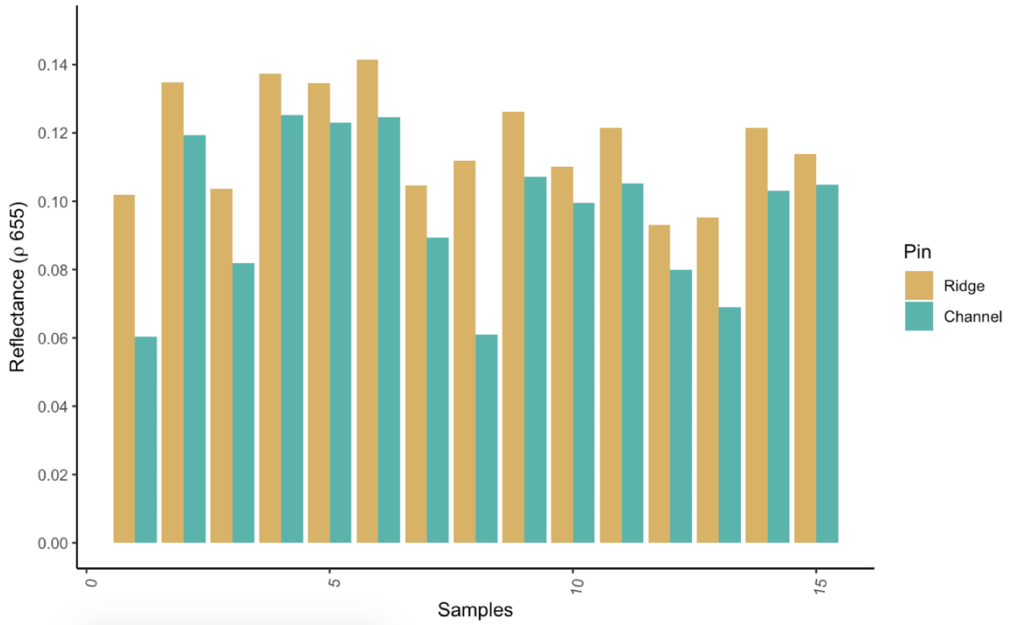

Figure 3.4: Sample reflectance over the ridge and channel of the HMB in 15 images. The ridge had higher reflectance than the channel for each sample, and the ridge and channel had similar patterns of variation among images.

Wind speed can affect surface reflectance by generating waves that resuspend sediment through increased turbulence. Reflectances over the ridge and channel in both wave bands were correlated positively with wind speeds up to 12 m/s [Figure 3.5; Table 3.3]. At higher wind speeds reflectances were lower, which can be explained by incorporation of foam into the sea surface once wind speed is over 12 m/s (Frouin, 1996).

Water level can affect surface reflectance when sediment supply is limited. If the supply of slowly sinking particles that affect surface reflectance is limited, then a deeper water column will lower the concentration of suspended sediment throughout the column, including at the surface. Reflectances over the ridge and channel in both bands were negatively correlated with water level [Figure 3.6; Table 3.3].

Precipitation in the days before an image is taken can raise reflectance levels if continentally discharged sediment contributes to the overall surficial sediment load, due to increased river discharge. There were only weak positive correlations between precipitation and reflectance levels, leading to no significant effects at this site [Table 3.3].

Pearson Test	Band 4 Ridge	Band 4 Channel	Band 5 Ridge	Band 5 Channel
Wind	0.7633176**	0.7883925**	0.6371322*	0.7952895**
Water Level	-0.3876063*	-0.5765028*	-0.3809794*	-0.4523233**
Precipitation	0.09438585	0.08353124	0.03400967	0.1380594

Table 3.3: Pearson correlation results between environmental variables and band channels and locations. Strongest correlations are found to be between windspeed and water levels. No asterisks indicates $p > 0.05$; one asterisk means $0.01 < p < 0.05$; two asterisks means $0.001 < p < 0.01$; and three asterisks means $p < 0.001$.

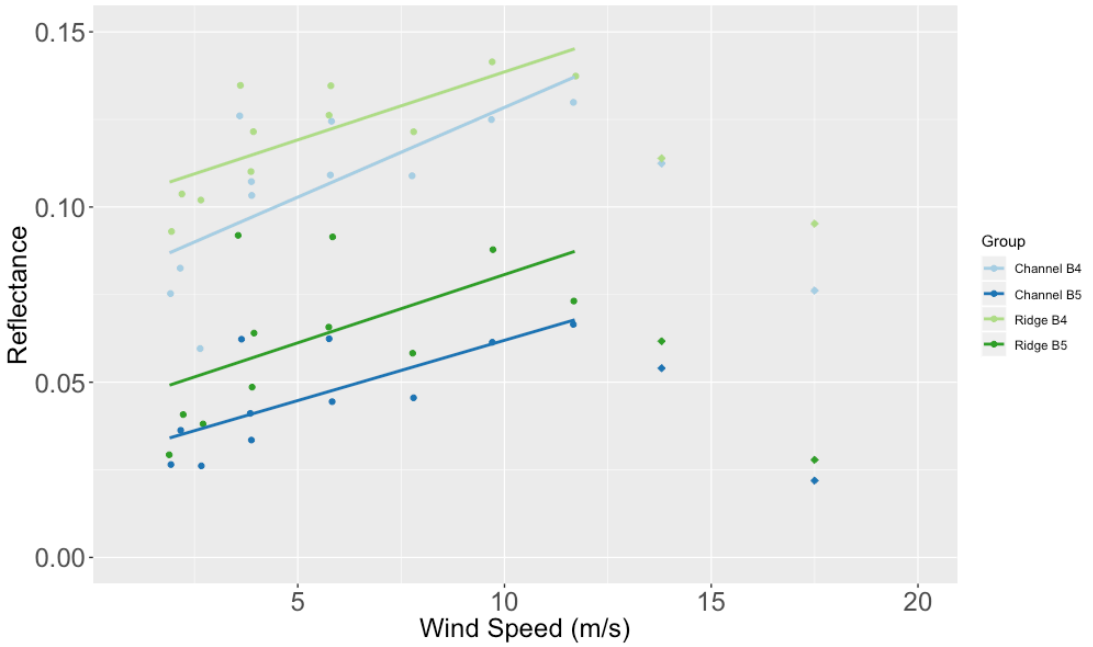

Figure 3.5: Scatterplot of reflectance versus wind speeds. Note how reflectance levels (diamonds excluded from trendline) were lower at wind speeds larger than 12 m/s.

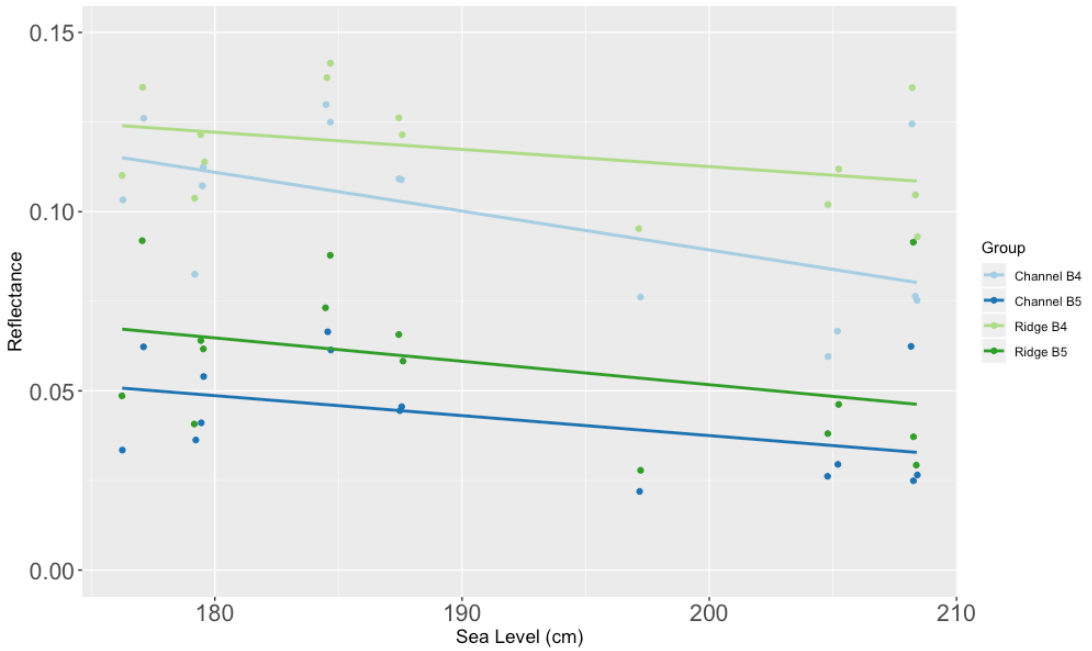

Figure 3.6: Scatterplot of reflectance against sea level.

3.3 – Controls on Reflectance at Secondary Sites

Similar analyses of reflectance were carried out in sites that share the strong tidal flows and high suspended sediment concentrations of the HMB. Gyeonggi Bay (GB) had lower levels of reflectance [Figure 3.7] and showed a similar relationship between depth and mean reflectance to the HMB. Standard deviation from the mean was higher over the ridge than the channel in both bands. The Gulf of Khambhat (GOK) [Figure 3.8] had overall higher levels of reflectance and also had higher mean reflectance over the ridge than the channel. Standard deviation was higher over the channel in both bands at this location.

Both sites demonstrated similar characteristics to the HMB in their relationships between reflectance and bathymetry [Figure 3.9, Figure 3.10]. Generally, the reflectance lowered in both magnitude and levels of standard deviation with depth. Pearson correlations between reflectance and depth demonstrated that GB had a higher correlation in band 4 while the GOK had a higher correlation between depth and reflectance in band 5 [Table 3.5, Table 3.6]

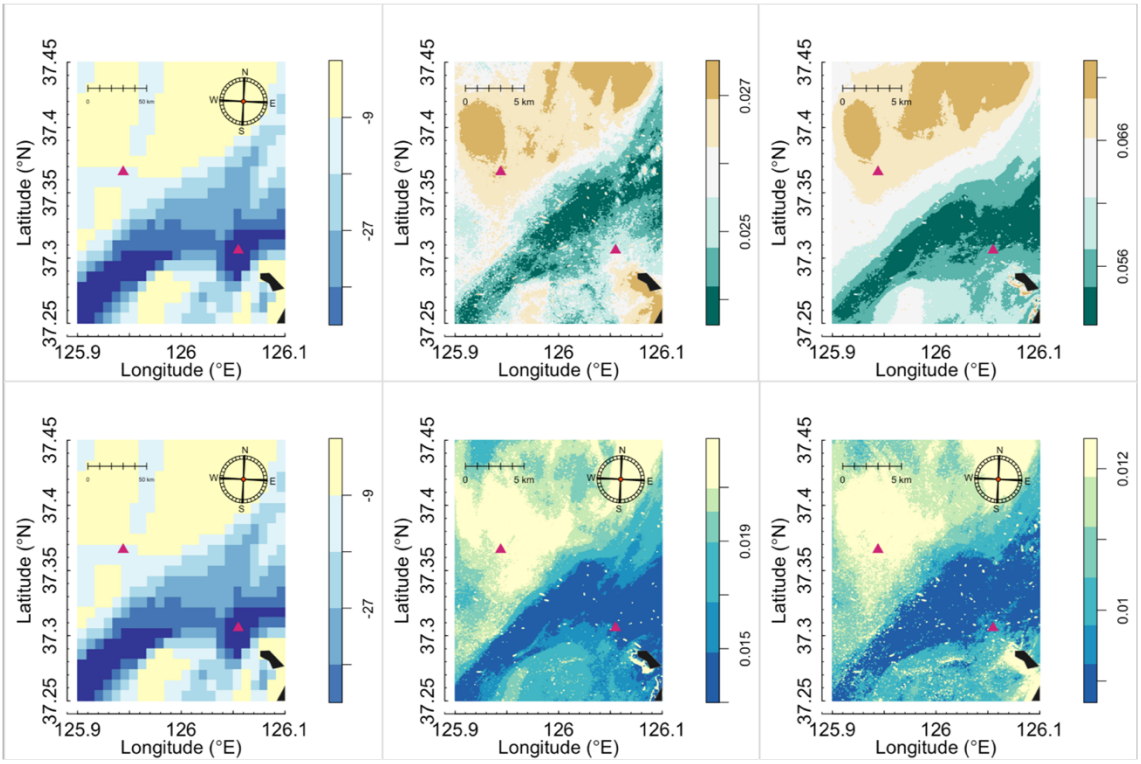

Fig. 3.7: Bathymetric map compared against reflectance behaviour observed over GB. A,D) Bathymetric map showing ridge and channel system. B) Mean reflectance pattern in band 4. C) Mean reflectance patterns in band 5. E, F) Higher level of standard deviation observed in both bands over the ridge.

A difference in mean reflectance between the ridge and channel of GB was found in band 4 ($p = 0.0453$), while the means between the ridge and channel in band 5 were not significantly different ($p = 0.6332$) [Table 3.4]. GOK reflectance tests behaved similarly to the HMB as the mean reflectance of the ridge was significantly higher than the channel [Table 3.5].

GB Independent T-Test	Band 4	Band 5
t	2.107	0.48283
p-value	0.0453	0.6332

Table 3.4: T-tests performed between the channel and ridge in both bands. Band 4 is saturated that the mean of the ridge is decisively higher than the channel, but suspended sediment levels are low enough that the ridge does not have a decisively higher mean than the channel in band 5.

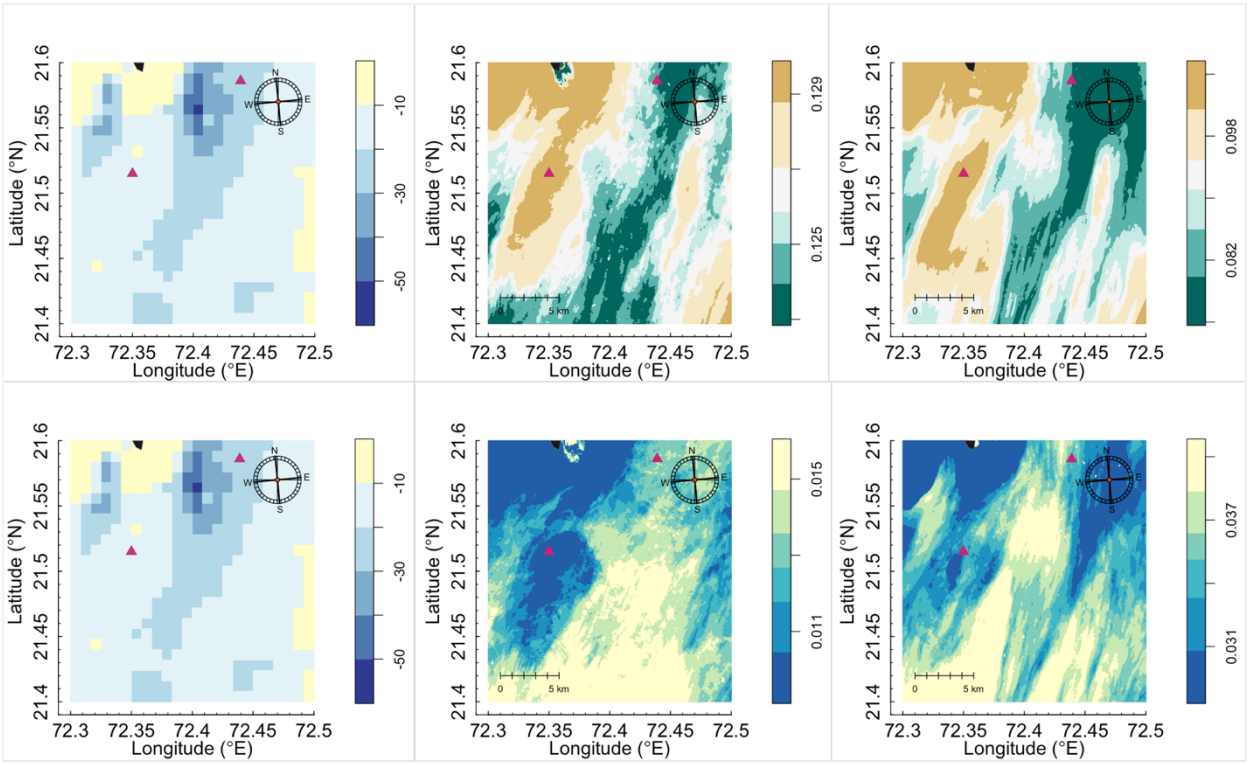

Fig. 3.8: A, D) Bathymetric map over study site in the GOK. B) Mean reflectance pattern in band 4. C) Mean reflectance in band 5. E) Standard Deviation in band 4, higher levels over the mid-depth channel, lower levels over the ridge. F) Similar pattern to band 4 standard deviation, with higher standard deviation found over the ridge, and lower in the channel.

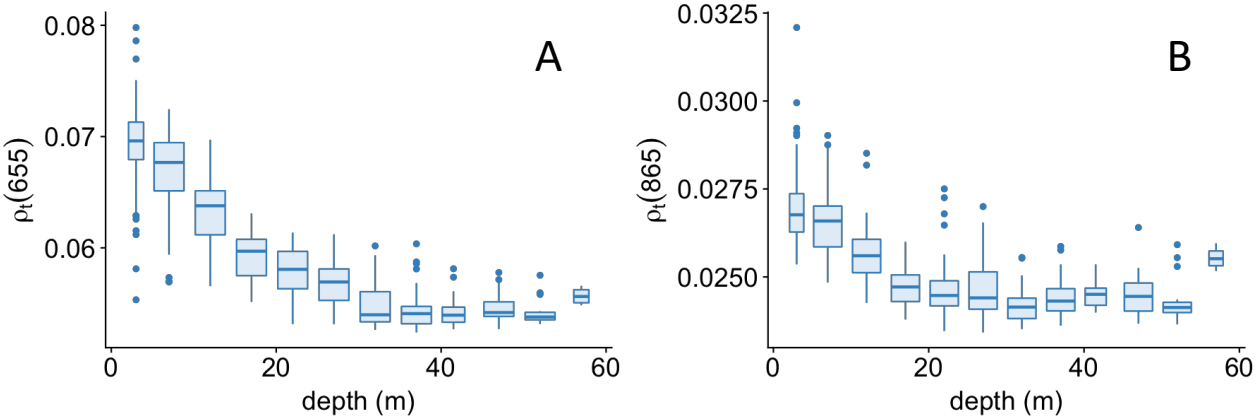

Figure 3.9: Reflectance against depth in GB. A) Band 4 reflectance had a negative correlation with depth. B) Band 5 reflectance also had a negative correlation with depth but it was more variable.

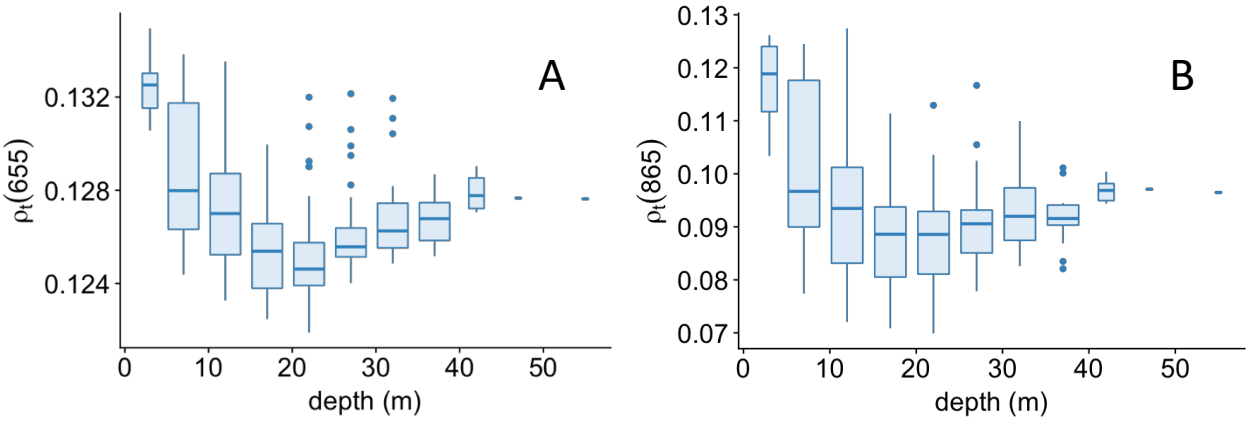

Figure 3.10: Reflectance against depth in the GOK. A negative trend is observed in both graph A and B. Standard deviation was smaller for depths greater than 20 m.

GOK Independent T-Test	Band 4	Band 5
t	3.2333	5.1881
p-value	0.00179	1.306e-06

Table 3.5: Independent t-tests of mean reflectance over ridge and channel in the GOK.

As in the HMB, GB reflectances over the ridge and channel were positively correlated with wind speed (p = 0.027) and had a non-significant negative correlation with water level (p = 0.497) and precipitation (p = 0.497) [Table 3.6, Figure 3.11, Figure 3.12, Figure 3.13].

GB Pearson Test	Band 4 Ridge	Band 4 Channel	Band 5 Ridge	Band 5 Channel
Wind Speed	0.5613868*	0.294745*	0.6026291	0.4472298
Water Level	-0.3083021	-0.1197965	-0.09315144	-0.2334466
Precipitation	-0.128481	-0.3692998	-0.2940493	-0.2993235

Table 3.6: Pearson correlation between reflectance levels and environmental variables.

Correlation between reflectance and environmental variables in the GOK was assessed only for wind speed and water level [Table 3.7]. Precipitation levels over the past 72 hours were omitted due to the arid climate in this region. Reflectance had a positive correlation with wind speed. Band 5 had a higher level of correlation in both sample locations, perhaps due to saturation of the band 4 sensor by large suspended sediment concentrations [Figure 3.14].

Reflectance was negatively correlated with water level, suggesting limitation of sediment supply from the seabed [Figure 3.15].

GOK Pearson Test	Band 4 Ridge	Band 4 Channel	Band 5 Ridge	Band 5 Channel
Wind Speed	0.2719985	0.447005**	0.4193551**	0.476447***
Water Level	-0.3527098*	-0.494334***	-0.4998607***	-0.5967319***

Table 3.7: Pearson correlation results between reflectance and environmental variables. Wind speed has a moderately positive correlation against reflectance, while water level has a moderately negative correlation against reflectance.

Figure 3.11: Scatterplot between wind speed and reflectance in GB.

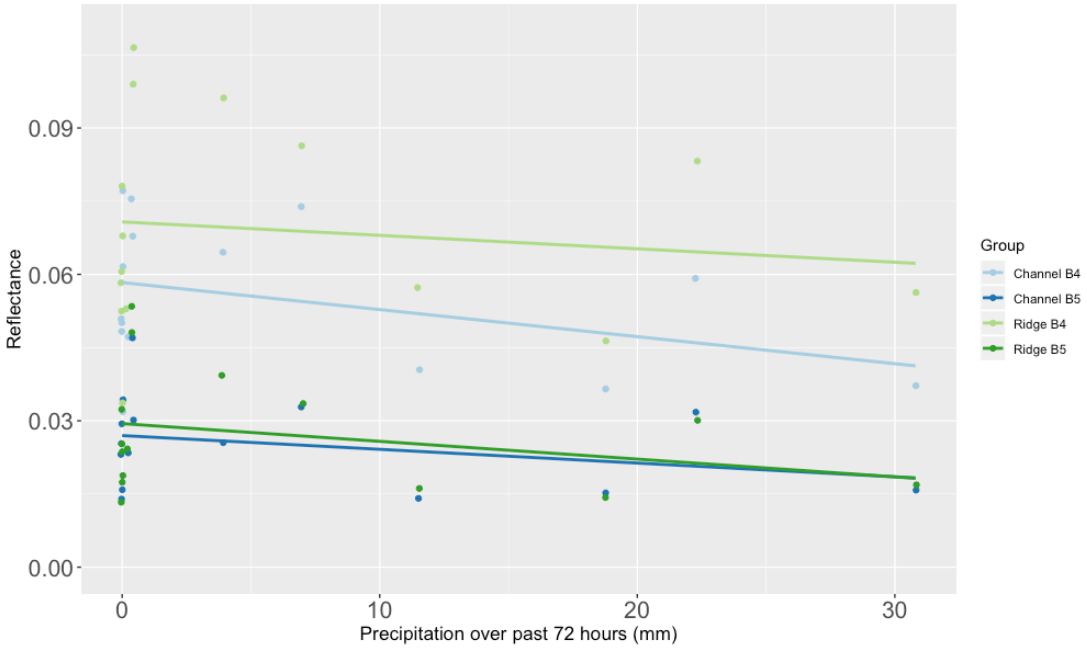

Figure 3.12: Scatterplot of precipitation against reflectance in GB.

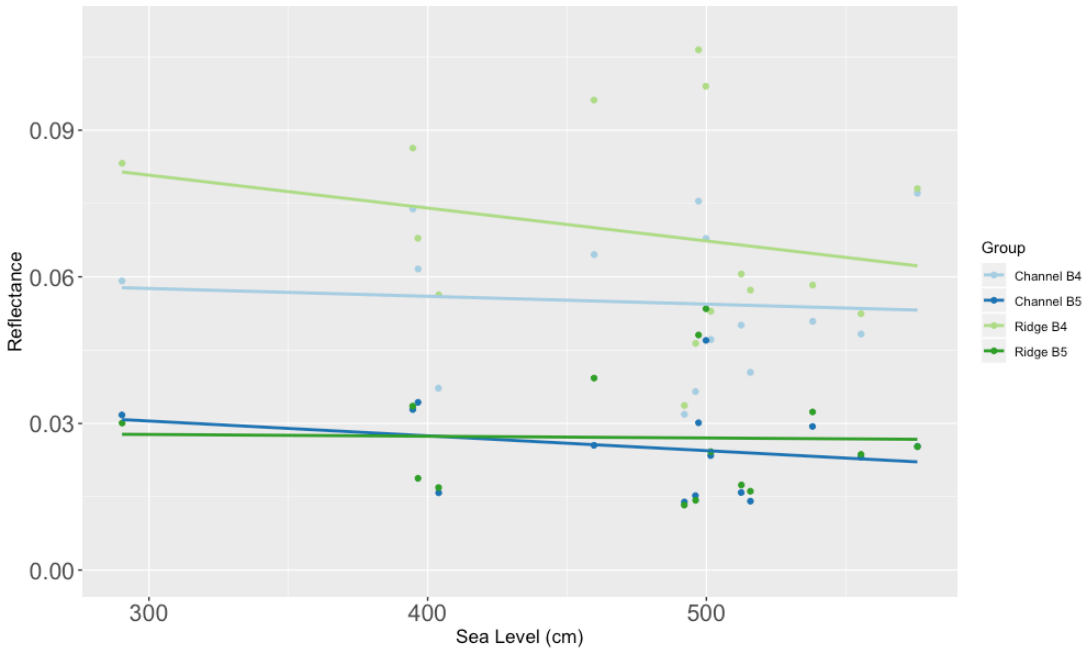

Figure 3.13: Relationship between sea level and reflectance in GB.

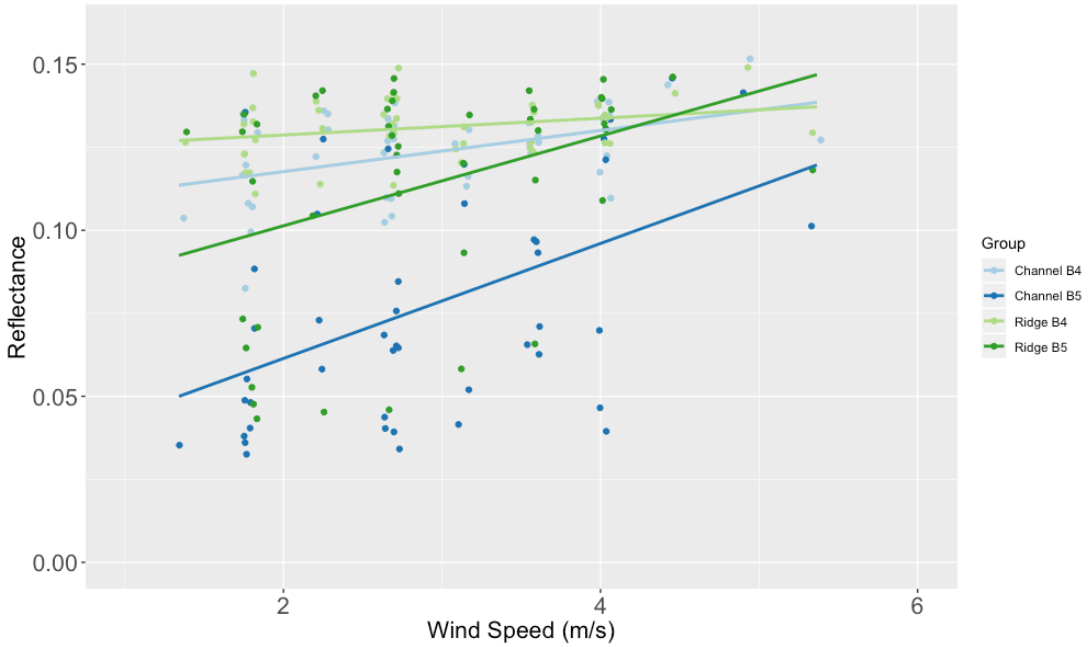

Figure 3.14: Reflectance plotted against wind speed in the GOK.

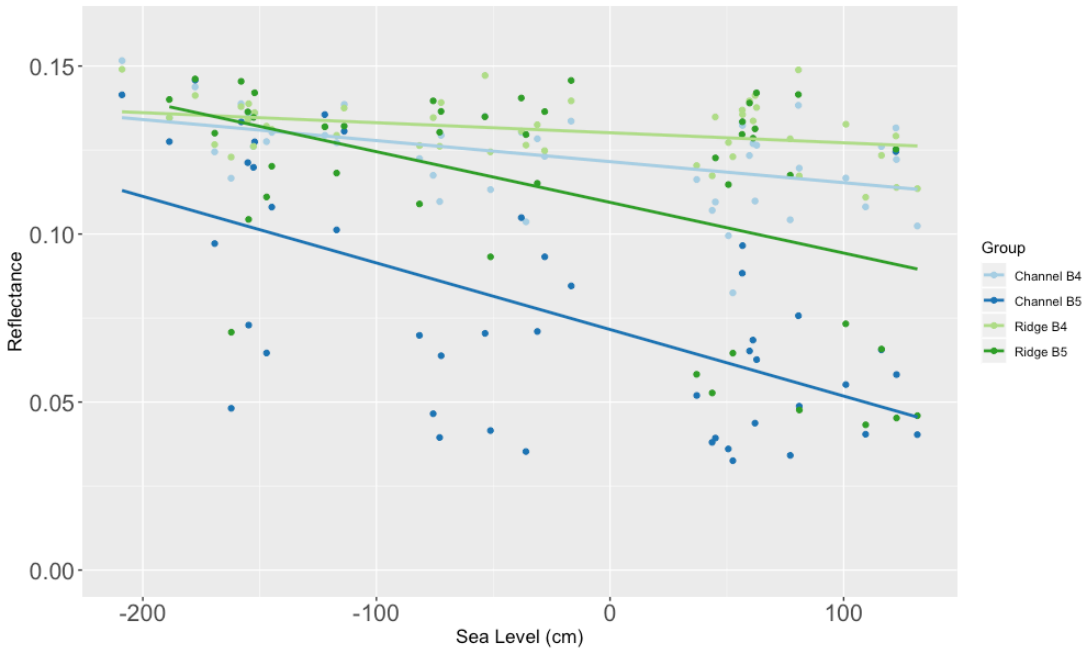

Figure 3.15: Relationship between sea level and reflectance in the GOK.

Chapter 4: Discussion

4.1 – Surface Reflectance and Stratification

Previous profiles of SPM in a tidal channel of the HMB produced the curious result that the integrated sediment load in the top half of the water column was higher at slack water than at peak flow (Hill, 2017). One proposed mechanism for this pattern of variability is suspended sediment stratification at peak flow. When flows are strongest, so much sediment is resuspended from the seabed that a dense suspension forms near the seabed. The gradient in density between sediment-laden water and the overlying surficial water – otherwise known as a lutocline – is great enough to limit upward turbulent mixing of sediment. As the flow decreases, sediment in the nearbed suspension begins to deposit, and turbulent mixing is again able to bring sediment to the surface. Standard deviation of reflectance in an area where a lutocline is suspected to be affecting stratification at peak flow should be lower than areas which have turbulent mixing throughout the tidal cycle.

This project's attempt to identify sediment stratification through the analysis of reflectance patterns depends on the saturation levels of reflectance in bands 4 and 5. Essentially, reflectance levels are determined by the level of surficial suspended sediment, which determines the ratio of backscattered to absorbed light. At low suspended sediment concentrations, SPM causes backscatter while water absorbs light, meaning that if surficial sediment concentration goes up then reflectance levels will rise as well. However, at high enough concentrations suspended sediment takes over as the primary absorber of light. Under these conditions, an increase in sediment concentration causes backscatter and absorption to increase, which means the reflectance level does not change, effectively saturating the wavelength and muting the satellite sensor's ability to detect variability in SPM at the water's surface. Shorter wavelengths become saturated before longer wavelengths

Through the correlation of reflectance and bathymetric graphs [Figure 3.1, 3.2], surficial patterns consistent with suspended sediment stratification were identifiable with remotely sensed reflectance. Surface reflectances were lower and had smaller variance at greater depths, where stratification occur.

In the HMB sediment concentrations, particularly over ridges, can be large. Sediment concentrations were high enough over the ridge to saturate band 4, so reflectance in this band did

not vary as much [Figure 3.3]. Band 5 was not saturated due to its longer wavelength, so it recorded greater variability in reflectance over the ridge than the channel.

4.2 – Surface Reflectance and Wind

Wind speed less than 12 m/s had significant positive correlations with reflectance in both bands 4 and 5 [Table 3.4]. This observation is consistent with the hypothesis that wave resuspension is the primary source for suspended sediment in the HMB. When winds are stronger, the increased stress from waves on the seabed is larger, which resuspends more sediment.

The two samples that had wind speeds over 12 m/s at the time of image capture lowered the overall correlation between reflectance and wind speed. Higher winds likely bring large concentrations of SPM to the surface, but the scattering created by sea foam that develops on the surface lowers reflectance.

4.3 – Surface Reflectance and Water Level

A significant negative correlation between reflectance and water level existed over both the ridge and the channel. If sediment supply is limited as water levels lower, the same amount of sediment occupies a smaller volume. This process causes a higher concentration of SPM in the water column.

4.4 – Comparison to Secondary Sites

Mean reflectance at the secondary sites correlated well with reflectance patterns over the HMB [Figure 3.7, 3.8]. Reflectance had similar patterns of mean variability against depth, suggesting similar subsurface processes [Figure 3.9, 3.10]. Saturation is more likely at GOK because of higher sediment concentrations, and it is less likely at GB because of lower sediment concentrations.

Wind speed was the most impactful environmental variable on reflectance relative to water level and precipitation in GB due to increased turbulence from waves resuspending sediment. Differences between high and low variance over the ridge and channel in each of the two bands correlates with the HMB's reflectance behaviour in band 5. Sediment concentrations are likely so low that the ratio of signal to noise masks the differences between the ridge and

channel in band 5 [Table 3.7]. Low levels of variance over the channel could also be linked to the surficial behaviour observed over the HMB during the development of a lutocline.

In the GOK the mean reflectance pattern also matches the bathymetric map [Figure 3.8]. However, high levels of SPM may be causing saturation in both bands over the ridge, so surface variability in shallower regions is not well resolved. Reflectance levels over the ridge are highly influenced by water level, as low water levels have higher reflectance than higher water.

Higher variance over the channel in the GOK may arise in two ways. The first is that the saturation over the ridge is so high that despite actual SPM variance being greater at shallower depths, the changes in surficial suspended sediment are not registered, causing the variance over the channel to appear to be greater. This is the mechanism proposed for the HMB in band 4. The other option could be that there are different subsurface mechanisms at play. Instead of the pattern observed over the HMB in band 5 – in which the difference between reflectance at peak flow and slack water are close due to suspected stratification of suspended sediment – there may be no stratification. If so, the increased turbulence during peak flow would increase SSC throughout the water column, which would explain the higher variance in the channel.

4.5 – Implications

The ability to identify areas affected by suspended sediment stratification with remote sensing methods has promising implications for future work. This method allows for preliminary site analysis and identification of subsurface sediment stratification in areas with high levels of SPM. The analysis of secondary sites demonstrates that this method could be applied to a much wider series of sites. The correlation of reflectance with bathymetry may allow for general bathymetric mapping in areas where mapping through traditional methods is difficult.

4.6 – Recommendations for Future Work

Limitations to the study are primarily the number of samples. The initial in situ data which prompted this project only has one sample to analyze. Further measurements of SPM over a ridge and channel throughout a tidal cycle would demonstrate whether surface SPM is highest at peak flow over the ridge, as predicted.

The limit on the number of images is also a factor to consider, as only 15 samples of Landsat 8 images were suitable for the project. As this project progresses, more imagery from

different satellites will be gathered from other sources in order to have a more robust sample collection. Ideally an approximately equal number of samples from different tidal stages would create a more reliable dataset.

Finally, possible analysis in other bands in Landsat imagery could be made to see whether longer wavelengths which are not as easily saturated could read SSC levels reliably. Part of the scientific community is currently exploring the usefulness of the two short wave infrared bands on Landsat 8, which are not as easily saturated as bands 4 and 5 but have the drawback of reading more noise than shorter wavelengths. A preliminary analysis into whether these bands could provide insight into the surficial sediment behaviour over areas with high reflectance such as the GOK would help in being certain that behaviour seen in bands 4 and 5 are reliable.

Chapter 5: Conclusion

5.1 – Conclusions

Surface reflectance patterns are consistent with the hypothesis of the presence of a lutocline over the HMB. Mean reflectance has been proven to correlate negatively with depth. Measurements of reflectance points over the channel and the ridge show that the latter has higher reflectance. Standard deviation over the ridge is lower in band 4 and higher in band 5, with the different results most likely due to saturation. Tests against environmental variables show that reflectance correlates well with wind speed, most likely due to resuspension of sediment at shallower depths.

Similar results have been obtained at secondary sites, with GB and the GOK demonstrating the same behaviour in both mean and sample point reflectance. Standard deviation is higher over the ridge in GB in both bands, while in the GOK suspected high saturation levels over the ridge causes the channel to have higher variance.

While further analysis is needed through observation of suspended sediment behaviour over a ridge and channel in a macrotidal environment, the results obtained in this project suggest that suspended sediment stratification might be possible to identify over the HMB. Similar patterns observed in similar environments suggest suspended sediment stratification may be active in other tidal seas.

References

Barsi, J. A. (2014). The Spectral Response of the Landsat-8 Operational Land Imager. *Remote Sensing, 6*, 10232-10251.

British Oceanographic Data Centre. (2018). *Gridded Bathymetry Data*. Retrieved from Gebco Bathymetric Chart of the Ocean: https://www.gebco.net/data_and_products/gridded_bathymetry_data/

Choi, J.-K. e. (2012). GOCI, the world's first geostationary ocean color observation satellite, for the monitoring of temporal variability in coastal water turbidity. *Journal of Geophysical Research, 117*(C9).

Earth & Space Research. (2019). *TMD Matlab Toolbox*. Retrieved from Earth & Space Research - A Non-Profit Institute: https://www.esr.org/research/polar-tide-models/tmd-software/

Egbert, G. D., & Erofeeva, L. (2010). *Regional and Local Tidal Solutions*. Retrieved from OSU Tidal Data Inversion: http://volkov.oce.orst.edu/tides/region.html

Frouin, R. (1996). Spectral reflectance of sea foam in the visible and near-infrared: In situ measurements and remote sensing implications. *Journal of Geophysical Research, 101*, 14,361-14,371.

Hill, P. (2017). *unpublished data.*

Ichikawa, K. (1997). Co-tidal and Co-range Charts for the East China Sea and the Yellow Sea Derived from Satellite Altimetric Data. *Journal of Oceanography, 53*, 303-309.

Kim, T. S. (2018). Modulation of Tidal Channel Signatures on SAR Images Over Gyeonggi Bay in Relation to Environmental Factors. *Remote Sensing, 10*.

Korean Meteoroligical Administration. (2009). *Climate*. Retrieved from Korean Meteoroligical Administration: https://web.kma.go.kr/eng/biz/climate_01.jsp

Lee, H. J. (2014). A Review of Sediment Dynamical Processes in the West Coast of Korea, Eastern Yellow Sea. *Ocean Science Journal*, 85-95.

Lee, H. J. (2015). A Review on the Holocene evolution of an Inner-shelf Mud Deposit in the Southeastern Yellow Sea: the Huksan Mud Belt. *Ocean Science Journal, 50*, 615-621.

Lee, H. J., & Chu, Y. S. (2001). Origin of Inner-Shelf Mud Deposit in the Southeastern Yellow Sea: Huksan Mud Belt. *Journal of Sedimentary Research 71*, 144-154.

NDBC. (2018). *NDBC - Station 22102 Recent Data*. Retrieved from National Oceanic and Atmospheric Administration's National Data Buoy Center: https://www.ndbc.noaa.gov/station_page.php?station=22102

NDBC. (2018). *Station 22101 Recent Data*. Retrieved from National Oceanographic and Atmospheric Administration's National Data Buoy Center: https://www.ndbc.noaa.gov/station_page.php?station=22101

Novoa, S. e. (2017). Atmospheric Corrections and Multi-Conditional Algorithm for Multi-Sensor Remote Sensing of Suspended Particulate Matter in Low-to-High Turbidity Levels Coastal Waters. *Remote Sensing*.

Permenant Service for Mean Sea Level. (2018). *Revised Local Reference fot Heuksando*. Retrieved from Permenants Service for Mean Sea Level: https://www.psmsl.org/data/obtaining/rlr.diagrams/1489.php

Ramakrishnan, D. e. (2013). A technique for estimation of suspended sediment concentration in very high turbid coastal waters: An investigation from Gulf of Cambay, India. *Marine Geology*, 256-261.

Royal Belgian Institute of Natural Sciences. (2019). *ACOLITE*. Retrieved from Royal Belgian Institute of Natural Sciences: https://odnature.naturalsciences.be/remsem/software-and-data/acolite

Shapiro, S. S., & Wilk, M. B. (1965). An analysis of variance test for normality (complete samples). *Biometrika, 52(3–4)*, 591–611.

Student. (1908). The probable error of a mean. *Biometrika, Volume 6, Issue 1*, 1-25.

Trowbridge, J. H., & Kineke, G. (1994). Structure and dynamics of fluid muds on the Amazon continental shelf. *Journal of Geophysical Research, 99*(C1), 865-874.

Vanhellemont, Q., & Ruddick, K. (2018). Atmospheric correction of metre-scale optical satellite data for inland and coastal water applications. *Remote Sensing of Environment, 216*, 586-597.

Wolanski, E. e. (1988). Fluidization of Mud in Estuaries. *Journal of Geophysical Research, 93*(C3), 2351-2361.

Appendix A – Data Tables

HMB Data Table

Entry	Image Capture Date	Ridge Band 4	Ridge Band 5	Channel Band 4	Channel Band 5	Wind (m/s)	Precipitation (mm)	Season	Tide Level	Water Height (m)	Actual Sea Level (cm)
1	2013-09-16	0.1019762	0.038079556	0.059594795	0.02613064	2.68	18.6	Fall	High	4	204.764168
2	2014-01-06	0.13470908	0.091914095	0.12602657	0.062263113	3.6	0	Winter	Low	0.72	177.095033
3	2014-03-11	0.103723034	0.040759847	0.08253382	0.036277987	2.2	0.2	Winter	High	3.95	179.195797
4	2015-04-15	0.13737589	0.073179044	0.1298592	0.06648687	11.7	20	Winter	High	4.5	184.521417
5	2015-08-05	0.13459991	0.09148443	0.12447773	0.06240208	5.8	2.9	Summer	Low	0.9	208.206912
6	2016-04-17	0.14144063	0.087822095	0.12496606	0.061407994	9.7	22.1	Winter	High	4.1	184.702622
7	2016-08-07	0.1047082	0.037188355	0.07639767	0.024918566	0	0.1	Summer	Low	0.96	208.297515
8	2016-09-24	0.1118978	0.046202406	0.06664812	0.02949295	0	0	Fall	Mid	2.5	205.217182
9	2016-11-11	0.12619762	0.06572027	0.10913463	0.04446681	5.8	31.3	Fall	High	4.25	187.472865
10	2017-02-15	0.11011137	0.048601348	0.1033025	0.03347949	3.9	0.2	Winter	Low	0.74	176.250582
11	2017-03-18	0.12152625	0.064009696	0.10723581	0.041094065	3.9	0	Winter	Low	2.16	179.467605
12	2017-08-10	0.0930137	0.029280247	0.07528056	0.026509698	1.9	23.4	Summer	Low	0.97	208.388118
13	2017-10-13	0.095253125	0.027842289	0.07615607	0.021925988	17.5	8.9	Fall	Mid	2.5	197.175725
14	2017-11-14	0.121484265	0.058294386	0.10890932	0.04556469	7.8	0	Fall	High	4.1	187.563468
15	2018-03-06	0.11390375	0.061714664	0.11243935	0.054003373	13.8	15.1	Winter	Low	0.75	179.558208

GB Data Table

Sample	Date	Channel B4	Channel B5	Ridge B4	Ridge B5	Wind	Actual Sea Level (cm)	Tide	Precipitation
1	2013-09-16	0.03651146	0.01523067	0.0463695	0.01428691	0.5	496.1042	Mid	18.8
2	2014-09-19	0.03186203	0.01394799	0.0336885	0.01330298	1.2	492.1225	Mid	0
3	2014-10-05	0.04718341	0.02344006	0.05295738	0.02423748	6.7	501.5706	Mid	0.2
4	2015-03-14	0.07711154	0.0253206	0.07805806	0.02523611	4.5	575.7091	High	0
5	2015-09-22	0.05088375	0.02937745	0.05830111	0.03234355	5.2	538.1083	Mid	0
6	2016-05-19	0.06159741	0.03432877	0.06787846	0.018778	2.3	396.5134	Low	0
7	2016-10-10	0.04044455	0.01408922	0.05729076	0.01612378	7.6	515.7881	Mid	11.5
8	2017-05-06	0.06783201	0.04698243	0.0989781	0.05344858	12.8	499.8332	Mid	0.4
9	2017-07-25	0.05916346	0.03175989	0.0832219	0.03007484	6.9	290.3266	Low	22.3
10	2017-08-26	0.03719308	0.01578993	0.05630017	0.01687784	6.4	403.8988	Mid	30.8
11	2017-11-14	0.06454186	0.02550896	0.09617495	0.03929315	11.3	459.7128	Mid	3.9
12	2017-11-30	0.07547326	0.03013712	0.1064584	0.04811435	3.8	497.174	Mid	0.4
13	2018-03-22	0.07388864	0.03283927	0.08633741	0.03354374	3.9	394.6639	Mid	7
14	2018-05-09	0.0483159	0.02310418	0.05244858	0.02365144	1.7	555.5205	High	0
15	2018-11-01	0.05009703	0.01587823	0.06058652	0.01740149	3.9	512.5176	High	0

GOK Data Table

Sample	Date	Channel B4	Channel B5	Ridge B4	Ridge B5	Tide	Actual Sea Level (cm)	Wind (m/s)
1	2014-03-11	0.1196094	0.048789	0.1173206	0.0476332	High	80	1.78816
2	2014-04-12	0.1036457	0.035271	0.1264626	0.1296114	Mid	210	1.34112
3	2014-04-28	0.1350281	0.0729041	0.1387924	0.1043569	Mid	290	2.2352
4	2014-05-30	0.1516156	0.1414293	0.1490388	0.1626598	Low	360	4.91744
5	2014-10-05	0.1333059	0.0883554	0.1368993	0.1296541	Mid	150	1.78816
6	2014-10-21	0.1283532	0.0710119	0.1325255	0.1150931	Mid	210	3.57632
7	2014-11-06	0.1293892	0.1355524	0.1319508	0.1319325	Mid	270	1.78816
8	2014-11-22	0.1275184	0.0646042	0.132101	0.1110433	Low	310	2.68224
9	2014-12-24	0.138791	0.1333832	0.1379425	0.1454461	Low	310	4.02336
10	2015-01-09	0.1224477	0.0698429	0.1263342	0.1089646	Mid	250	4.02336
11	2015-02-26	0.1315906	0.1245302	0.1291902	0.12526	High	70	2.68224
12	2015-05-01	0.1350207	0.0704512	0.147201	0.1349112	Mid	230	1.78816
13	2015-05-17	0.1166202	0.0481415	0.1229101	0.0707836	Mid	290	1.78816
14	2015-12-27	0.1244785	0.0971719	0.1266259	0.1300329	Low	340	3.57632
15	2016-01-12	0.133778	0.1212515	0.1340161	0.1363548	Low	300	4.02336
16	2016-01-28	0.1174794	0.0465246	0.1346526	0.1396407	Mid	240	4.02336
17	2016-02-13	0.1336113	0.0845727	0.1396407	0.1457058	Mid	200	2.68224
18	2016-02-29	0.1162353	0.0519683	0.1203884	0.0582534	Mid	160	3.12928
19	2016-03-16	0.1221897	0.0581869	0.1138818	0.0452525	High	60	2.2352
20	2016-04-01	0.1081078	0.0404233	0.1109566	0.0432345	High	30	1.78816
21	2016-04-17	0.1264255	0.0626301	0.1376689	0.1420329	Mid	120	3.57632
22	2016-05-03	0.0995123	0.036051	0.1272501	0.1147314	Mid	150	1.78816
23	2016-10-26	0.1042497	0.0341282	0.1283479	0.1175212	Mid	120	2.68224
24	2016-11-11	0.1269249	0.0684477	0.1336751	0.1285345	Mid	140	2.68224
25	2016-11-27	0.1132444	0.0415167	0.1244556	0.093224	Mid	230	3.12928
26	2016-12-13	0.127208	0.1012424	0.12938	0.1181512	Mid	270	5.36448
27	2016-12-29	0.1302755	0.108028	0.1311572	0.1201862	Low	330	3.12928
28	2017-01-14	0.1437886	0.1457967	0.1412438	0.1461698	Low	330	4.4704
29	2017-01-30	0.126071	0.1198518	0.1260957	0.1347207	Low	300	3.12928
30	2017-02-15	0.1293765	0.0637921	0.1391344	0.1365038	Mid	230	2.68224
31	2017-03-03	0.1231379	0.0932365	0.1248139	0.1364516	Mid	200	3.57632
32	2017-03-19	0.107054	0.0380066	0.1173508	0.0527041	Mid	150	1.78816
33	2017-05-06	0.1233735	0.0651991	0.139624	0.1389913	Mid	130	2.68224
34	2017-05-22	0.1095431	0.0392814	0.1348472	0.1226587	Mid	150	2.68224
35	2017-10-29	0.1024031	0.0403059	0.1135225	0.0459439	High	10	2.68224
36	2017-11-14	0.1383099	0.075688	0.1488666	0.1415242	Mid	120	2.68224
37	2017-11-30	0.1323238	0.0965571	0.1355691	0.1334405	Mid	140	3.57632
38	2018-01-01	0.1385828	0.1305989	0.1374993	0.1321263	Low	270	4.02336
39	2018-02-02	0.1345229	0.1275112	0.1346794	0.1400496	Low	330	4.02336
40	2018-02-18	0.1359534	0.1274462	0.1361405	0.1420474	Low	300	2.2352
41	2018-03-06	0.1096645	0.0394544	0.1261148	0.1303083	Mid	230	4.02336
42	2018-03-22	0.1302681	0.1048896	0.1306298	0.1404917	Mid	200	2.2352
43	2018-04-07	0.0825094	0.0325468	0.1230116	0.0645592	Mid	130	1.78816
44	2018-04-23	0.1260519	0.0655505	0.1234138	0.0657811	High	60	3.57632
45	2018-05-09	0.1166761	0.0552004	0.1326869	0.0732987	High	10	1.78816
46	2018-05-25	0.1098216	0.0437265	0.1412347	0.1313162	Mid	130	2.68224

Appendix B – Satellite Images (Post Correction): HMB

ρ_s RGB L8/OLI 2013-09-16 (02:13 UTC)

ρ_s RGB L8/OLI 2014-01-06 (02:13 UTC)

ρ_s RGB L8/OLI 2014-03-11 (02:12 UTC)

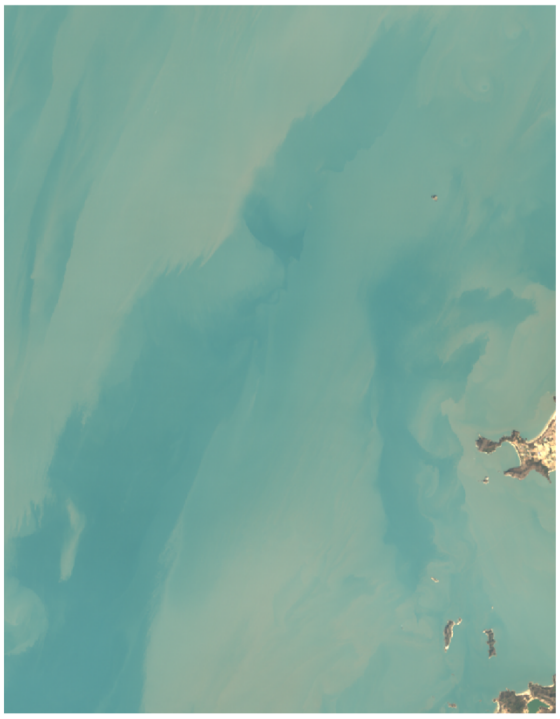

ρ_s RGB L8/OLI 2015-04-15 (02:11 UTC)

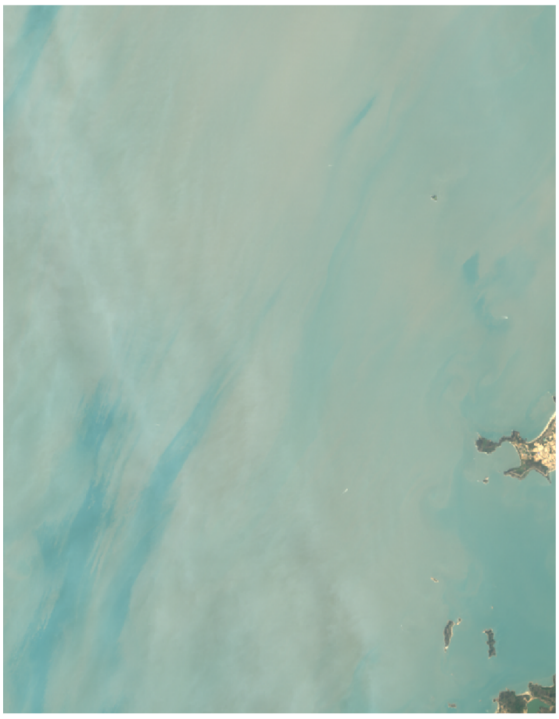

ρ_s RGB L8/OLI 2015-08-05 (02:11 UTC)

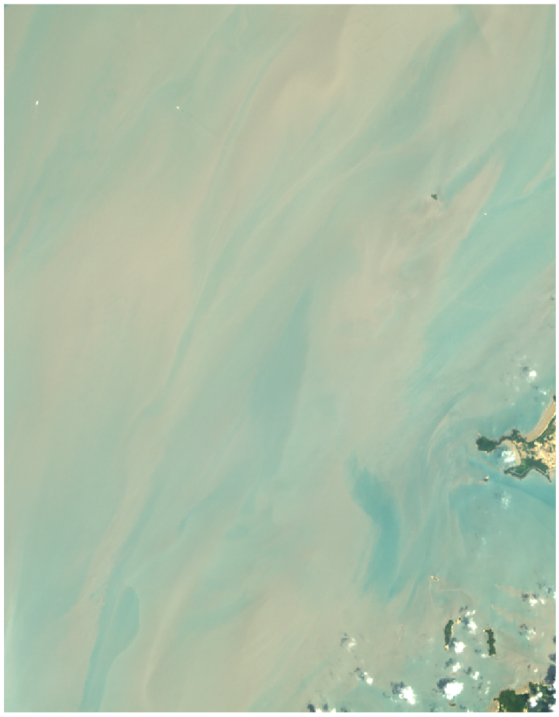

ρ_s RGB L8/OLI 2016-04-17 (02:11 UTC)

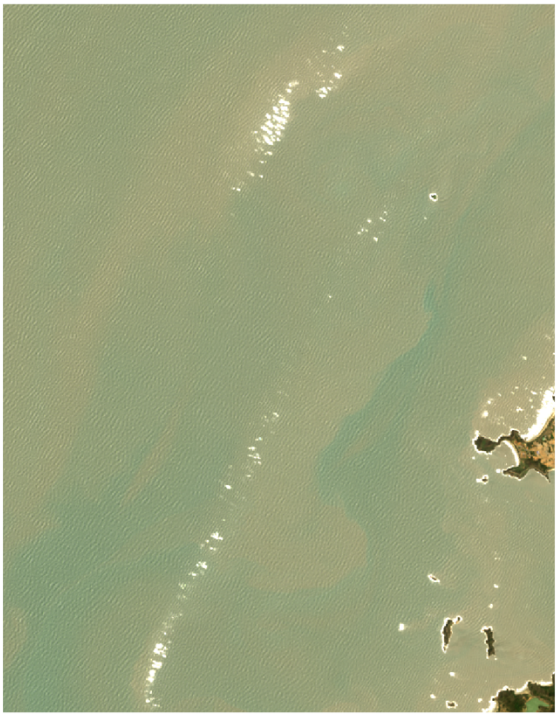

ρ_s RGB L8/OLI 2016-08-07 (02:11 UTC)

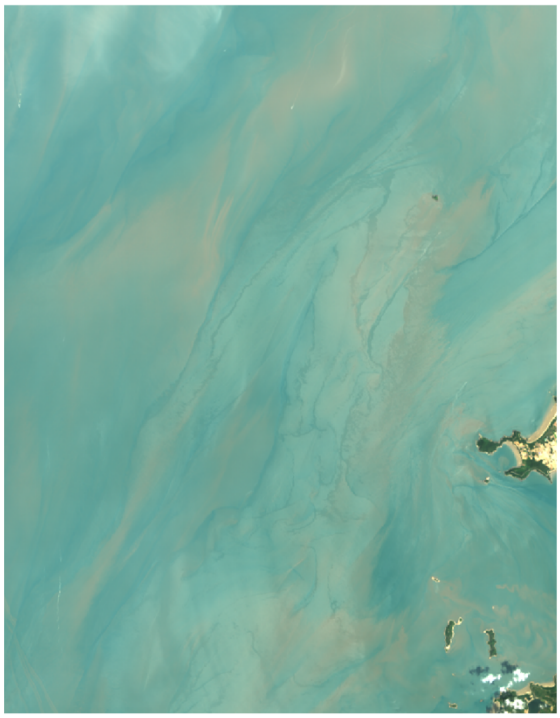

ρ_s RGB L8/OLI 2016-09-24 (02:12 UTC)

ρ_s RGB L8/OLI 2016-11-11 (02:12 UTC)

ρ_s RGB L8/OLI 2017-02-15 (02:11 UTC)

ρ_s RGB L8/OLI 2017-03-19 (02:11 UTC)

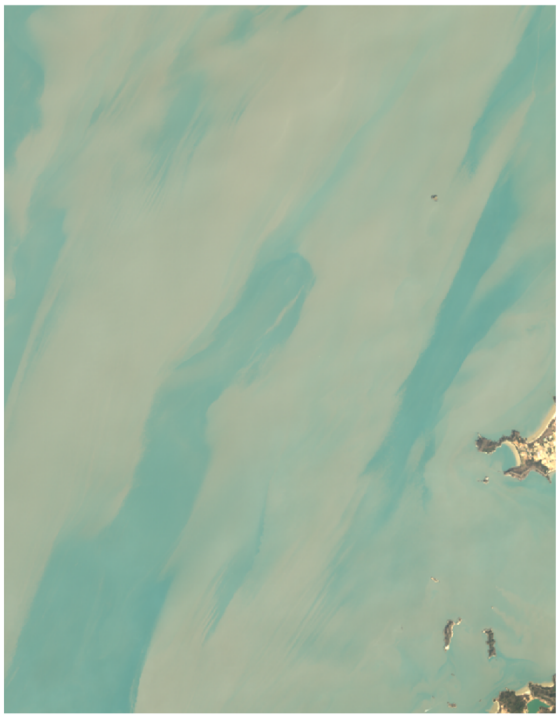

ρ_s RGB L8/OLI 2017-08-10 (02:11 UTC)

ρ_s RGB L8/OLI 2017-10-13 (02:12 UTC)

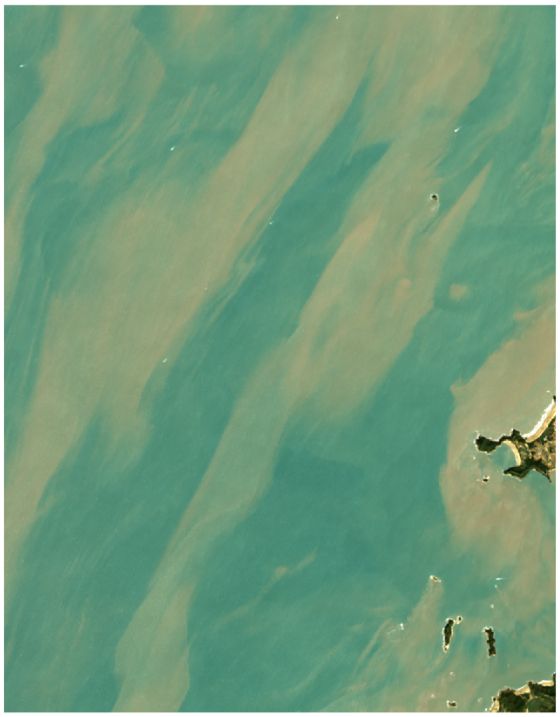

ρ_s RGB L8/OLI 2017-11-14 (02:12 UTC)

ρ_s RGB L8/OLI 2018-03-06 (02:11 UTC)

Satellite Images (Post Correction): GB

ρ_s RGB L8/OLI 2013-09-16 (02:13 UTC)

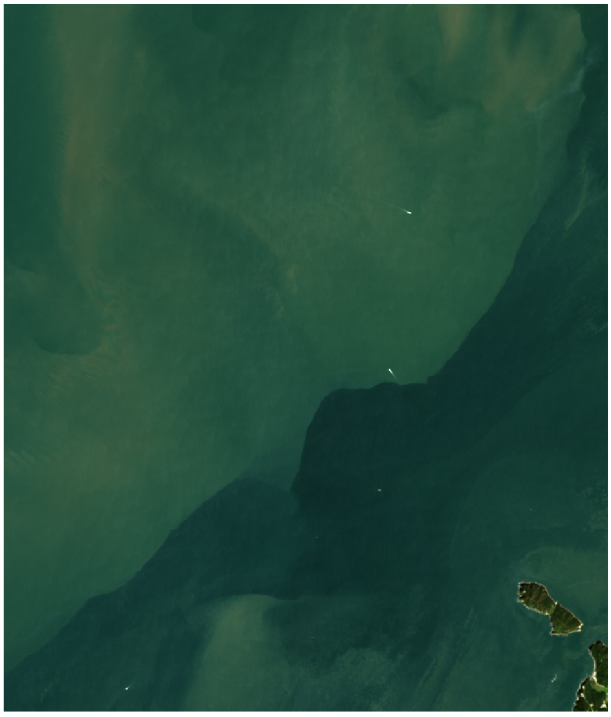

ρ_s RGB L8/OLI 2014-09-19 (02:11 UTC)

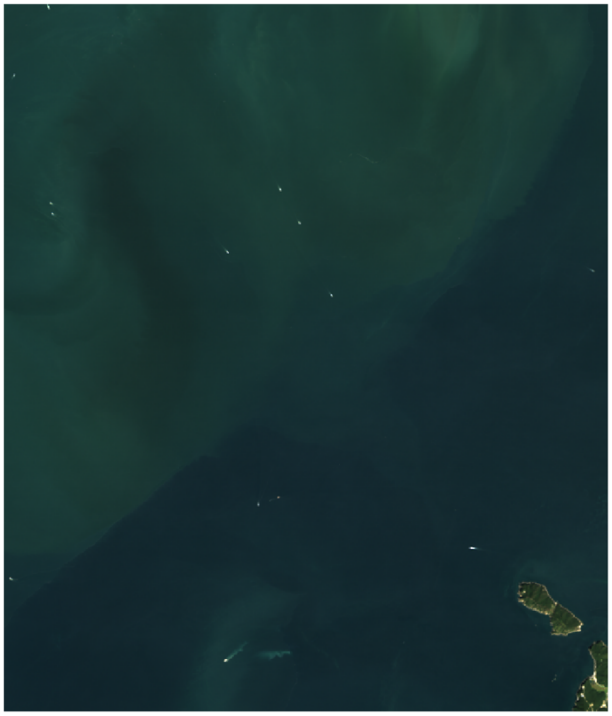

ρ_s RGB L8/OLI 2014-10-05 (02:11 UTC)

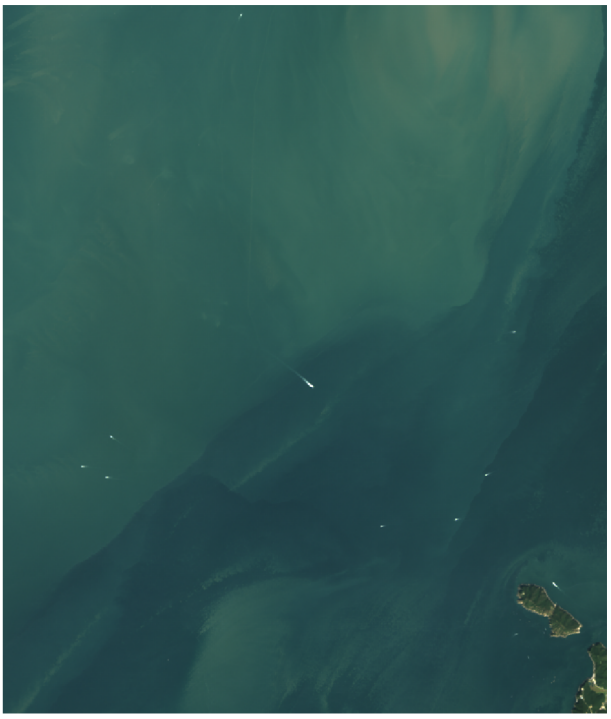

ρ_s RGB L8/OLI 2015-03-14 (02:10 UTC)

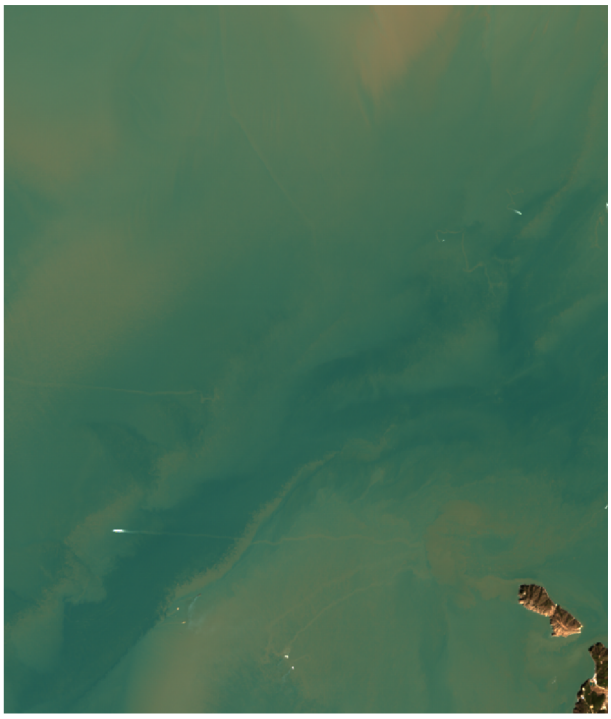

ρ_s RGB L8/OLI 2015-09-22 (02:11 UTC)

ρ_s RGB L8/OLI 2016-05-19 (02:10 UTC)

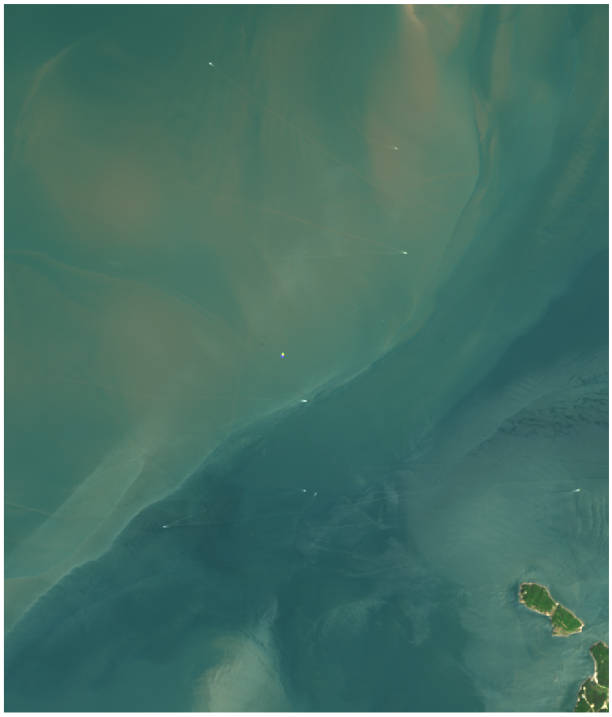

ρ_s RGB L8/OLI 2016-10-10 (02:11 UTC)

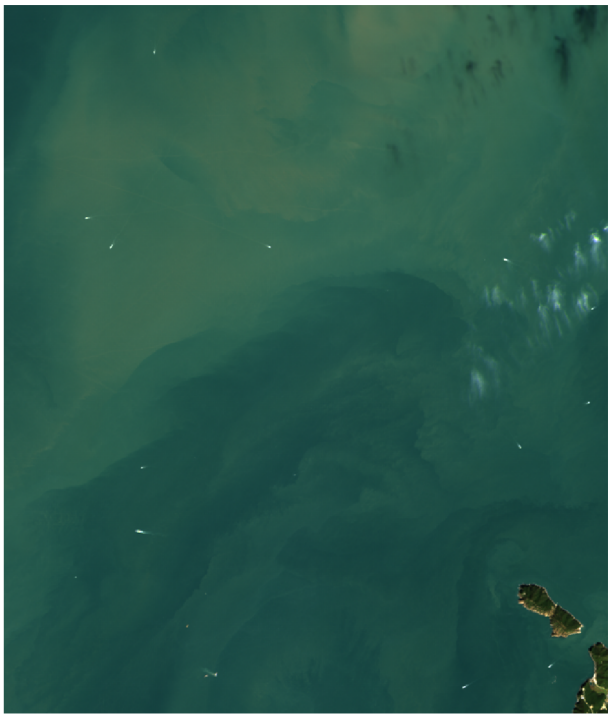

ρ_s RGB L8/OLI 2017-05-06 (02:10 UTC)

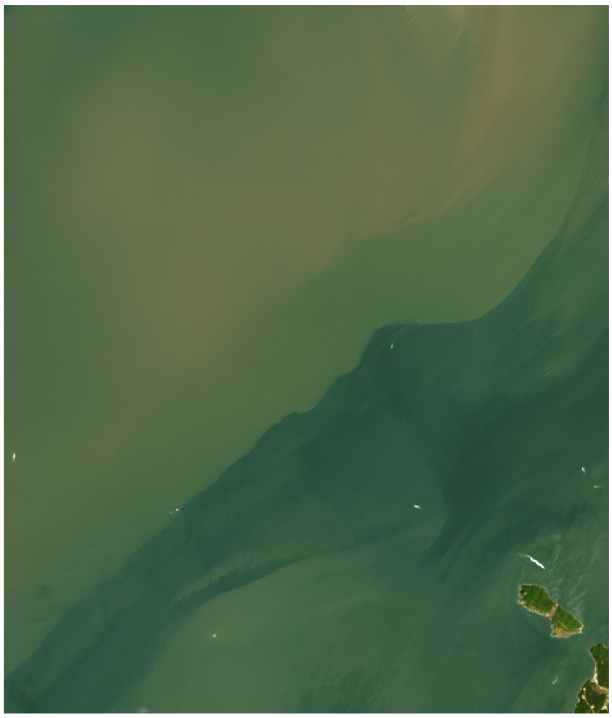

ρ_s RGB L8/OLI 2017-07-25 (02:10 UTC)

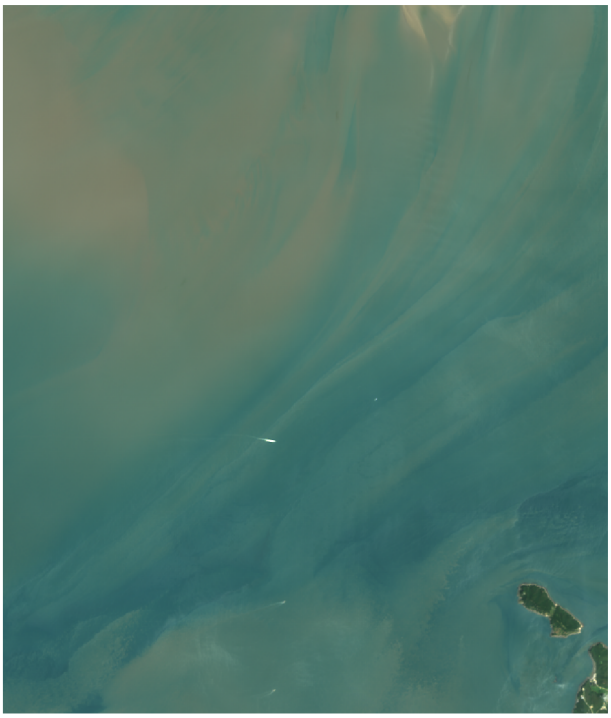

ρ_s RGB L8/OLI 2017-08-26 (02:11 UTC)

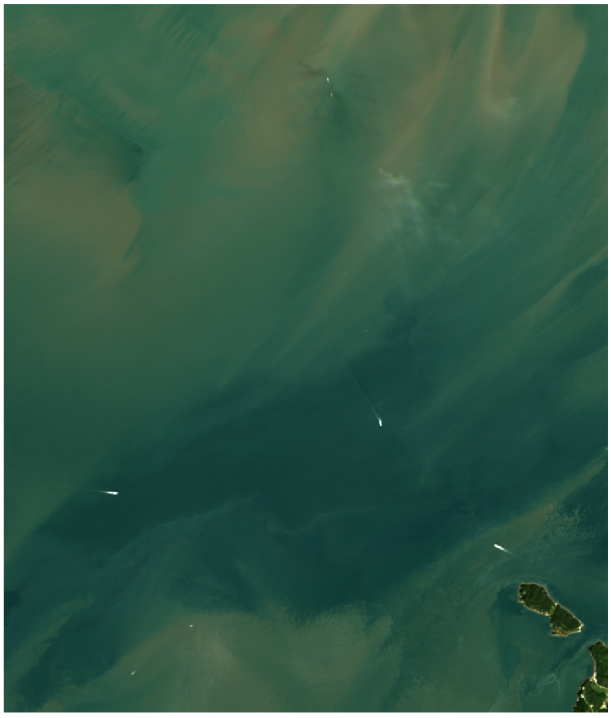

ρ_s RGB L8/OLI 2017-11-14 (02:11 UTC)

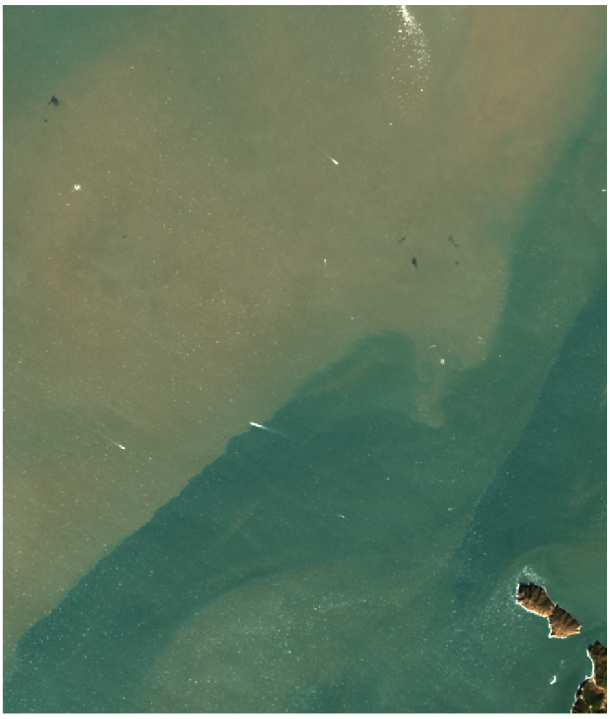

ρ_s RGB L8/OLI 2017-11-30 (02:11 UTC)

ρ_s RGB L8/OLI 2018-03-22 (02:10 UTC)

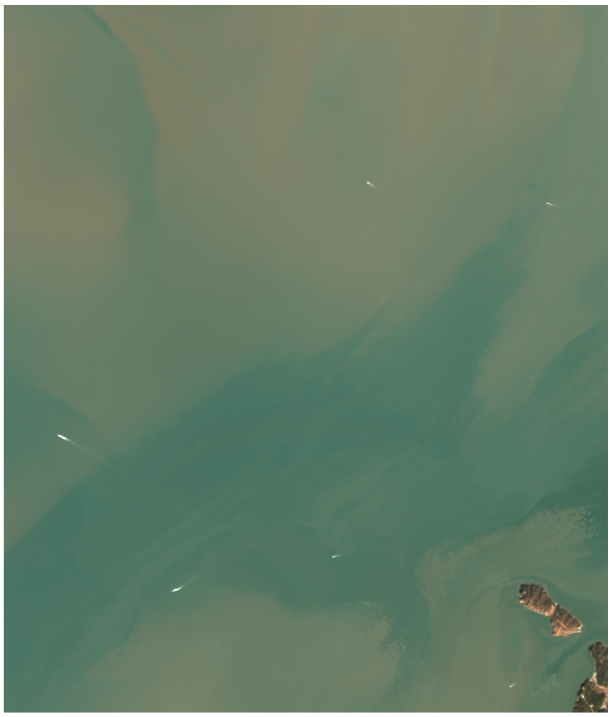

ρ_s RGB L8/OLI 2018-05-09 (02:10 UTC)

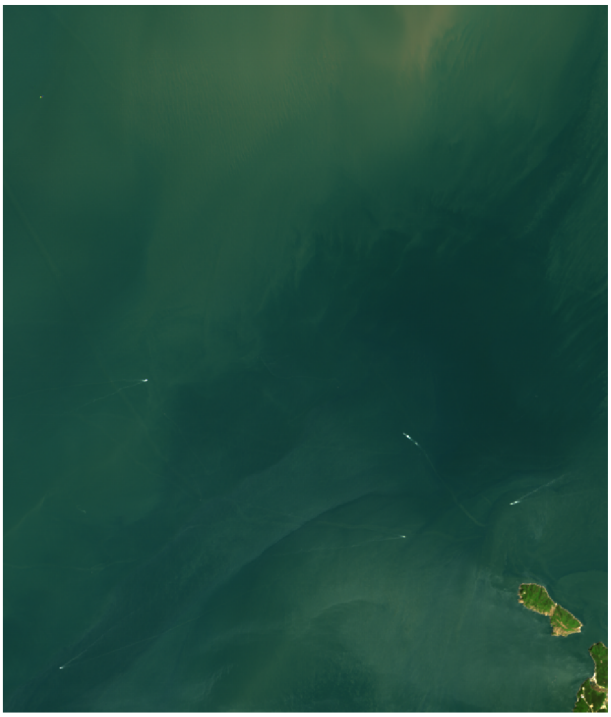

ρ_s RGB L8/OLI 2018-11-01 (02:10 UTC)

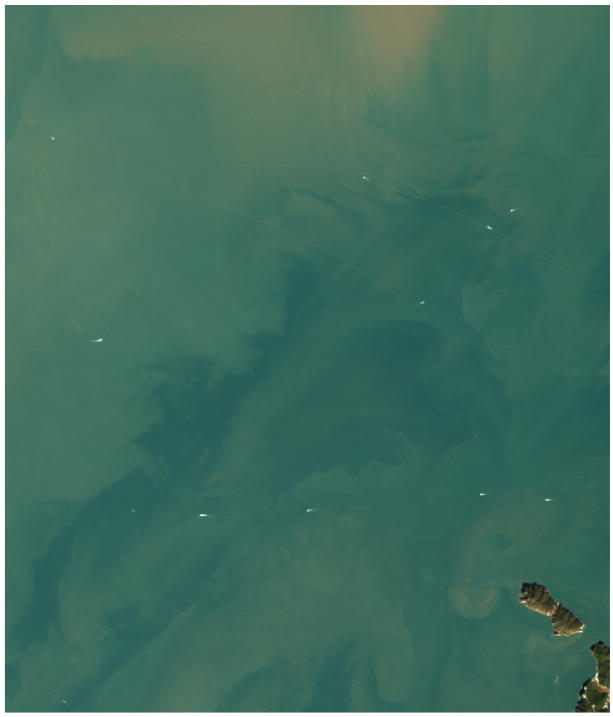

Satellite Images (Post Correction): GOK

ρ_s RGB L8/OLI 2014-03-11 (05:33 UTC)

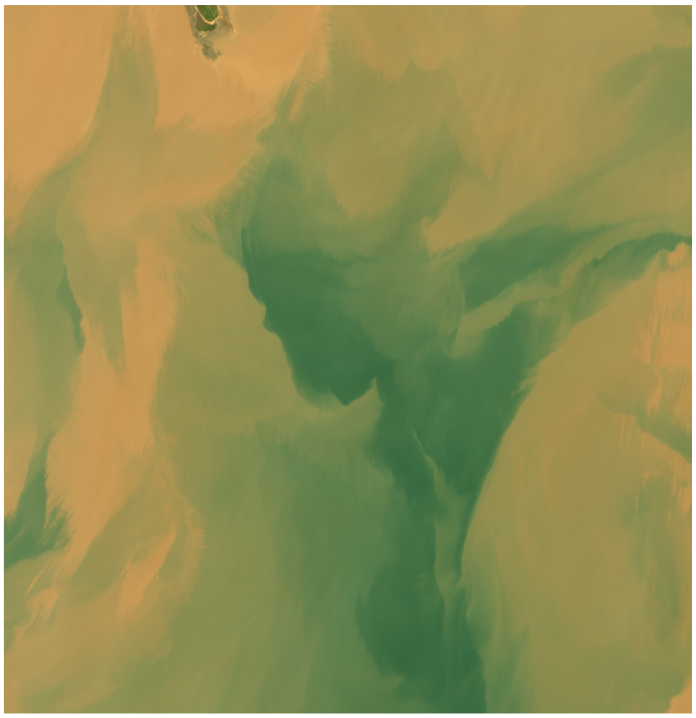

ρ_s RGB L8/OLI 2014-04-12 (05:33 UTC)

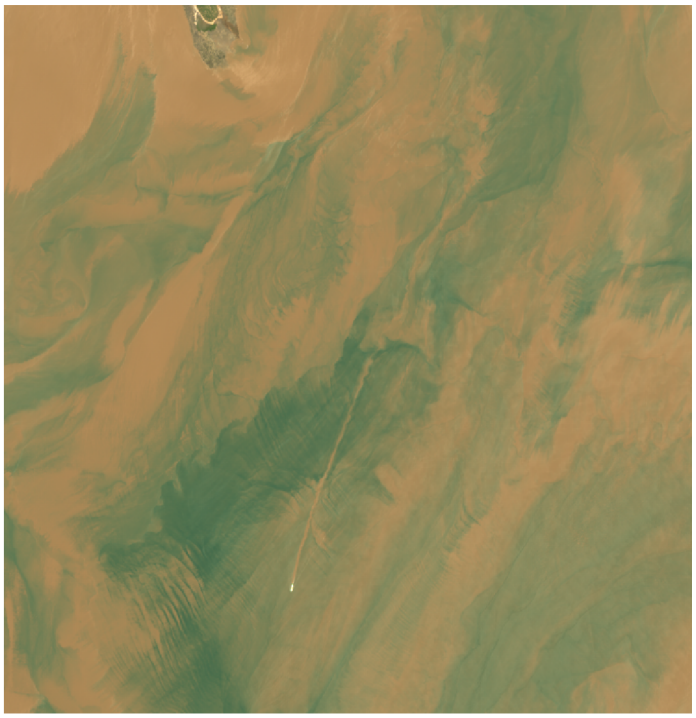

ρ_s RGB L8/OLI 2014-04-28 (05:32 UTC)

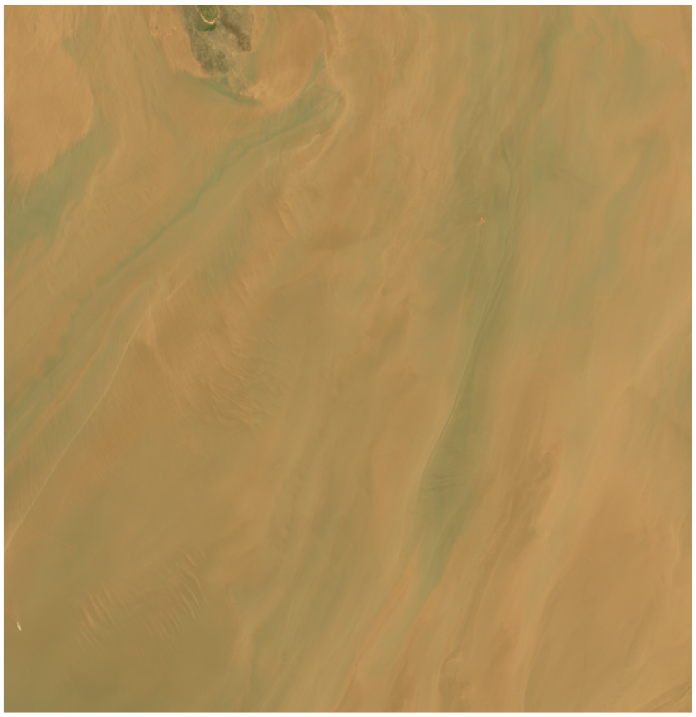

ρ_s RGB L8/OLI 2014-05-30 (05:32 UTC)

ρ_s RGB L8/OLI 2014-10-05 (05:33 UTC)

ρ_s RGB L8/OLI 2014-10-21 (05:33 UTC)

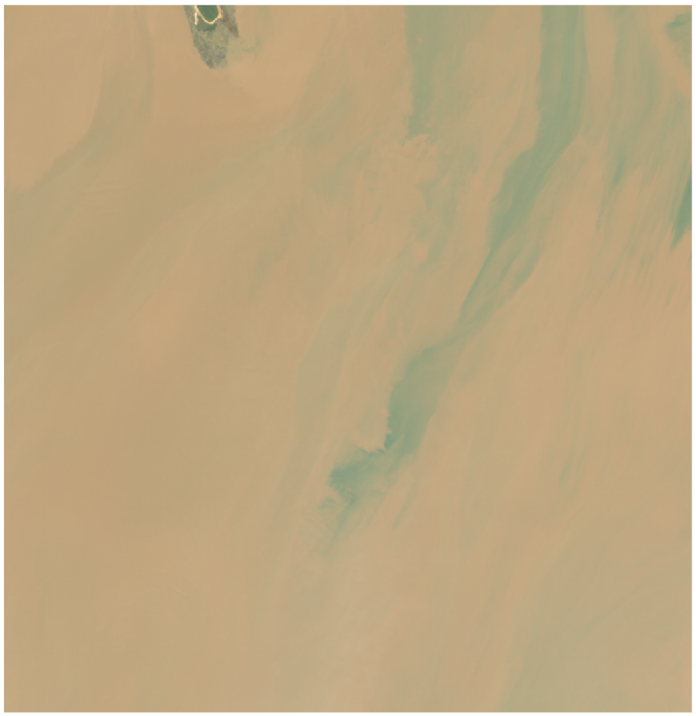

ρ_s RGB L8/OLI 2014-11-06 (05:33 UTC)

ρ_s RGB L8/OLI 2014-11-22 (05:33 UTC)

ρ_s RGB L8/OLI 2014-12-24 (05:33 UTC)

ρ_s RGB L8/OLI 2015-01-09 (05:33 UTC)

ρ_s RGB L8/OLI 2015-02-26 (05:32 UTC)

ρ_s RGB L8/OLI 2015-05-01 (05:32 UTC)

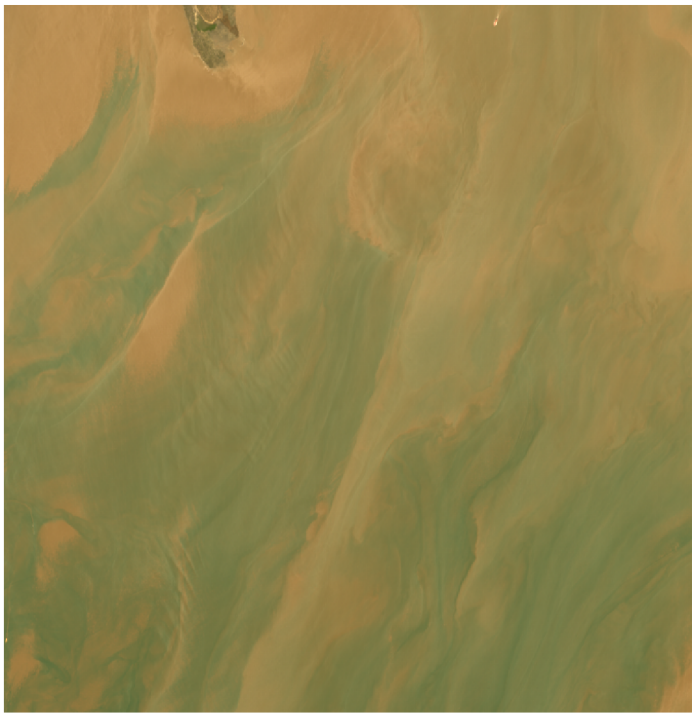

ρ_s RGB L8/OLI 2015-05-17 (05:32 UTC)

ρ_s RGB L8/OLI 2015-12-27 (05:33 UTC)

ρ_s RGB L8/OLI 2016-01-12 (05:33 UTC)

ρ_s RGB L8/OLI 2016-01-28 (05:33 UTC)

ρ_s RGB L8/OLI 2016-02-13 (05:33 UTC)

ρ_s RGB L8/OLI 2016-02-29 (05:33 UTC)

ρ_s RGB L8/OLI 2016-03-16 (05:33 UTC)

ρ_s RGB L8/OLI 2016-04-01 (05:32 UTC)

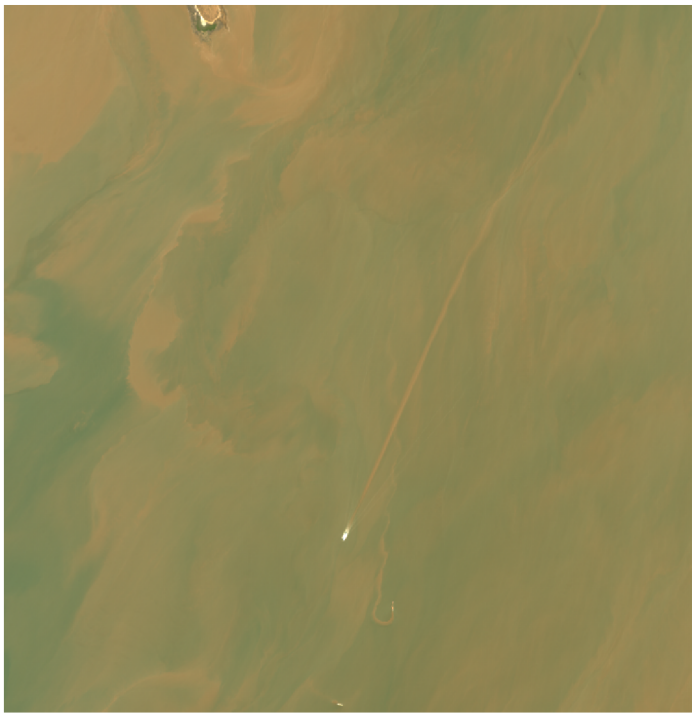

ρ_s RGB L8/OLI 2016-04-17 (05:32 UTC)

ρ_s RGB L8/OLI 2016-05-03 (05:32 UTC)

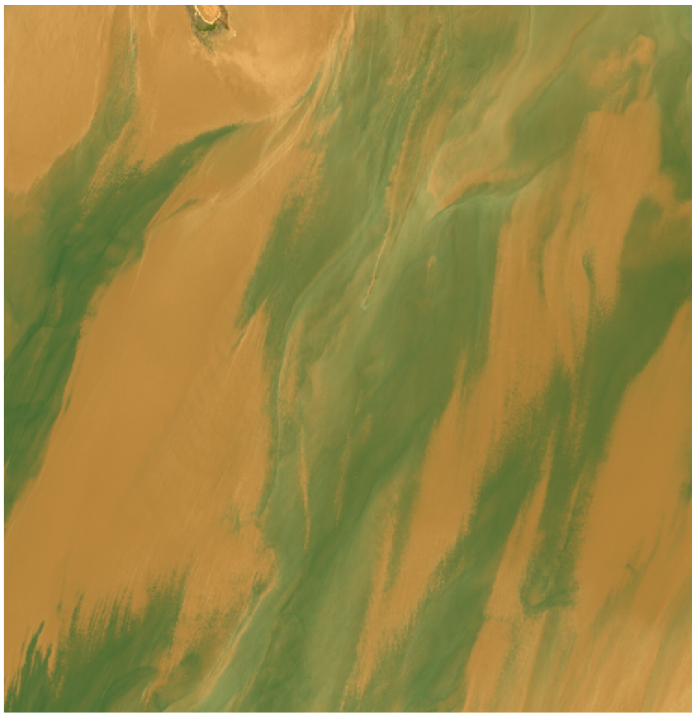

ρ_s RGB L8/OLI 2016-10-26 (05:33 UTC)

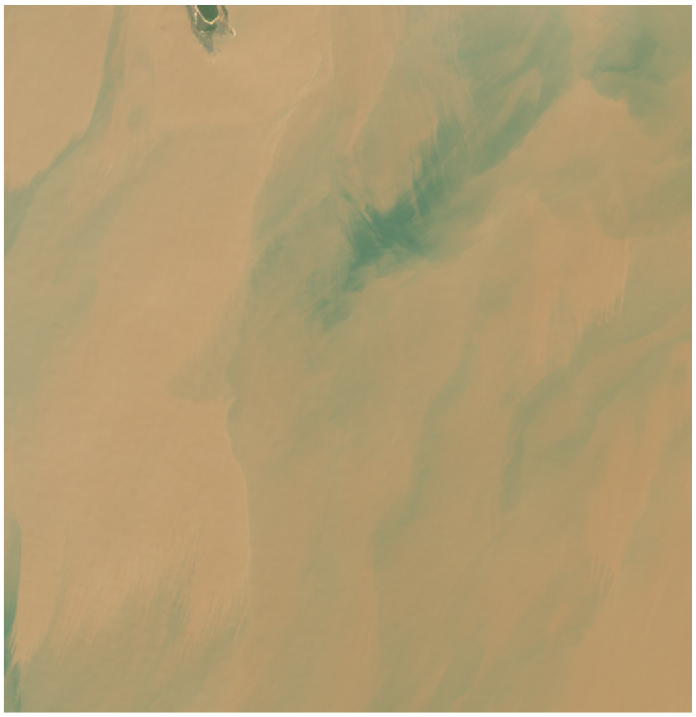

ρ_s RGB L8/OLI 2016-11-11 (05:33 UTC)

ρ_s RGB L8/OLI 2016-11-27 (05:33 UTC)

ρ_s RGB L8/OLI 2016-12-13 (05:33 UTC)

ρ_s RGB L8/OLI 2016-12-29 (05:33 UTC)

ρ_s RGB L8/OLI 2017-01-14 (05:33 UTC)

ρ_s RGB L8/OLI 2017-01-30 (05:33 UTC)

ρ_s RGB L8/OLI 2017-02-15 (05:33 UTC)

ρ_s RGB L8/OLI 2017-03-03 (05:33 UTC)

ρ_s RGB L8/OLI 2017-03-19 (05:32 UTC)

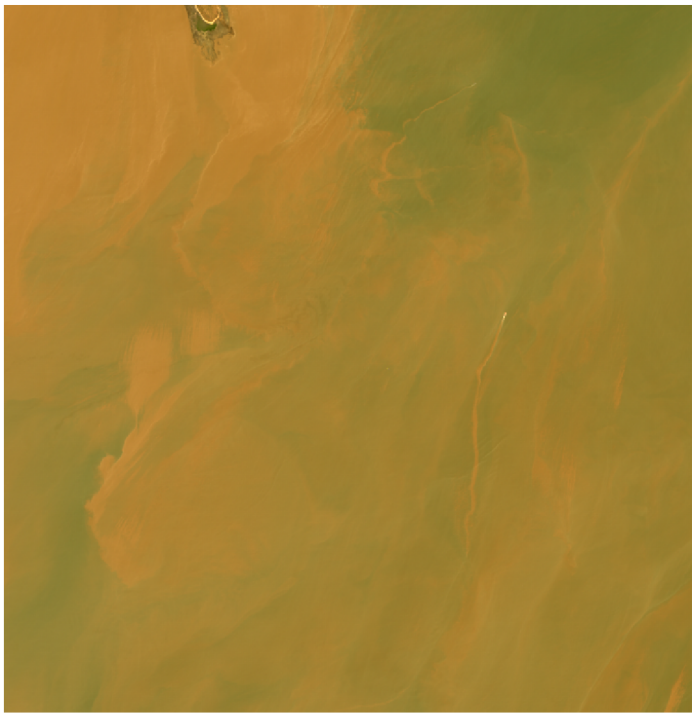

ρ_s RGB L8/OLI 2017-05-06 (05:32 UTC)

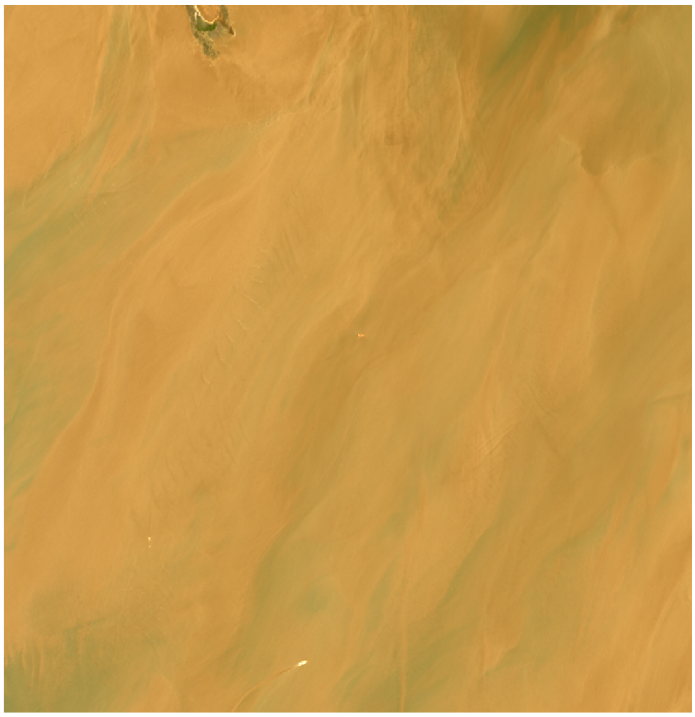

ρ_s RGB L8/OLI 2017-05-22 (05:32 UTC)

ρ_s RGB L8/OLI 2017-10-29 (05:33 UTC)

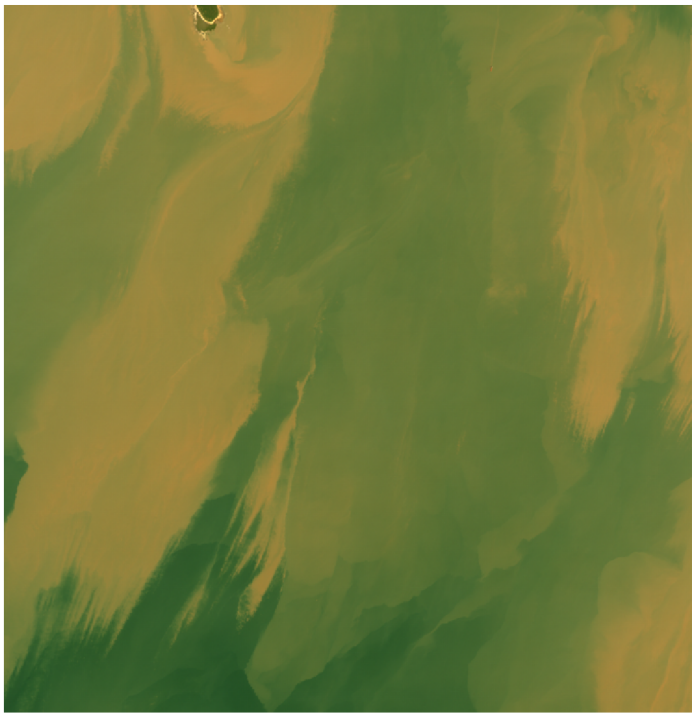

ρ_s RGB L8/OLI 2017-11-14 (05:33 UTC)

ρ_s RGB L8/OLI 2017-11-30 (05:33 UTC)

ρ_s RGB L8/OLI 2018-01-01 (05:33 UTC)

ρ_s RGB L8/OLI 2018-02-02 (05:33 UTC)

ρ_s RGB L8/OLI 2018-02-18 (05:32 UTC)

ρ_s RGB L8/OLI 2018-03-06 (05:32 UTC)

ρ_s RGB L8/OLI 2018-03-22 (05:32 UTC)

ρ_s RGB L8/OLI 2018-04-07 (05:32 UTC)

ρ_s RGB L8/OLI 2018-04-23 (05:32 UTC)

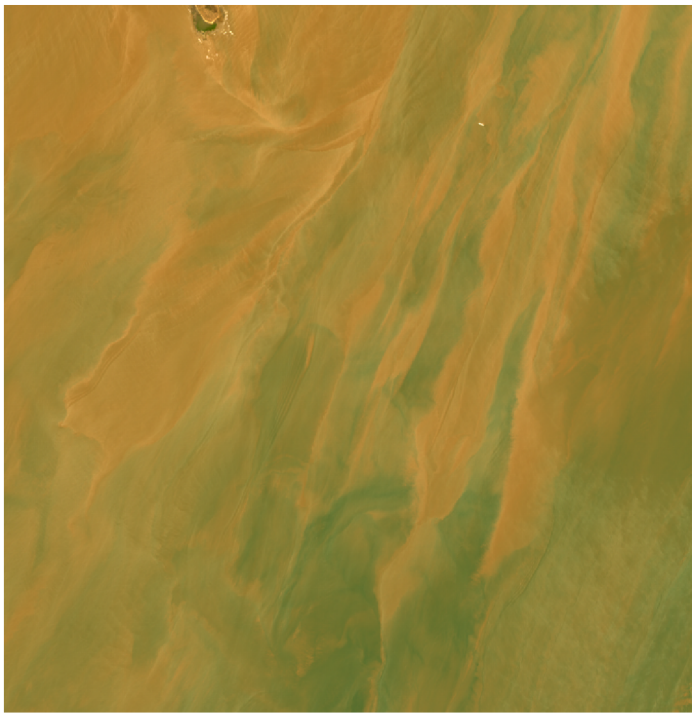

ρ_s RGB L8/OLI 2018-05-09 (05:32 UTC)

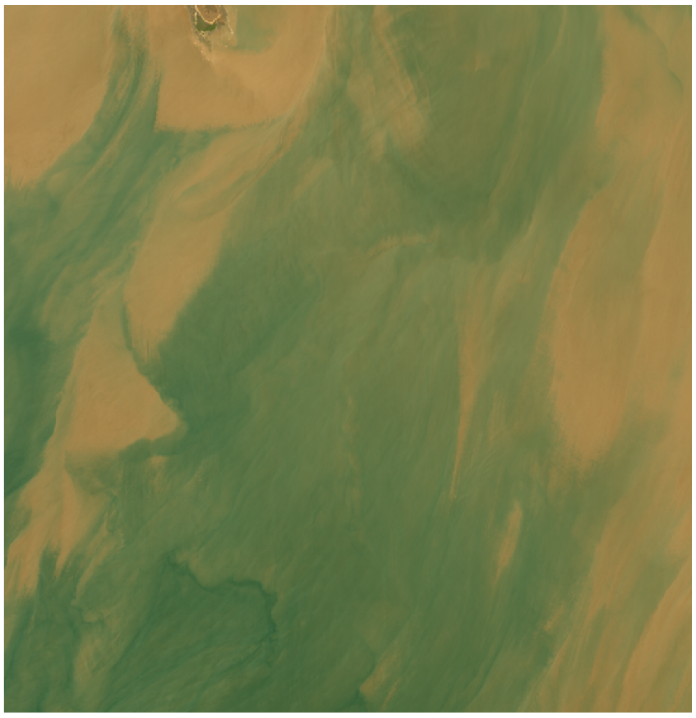

ρ_s RGB L8/OLI 2018-05-25 (05:32 UTC)

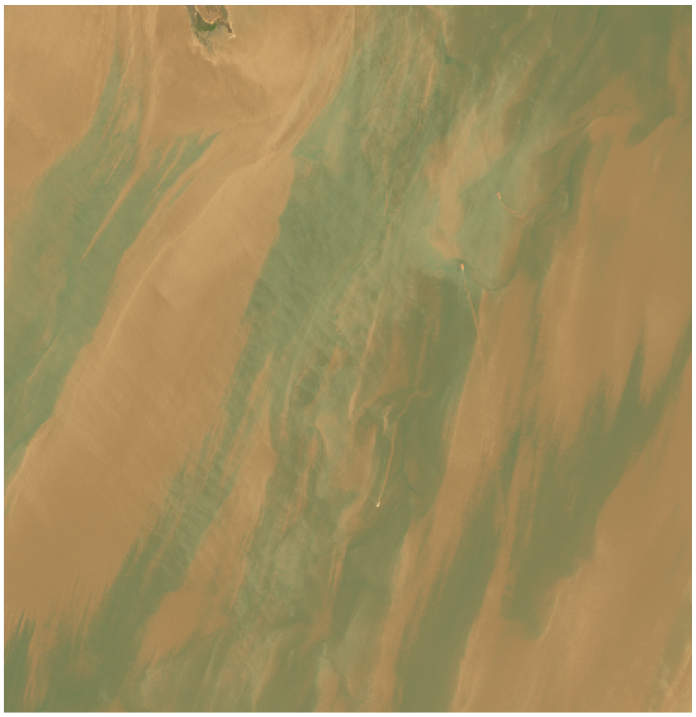

Appendix C – Tidal Graphs: HMB

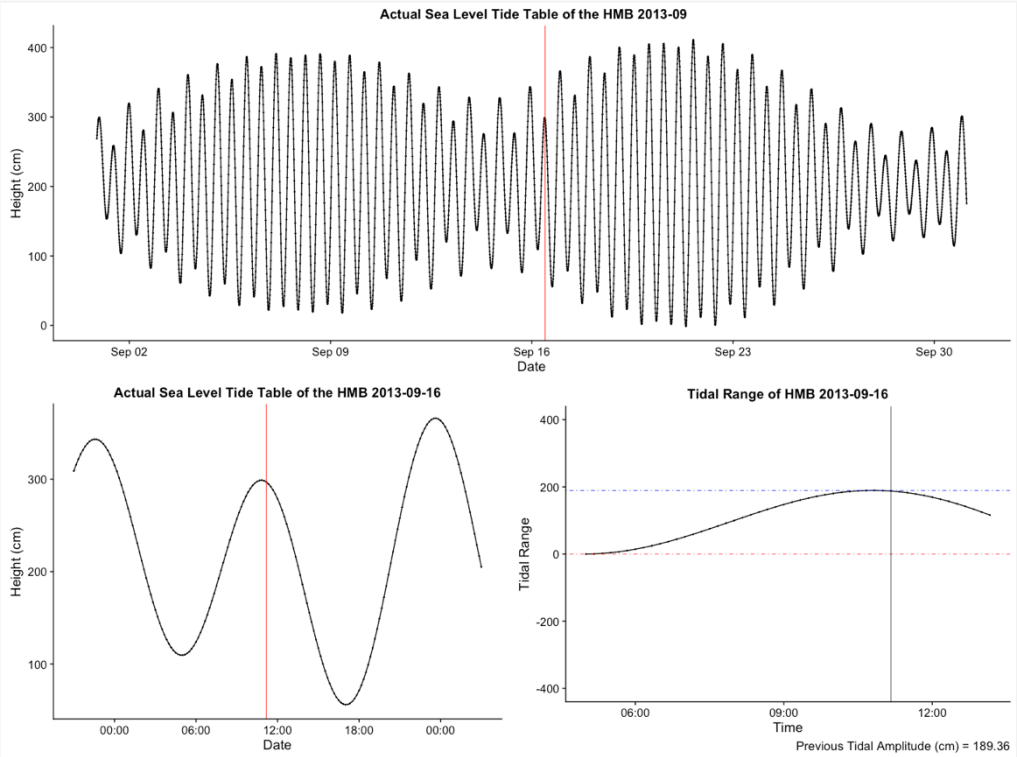

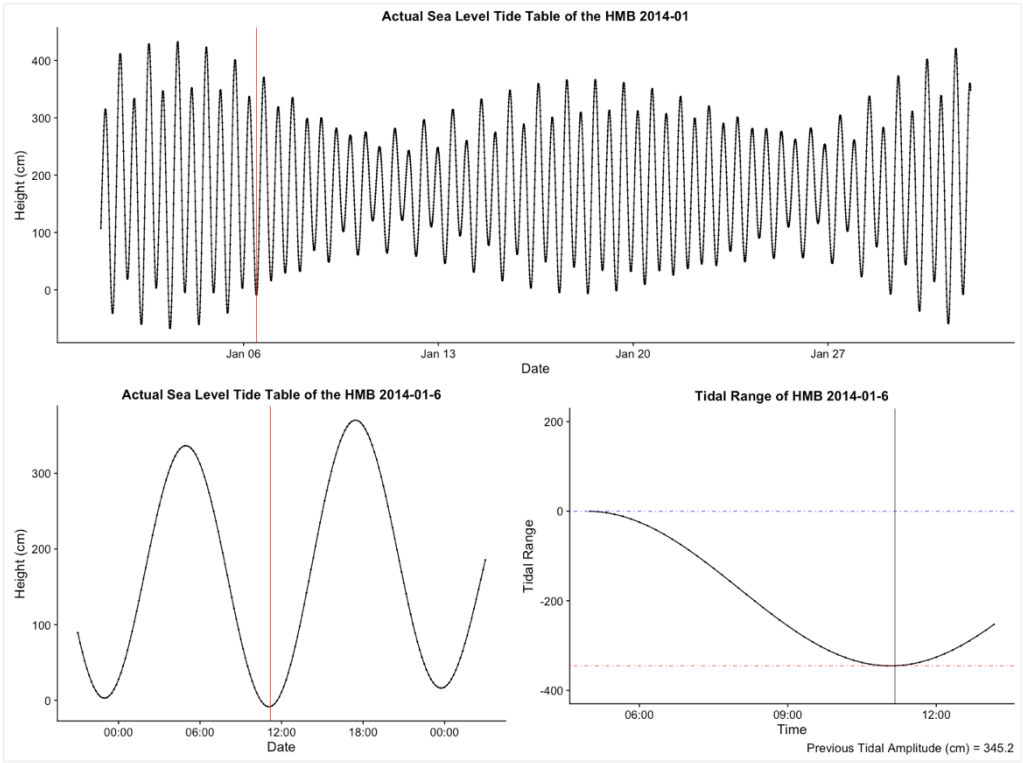
Actual Sea Level Tide Table of the HMB 2014-01
Height (cm)
400
300
200
100
0
Jan 06
Jan 13
Jan 20
Jan 27
Date
Actual Sea Level Tide Table of the HMB 2014-01-6
Height (cm)
300
200
100
0
00:00
06:00
12:00
18:00
00:00
Date
Tidal Range of HMB 2014-01-6
Tidal Range
200
0
-200
-400
06:00
09:00
12:00
Time
Previous Tidal Amplitude (cm) = 345.2

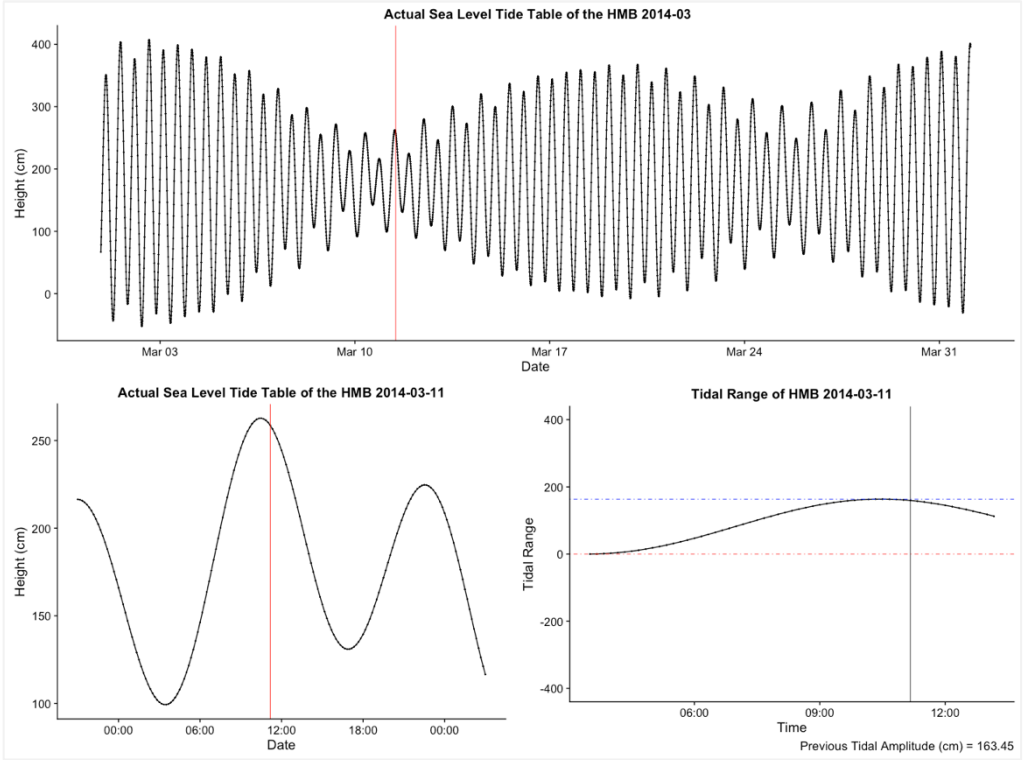
Actual Sea Level Tide Table of the HMB 2014-03
Height (cm)
400
300
200
100
0
Mar 03
Mar 10
Mar 17
Mar 24
Mar 31
Date
Actual Sea Level Tide Table of the HMB 2014-03-11
Height (cm)
250
200
150
100
00:00
06:00
12:00
18:00
00:00
Date
Tidal Range of HMB 2014-03-11
Tidal Range
400
200
0
-200
-400
06:00
09:00
12:00
Time
Previous Tidal Amplitude (cm) = 163.45

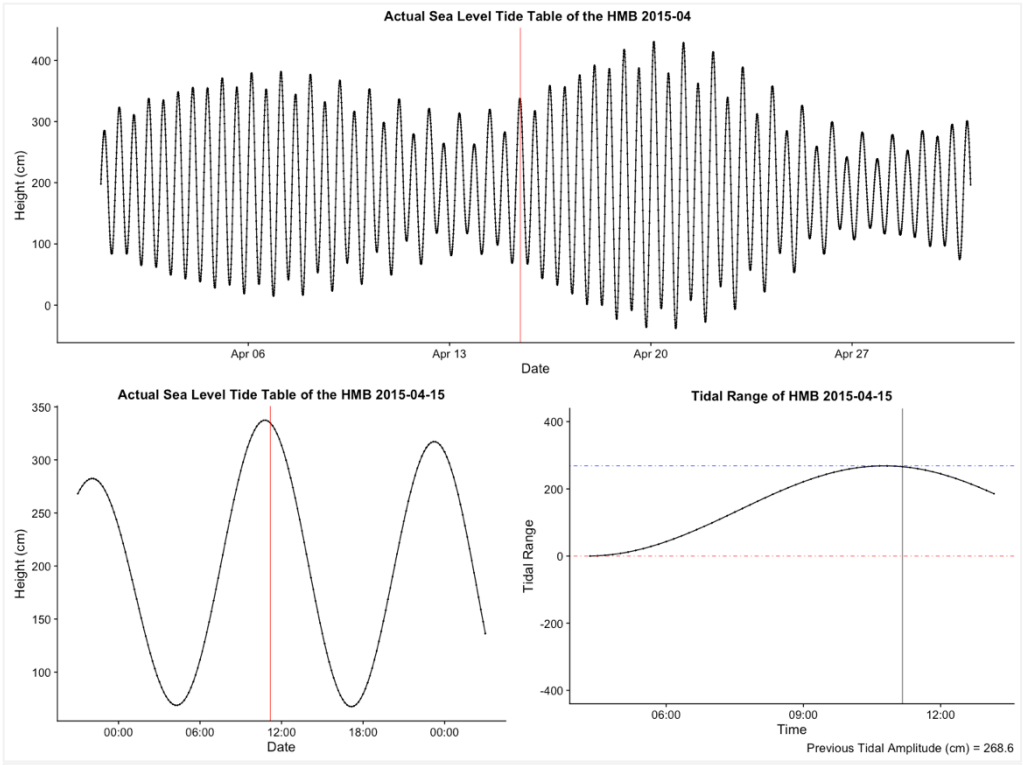
Actual Sea Level Tide Table of the HMB 2015-04
Height (cm)
Apr 06
Apr 13
Apr 20
Apr 27
Date
Actual Sea Level Tide Table of the HMB 2015-04-15
Height (cm)
00:00
06:00
12:00
18:00
00:00
Date
Tidal Range of HMB 2015-04-15
Tidal Range
06:00
09:00
12:00
Time
Previous Tidal Amplitude (cm) = 268.6

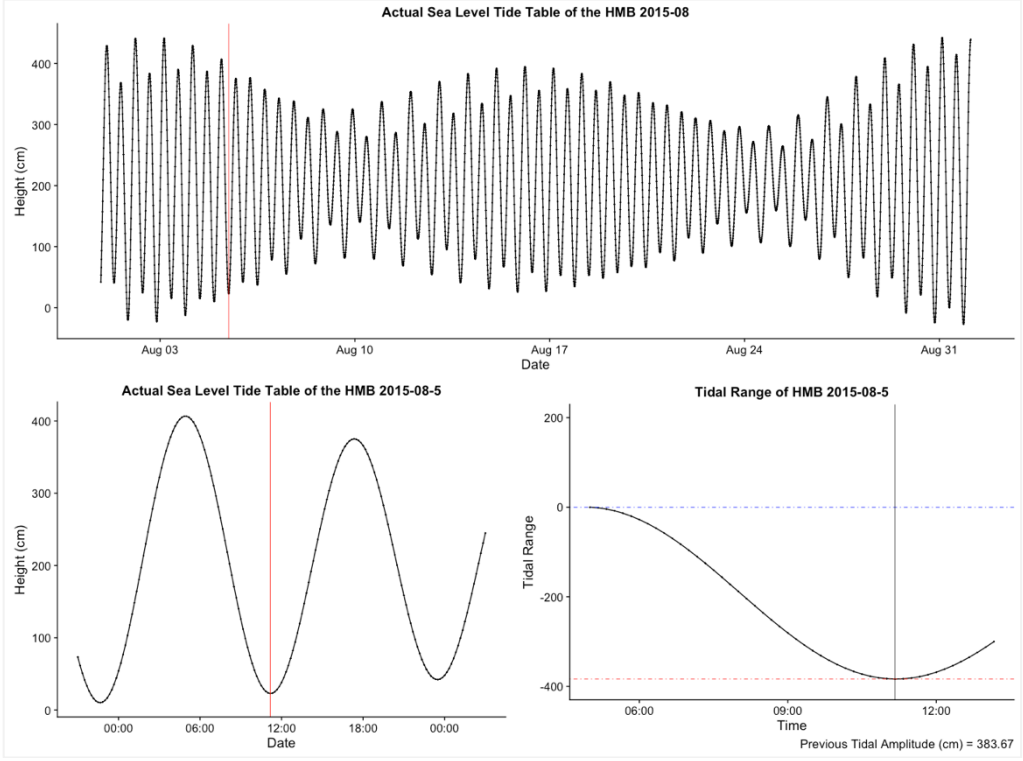
Actual Sea Level Tide Table of the HMB 2015-08
Height (cm)
Aug 03
Aug 10
Aug 17
Aug 24
Aug 31
Date
Actual Sea Level Tide Table of the HMB 2015-08-5
Height (cm)
00:00
06:00
12:00
18:00
00:00
Date
Tidal Range of HMB 2015-08-5
Tidal Range
06:00
09:00
12:00
Time
Previous Tidal Amplitude (cm) = 383.67

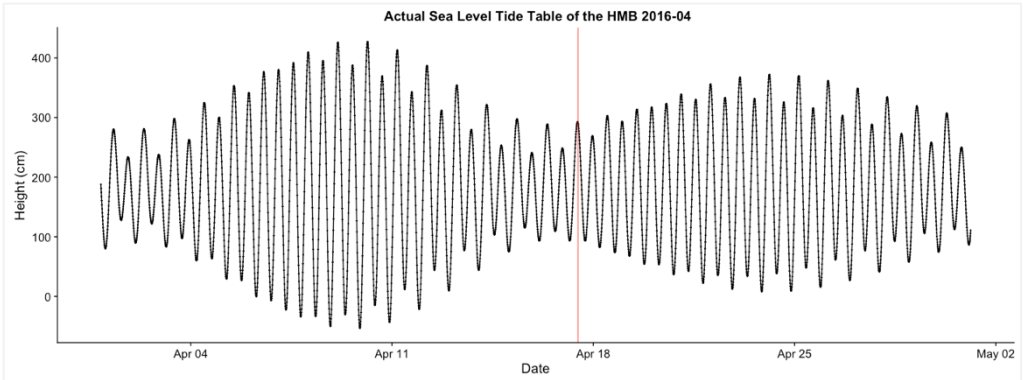

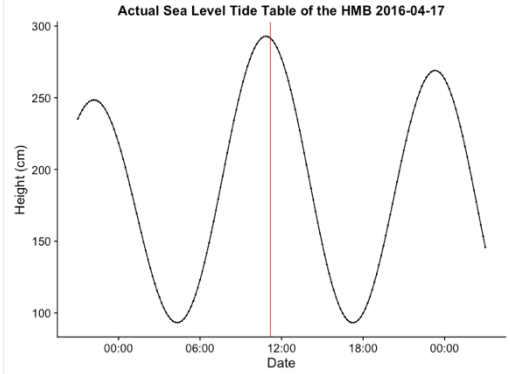

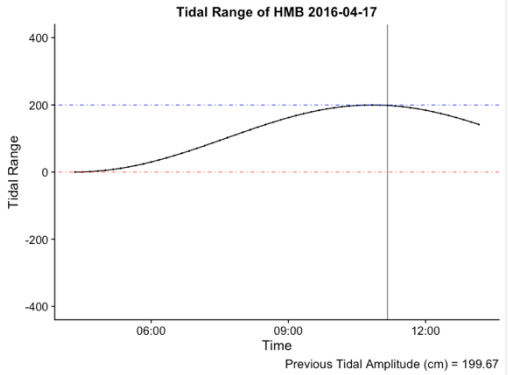

Previous Tidal Amplitude (cm) = 199.67

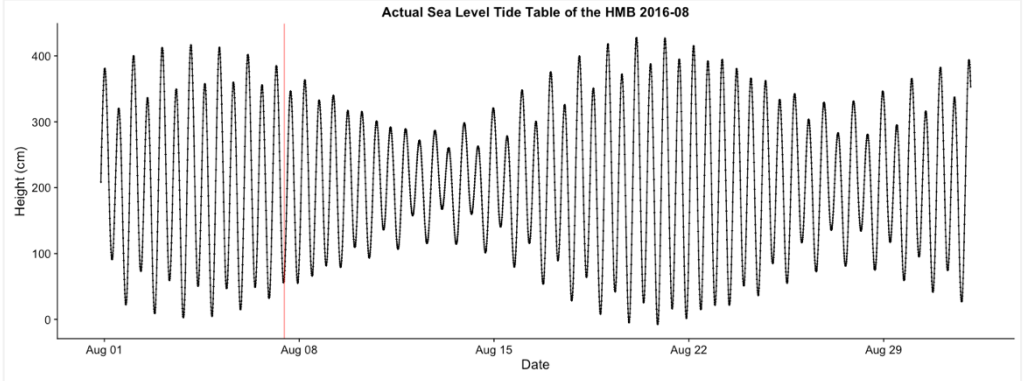

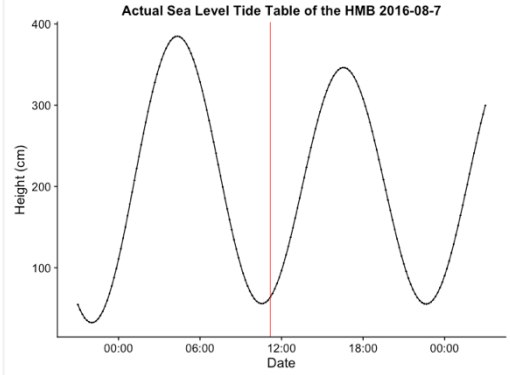

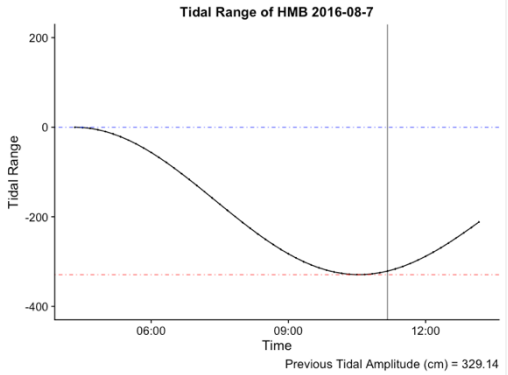

Previous Tidal Amplitude (cm) = 329.14

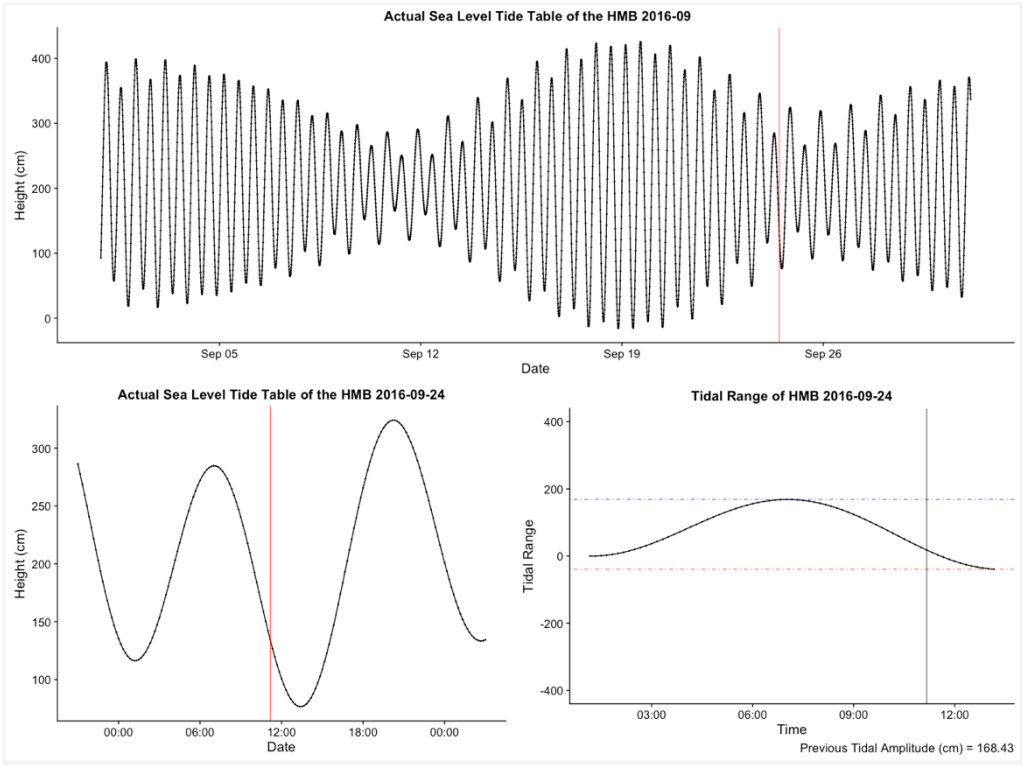
Actual Sea Level Tide Table of the HMB 2016-09
Height (cm)
400
300
200
100
0
Sep 05
Sep 12
Sep 19
Sep 26
Date
Actual Sea Level Tide Table of the HMB 2016-09-24
Height (cm)
300
250
200
150
100
00:00
06:00
12:00
18:00
00:00
Date
Tidal Range of HMB 2016-09-24
Tidal Range
400
200
0
-200
-400
03:00
06:00
09:00
12:00
Time
Previous Tidal Amplitude (cm) = 168.43

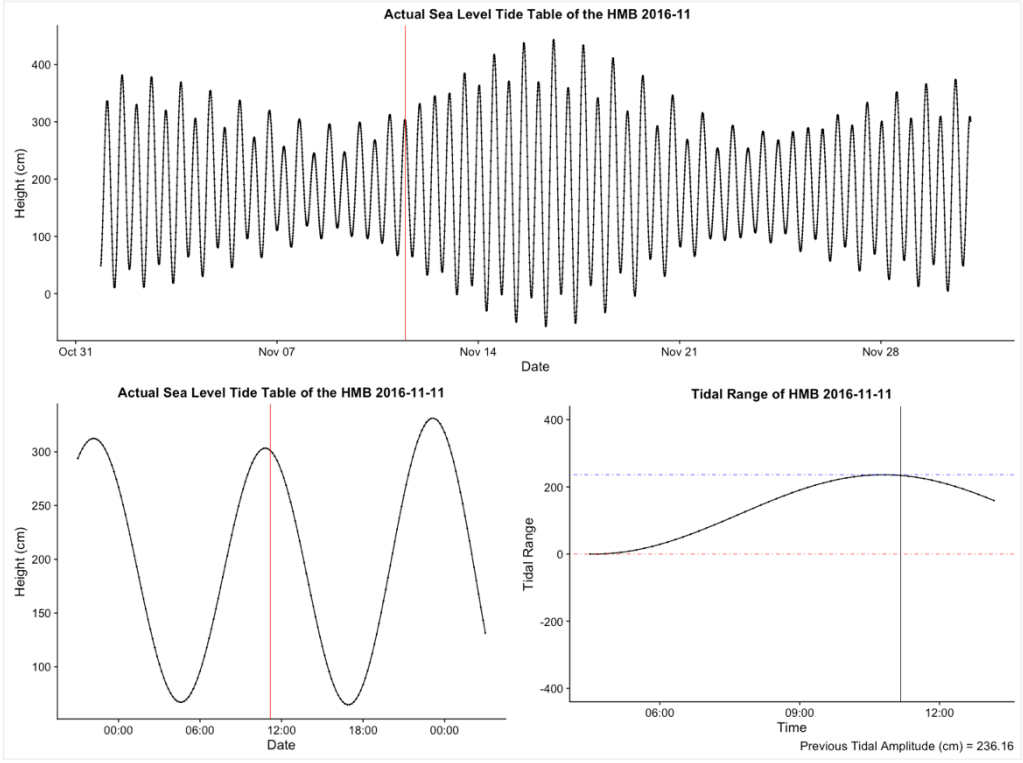
Actual Sea Level Tide Table of the HMB 2016-11
Height (cm)
400
300
200
100
0
Oct 31
Nov 07
Nov 14
Nov 21
Nov 28
Date
Actual Sea Level Tide Table of the HMB 2016-11-11
Height (cm)
300
250
200
150
100
00:00
06:00
12:00
18:00
00:00
Date
Tidal Range of HMB 2016-11-11
Tidal Range
400
200
0
-200
-400
06:00
09:00
12:00
Time
Previous Tidal Amplitude (cm) = 236.16

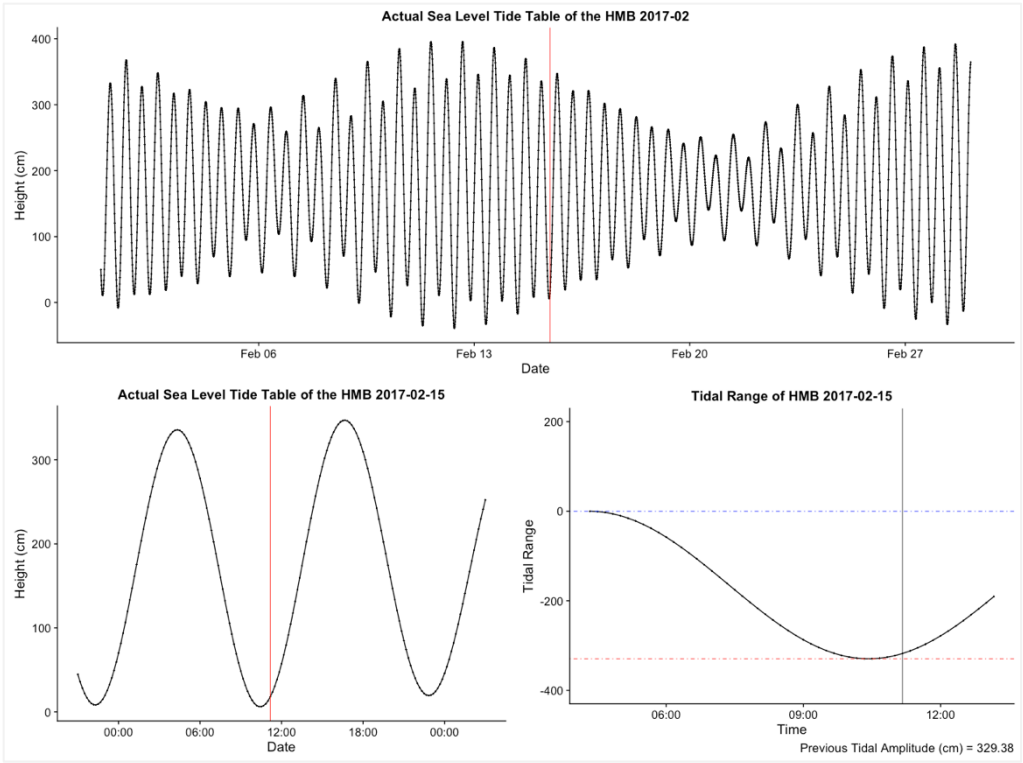
Actual Sea Level Tide Table of the HMB 2017-02
Height (cm)
400
300
200
100
0
Feb 06
Feb 13
Feb 20
Feb 27
Date
Actual Sea Level Tide Table of the HMB 2017-02-15
Height (cm)
300
200
100
0
00:00
06:00
12:00
18:00
00:00
Date
Tidal Range of HMB 2017-02-15
Tidal Range
200
0
-200
-400
06:00
09:00
12:00
Time
Previous Tidal Amplitude (cm) = 329.38

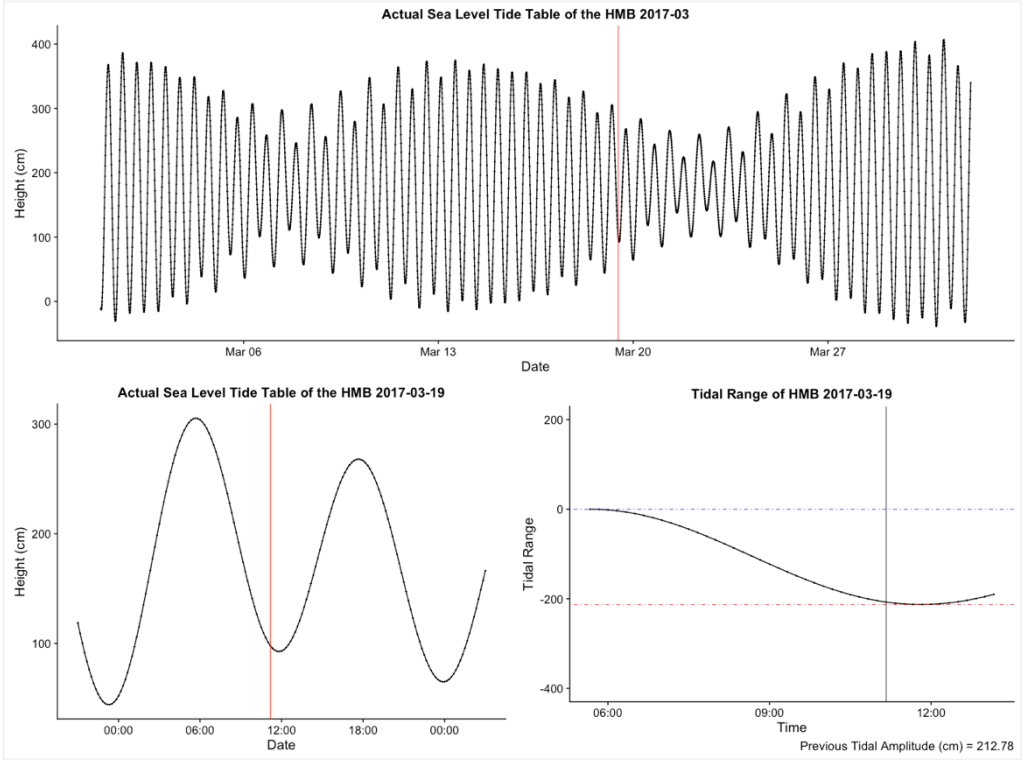
Actual Sea Level Tide Table of the HMB 2017-03
Height (cm)
400
300
200
100
0
Mar 06
Mar 13
Mar 20
Mar 27
Date
Actual Sea Level Tide Table of the HMB 2017-03-19
Height (cm)
300
200
100
00:00
06:00
12:00
18:00
00:00
Date
Tidal Range of HMB 2017-03-19
Tidal Range
200
0
-200
-400
06:00
09:00
12:00
Time
Previous Tidal Amplitude (cm) = 212.78

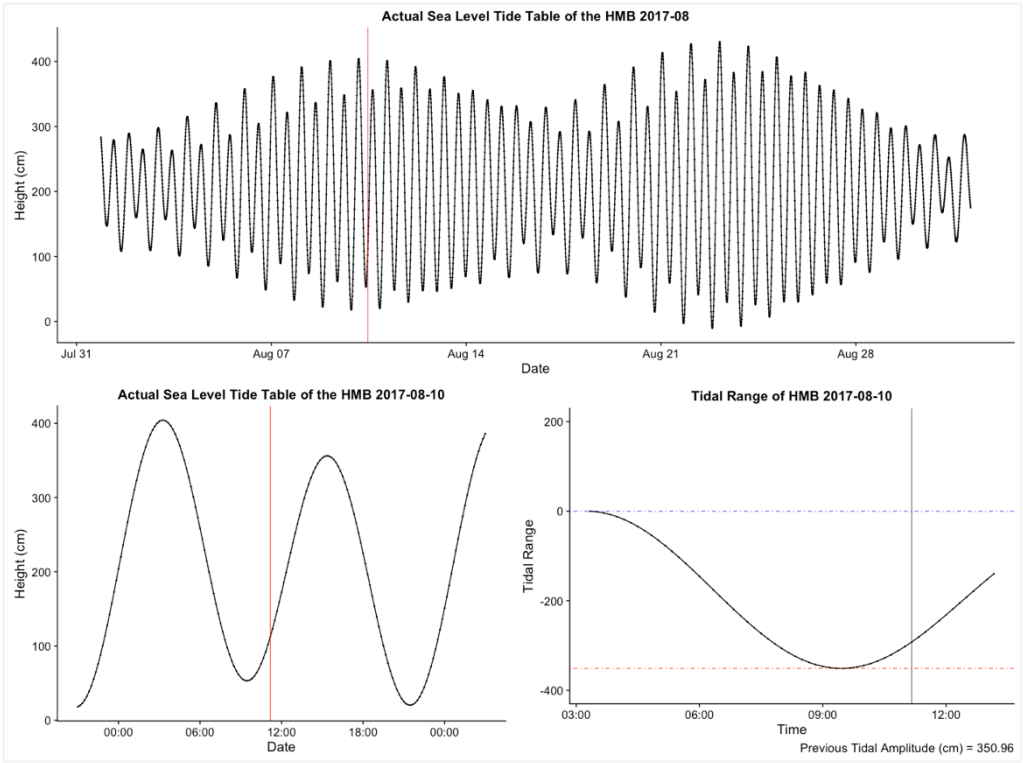
Actual Sea Level Tide Table of the HMB 2017-08
Height (cm)
Jul 31
Aug 07
Aug 14
Aug 21
Aug 28
Date
Actual Sea Level Tide Table of the HMB 2017-08-10
Height (cm)
00:00
06:00
12:00
18:00
00:00
Date
Tidal Range of HMB 2017-08-10
Tidal Range
03:00
06:00
09:00
12:00
Time
Previous Tidal Amplitude (cm) = 350.96

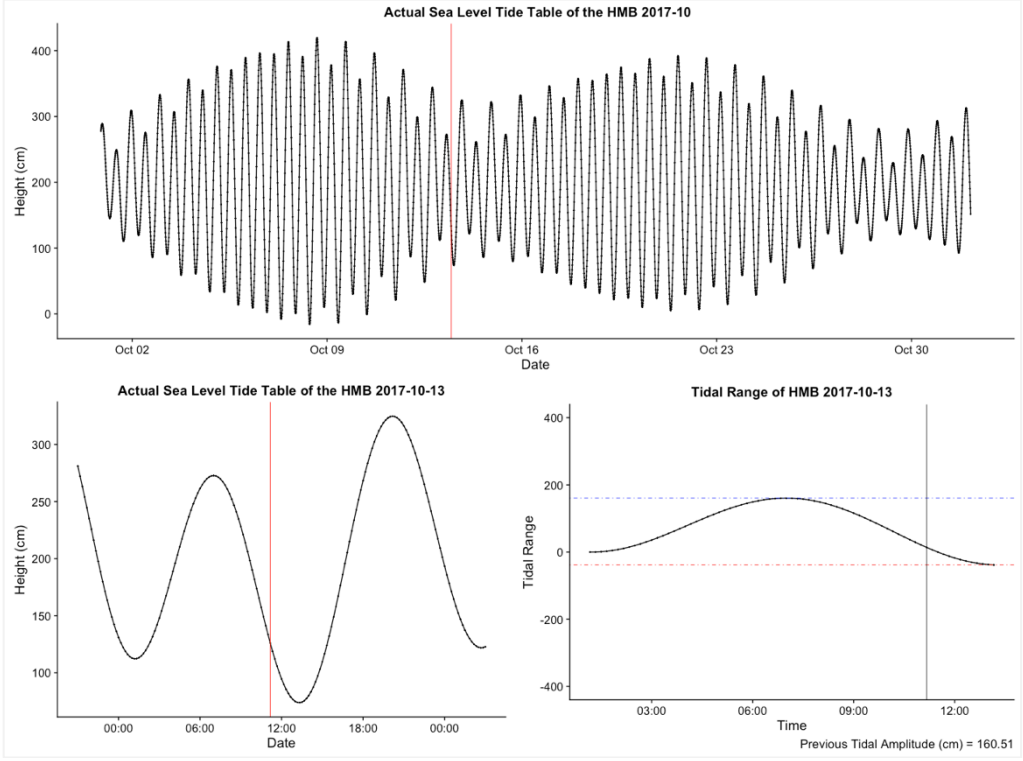
Actual Sea Level Tide Table of the HMB 2017-10
Height (cm)
Oct 02
Oct 09
Oct 16
Oct 23
Oct 30
Date
Actual Sea Level Tide Table of the HMB 2017-10-13
Height (cm)
00:00
06:00
12:00
18:00
00:00
Date
Tidal Range of HMB 2017-10-13
Tidal Range
03:00
06:00
09:00
12:00
Time
Previous Tidal Amplitude (cm) = 160.51

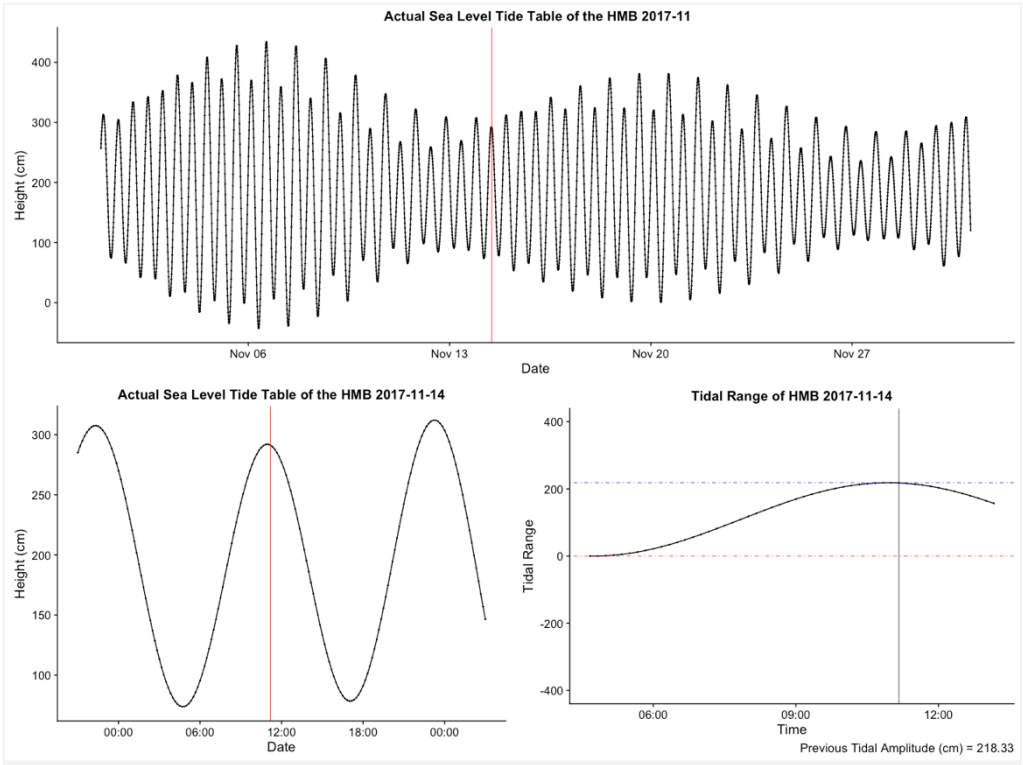
Actual Sea Level Tide Table of the HMB 2017-11
Height (cm)
400
300
200
100
0
Nov 06
Nov 13
Nov 20
Nov 27
Date
Actual Sea Level Tide Table of the HMB 2017-11-14
Height (cm)
300
250
200
150
100
00:00
06:00
12:00
18:00
00:00
Date
Tidal Range of HMB 2017-11-14
Tidal Range
400
200
0
-200
-400
06:00
09:00
12:00
Time
Previous Tidal Amplitude (cm) = 218.33

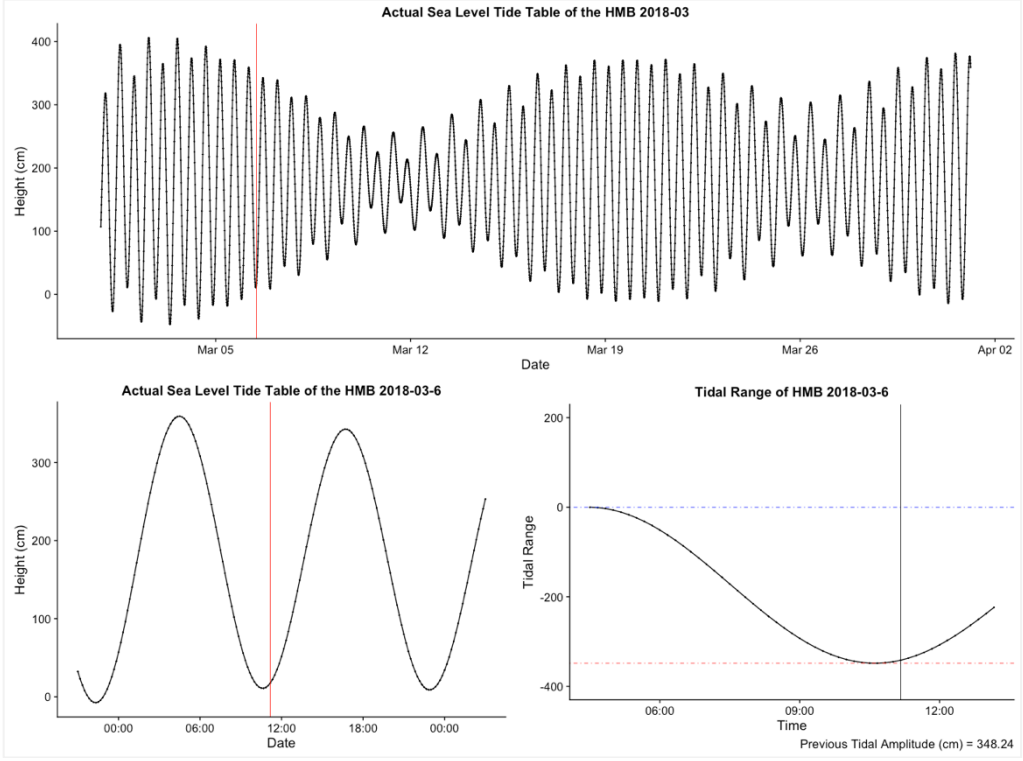
Actual Sea Level Tide Table of the HMB 2018-03
Height (cm)
400
300
200
100
0
Mar 05
Mar 12
Mar 19
Mar 26
Apr 02
Date
Actual Sea Level Tide Table of the HMB 2018-03-6
Height (cm)
300
200
100
0
00:00
06:00
12:00
18:00
00:00
Date
Tidal Range of HMB 2018-03-6
Tidal Range
200
0
-200
-400
06:00
09:00
12:00
Time
Previous Tidal Amplitude (cm) = 348.24

Tidal Graphs: GB

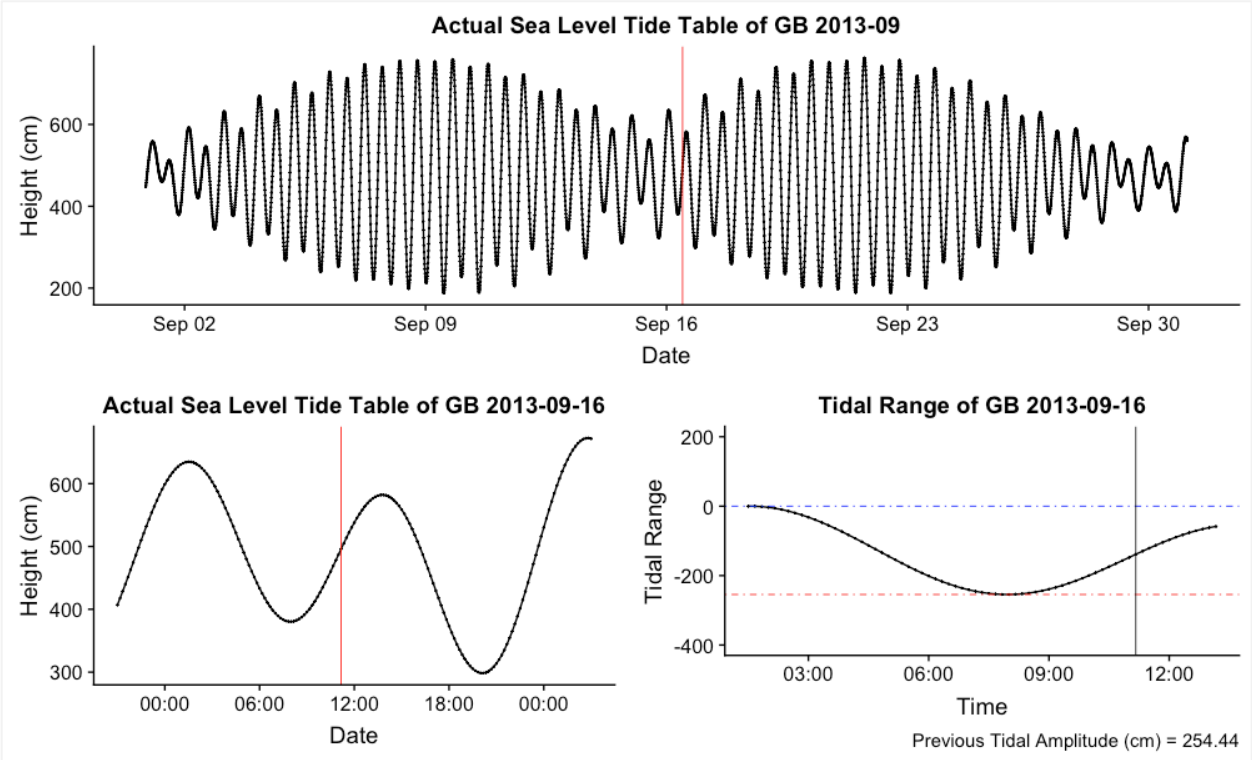

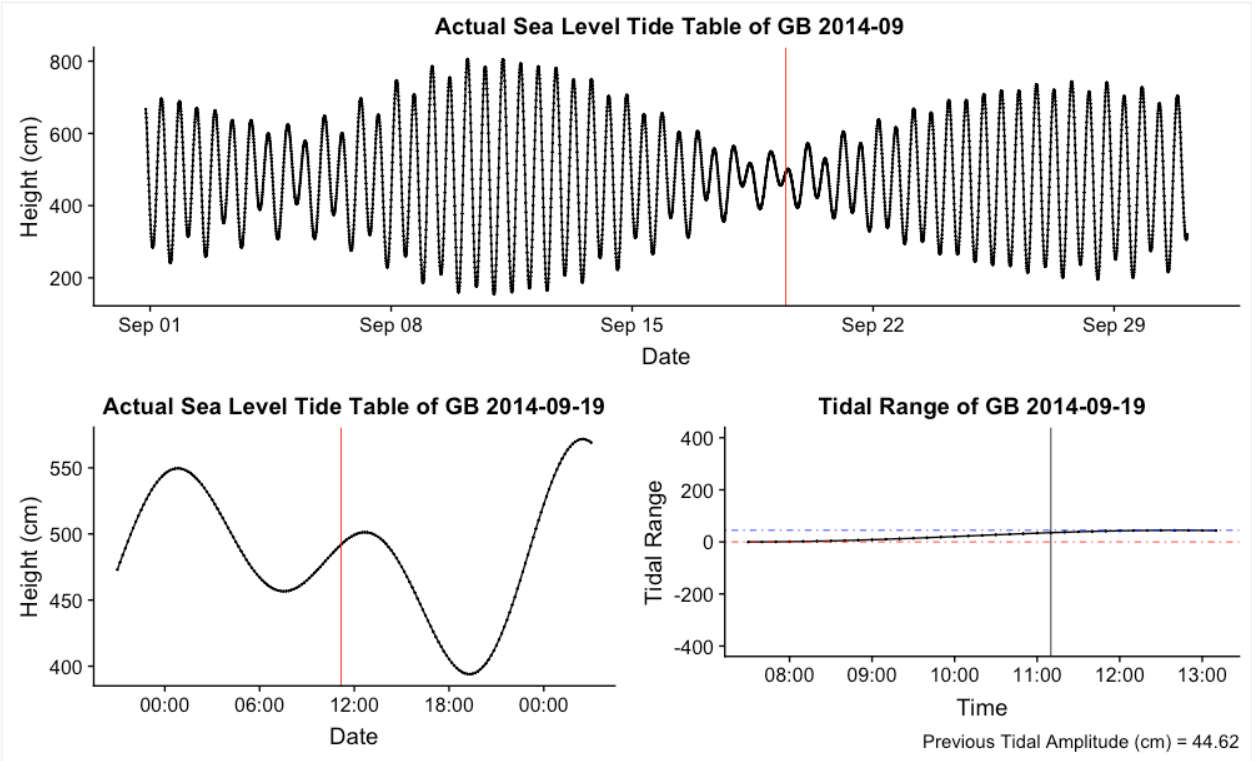

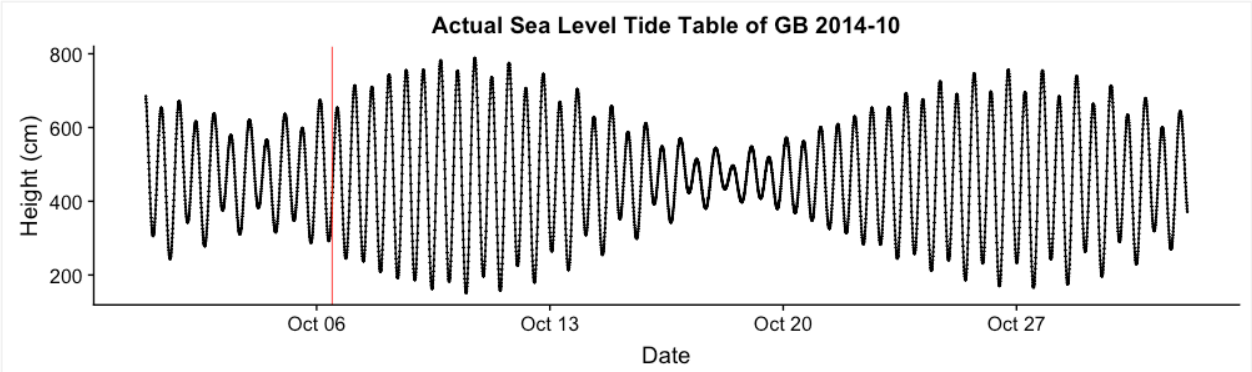

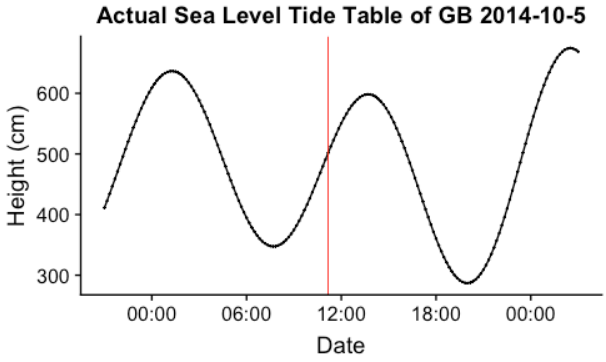

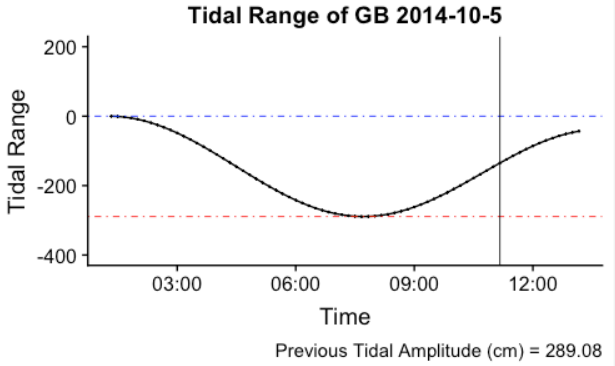

Previous Tidal Amplitude (cm) = 289.08

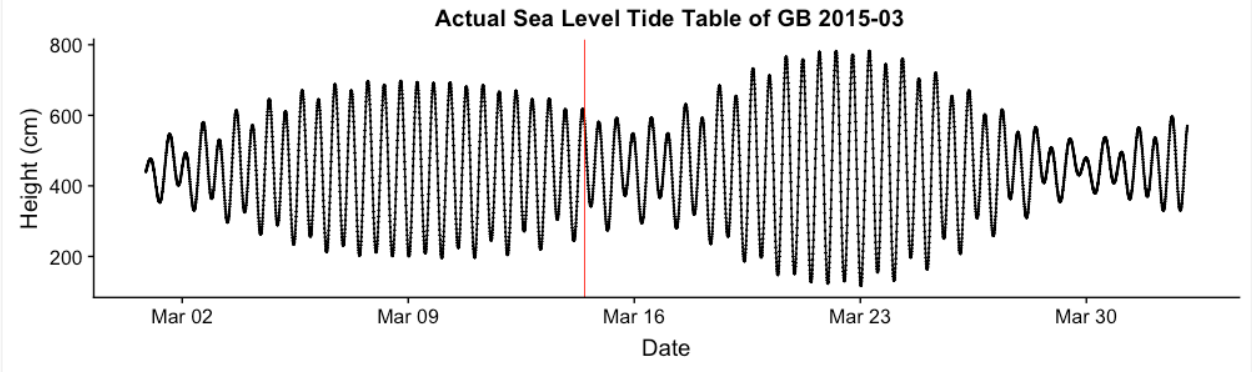

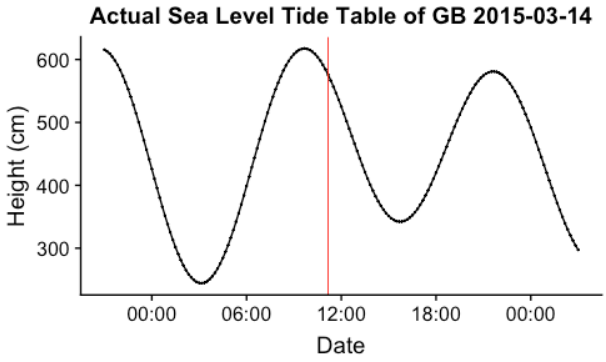

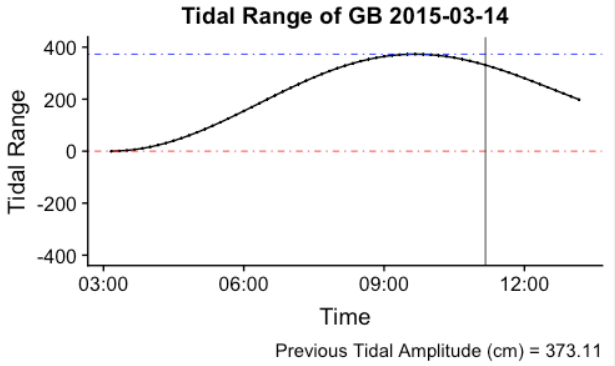

Previous Tidal Amplitude (cm) = 373.11

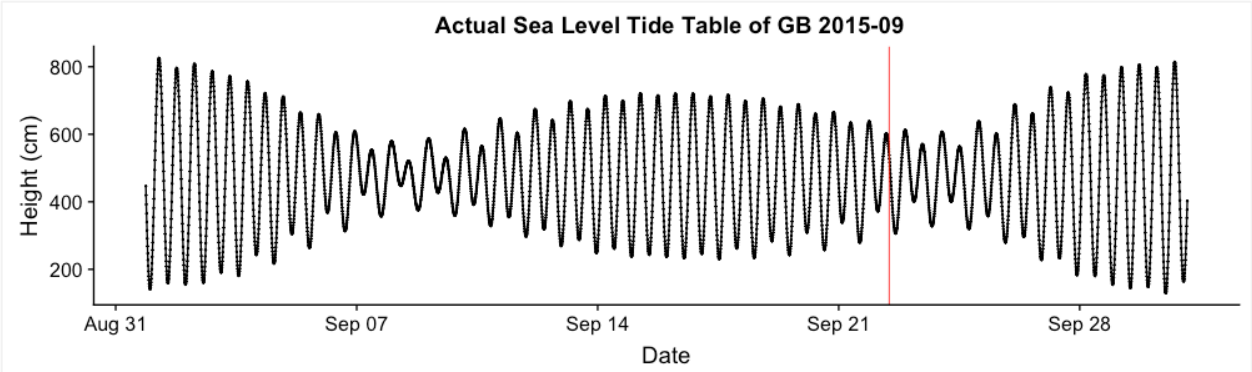

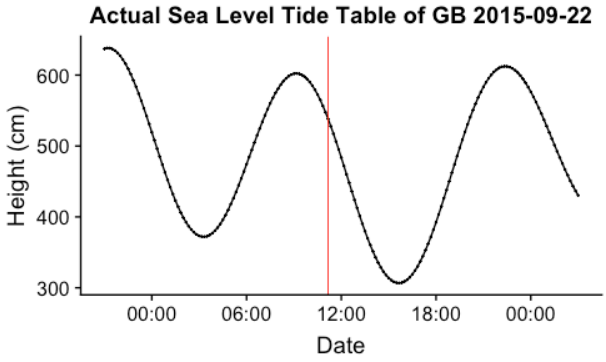

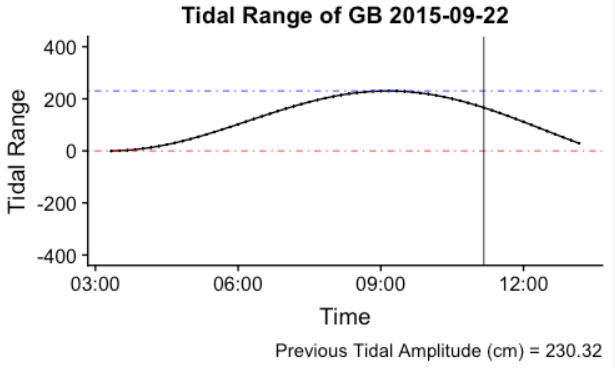

Previous Tidal Amplitude (cm) = 230.32

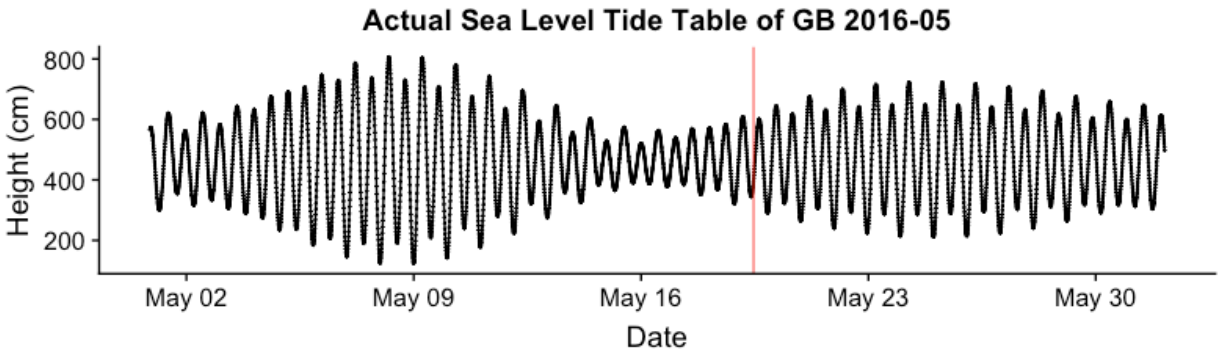

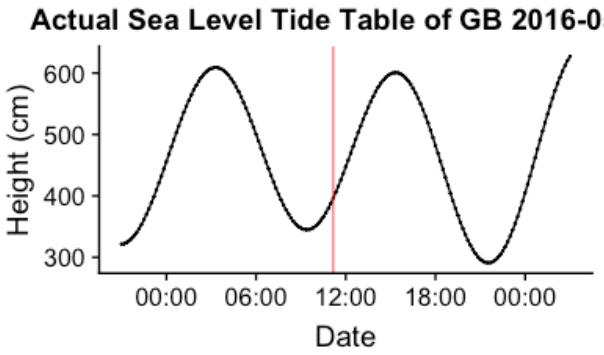

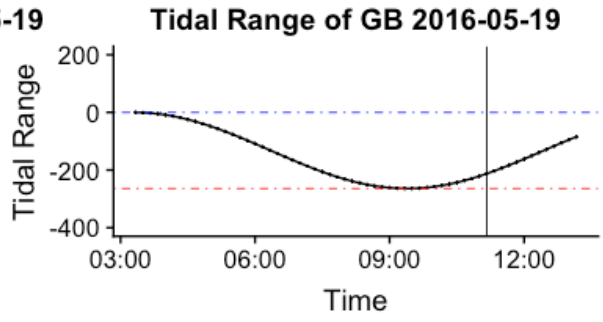

Previous Tidal Amplitude (cm) = 264.21

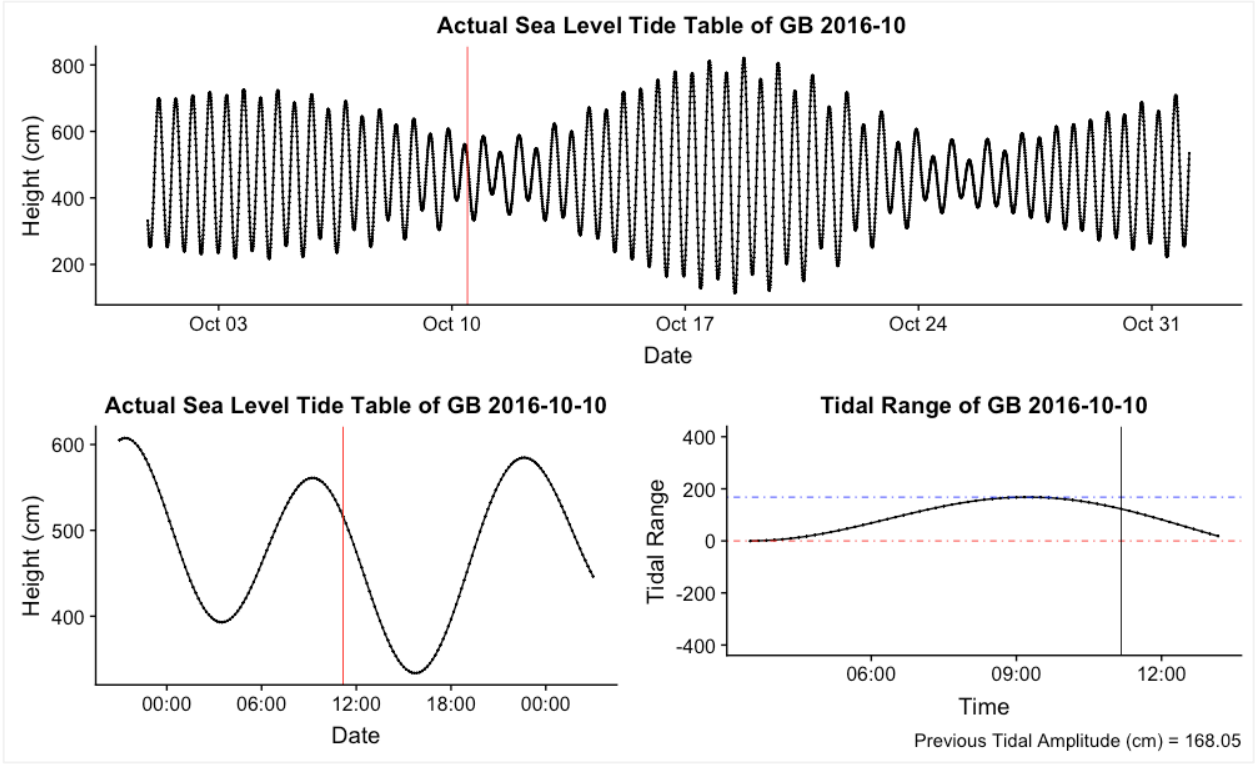
Actual Sea Level Tide Table of GB 2016-10
Height (cm)
800
600
400
200
Oct 03
Oct 10
Oct 17
Oct 24
Oct 31
Date
Actual Sea Level Tide Table of GB 2016-10-10
Height (cm)
600
500
400
00:00
06:00
12:00
18:00
00:00
Date
Tidal Range of GB 2016-10-10
Tidal Range
400
200
0
-200
-400
06:00
09:00
12:00
Time
Previous Tidal Amplitude (cm) = 168.05

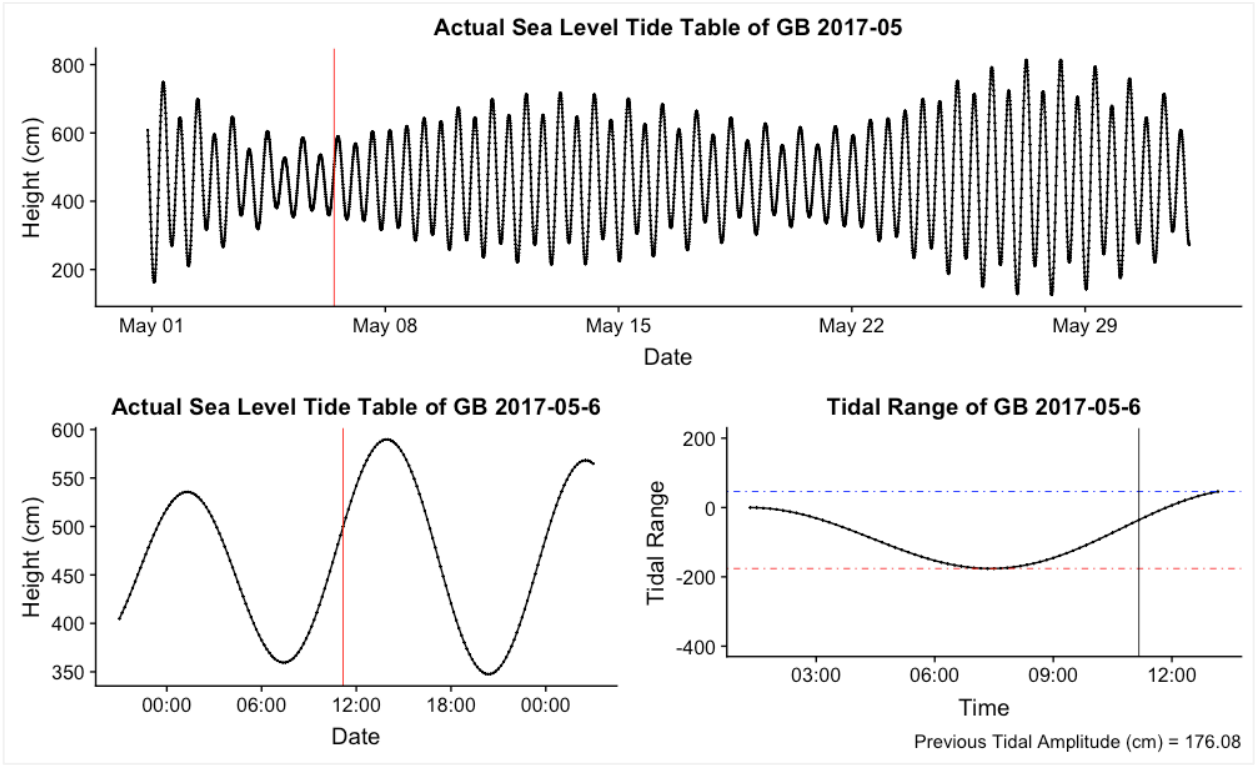
Actual Sea Level Tide Table of GB 2017-05
Height (cm)
800
600
400
200
May 01
May 08
May 15
May 22
May 29
Date
Actual Sea Level Tide Table of GB 2017-05-6
Height (cm)
600
550
500
450
400
350
00:00
06:00
12:00
18:00
00:00
Date
Tidal Range of GB 2017-05-6
Tidal Range
200
0
-200
-400
03:00
06:00
09:00
12:00
Time
Previous Tidal Amplitude (cm) = 176.08

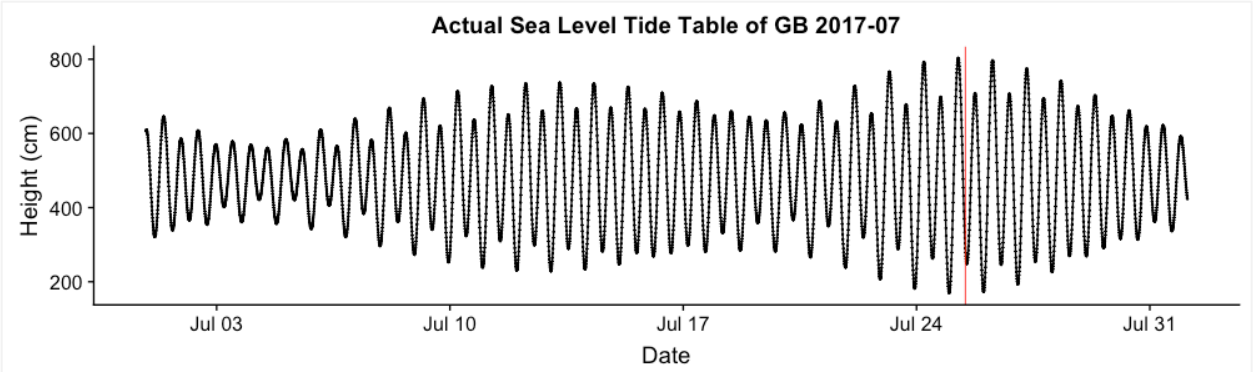
Actual Sea Level Tide Table of GB 2017-07
Height (cm)
800
600
400
200
Jul 03
Jul 10
Jul 17
Jul 24
Jul 31
Date

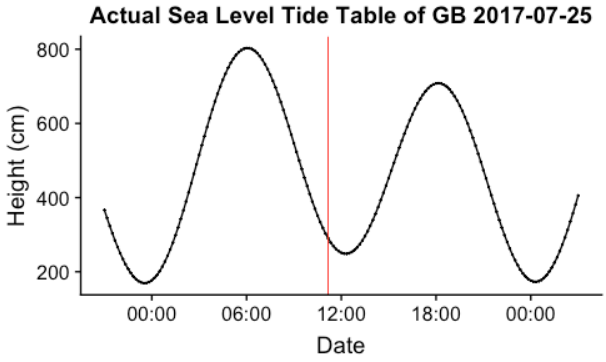
Actual Sea Level Tide Table of GB 2017-07-25
Height (cm)
800
600
400
200
00:00
06:00
12:00
18:00
00:00
Date

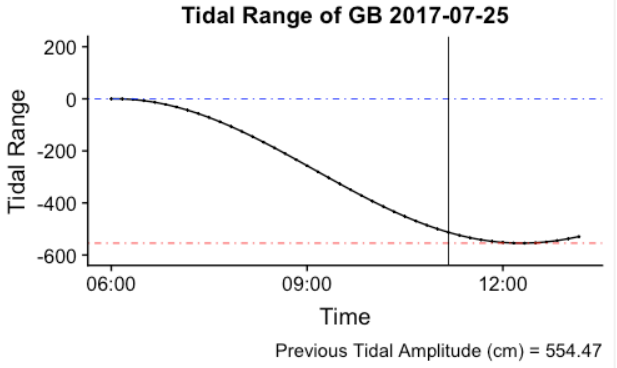
Tidal Range of GB 2017-07-25
Tidal Range
200
0
-200
-400
-600
06:00
09:00
12:00
Time
Previous Tidal Amplitude (cm) = 554.47

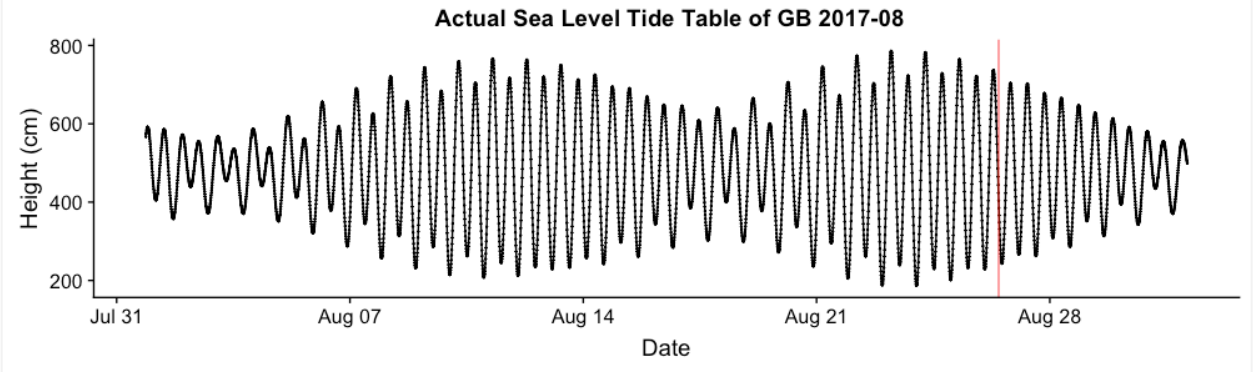
Actual Sea Level Tide Table of GB 2017-08
Height (cm)
800
600
400
200
Jul 31
Aug 07
Aug 14
Aug 21
Aug 28
Date

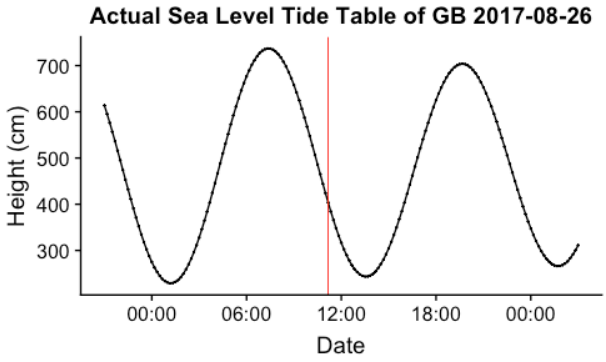
Actual Sea Level Tide Table of GB 2017-08-26
Height (cm)
700
600
500
400
300
00:00
06:00
12:00
18:00
00:00
Date

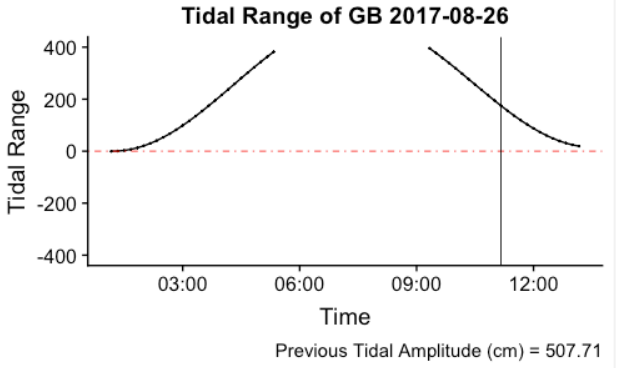
Tidal Range of GB 2017-08-26
Tidal Range
400
200
0
-200
-400
03:00
06:00
09:00
12:00
Time
Previous Tidal Amplitude (cm) = 507.71

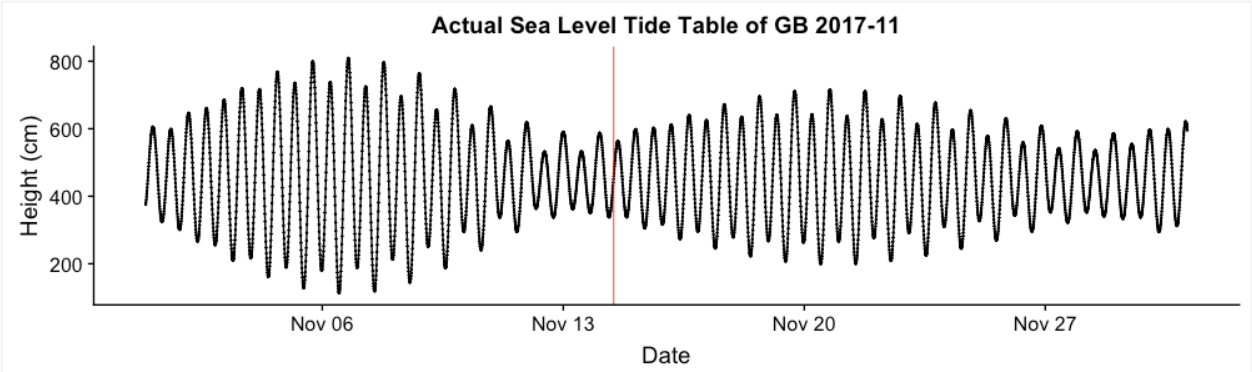

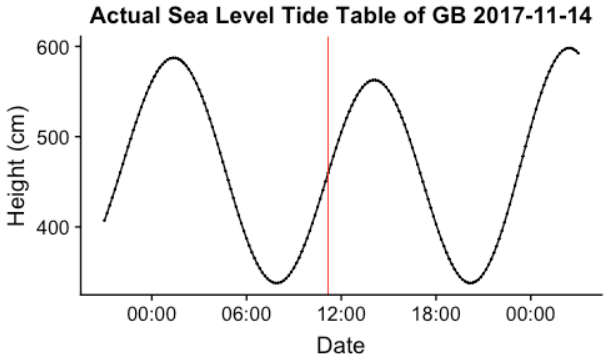

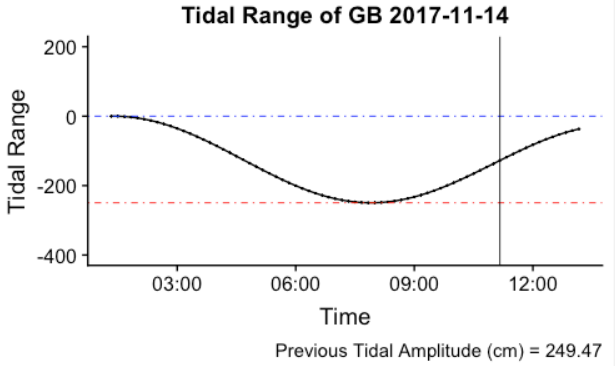

Previous Tidal Amplitude (cm) = 249.47

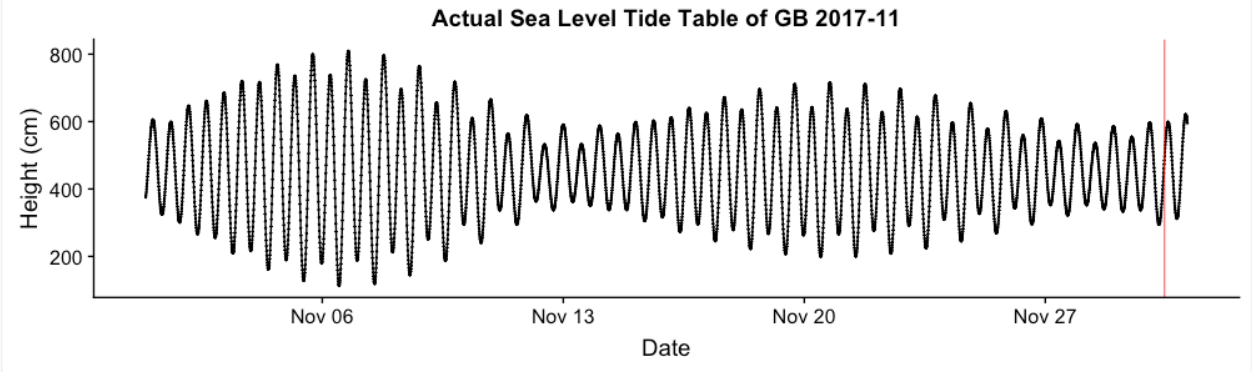

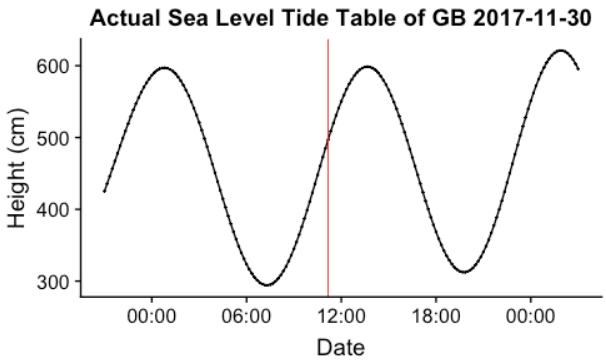

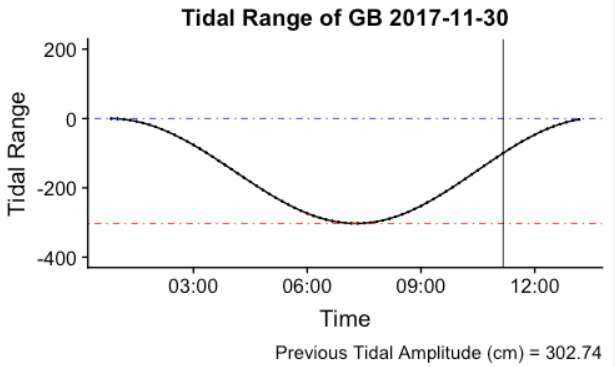

Previous Tidal Amplitude (cm) = 302.74

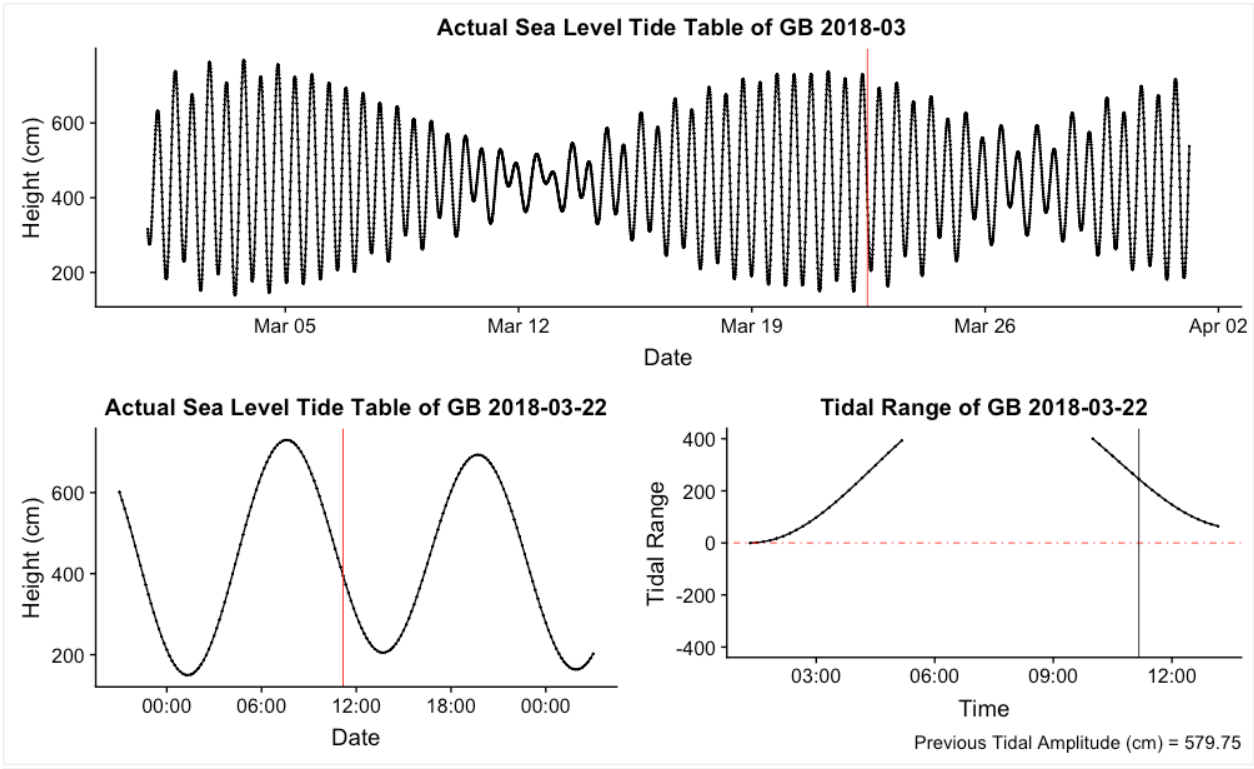
Actual Sea Level Tide Table of GB 2018-03
Height (cm)
600
400
200
Mar 05
Mar 12
Mar 19
Mar 26
Apr 02
Date
Actual Sea Level Tide Table of GB 2018-03-22
Height (cm)
600
400
200
00:00
06:00
12:00
18:00
00:00
Date
Tidal Range of GB 2018-03-22
Tidal Range
400
200
0
-200
-400
03:00
06:00
09:00
12:00
Time
Previous Tidal Amplitude (cm) = 579.75

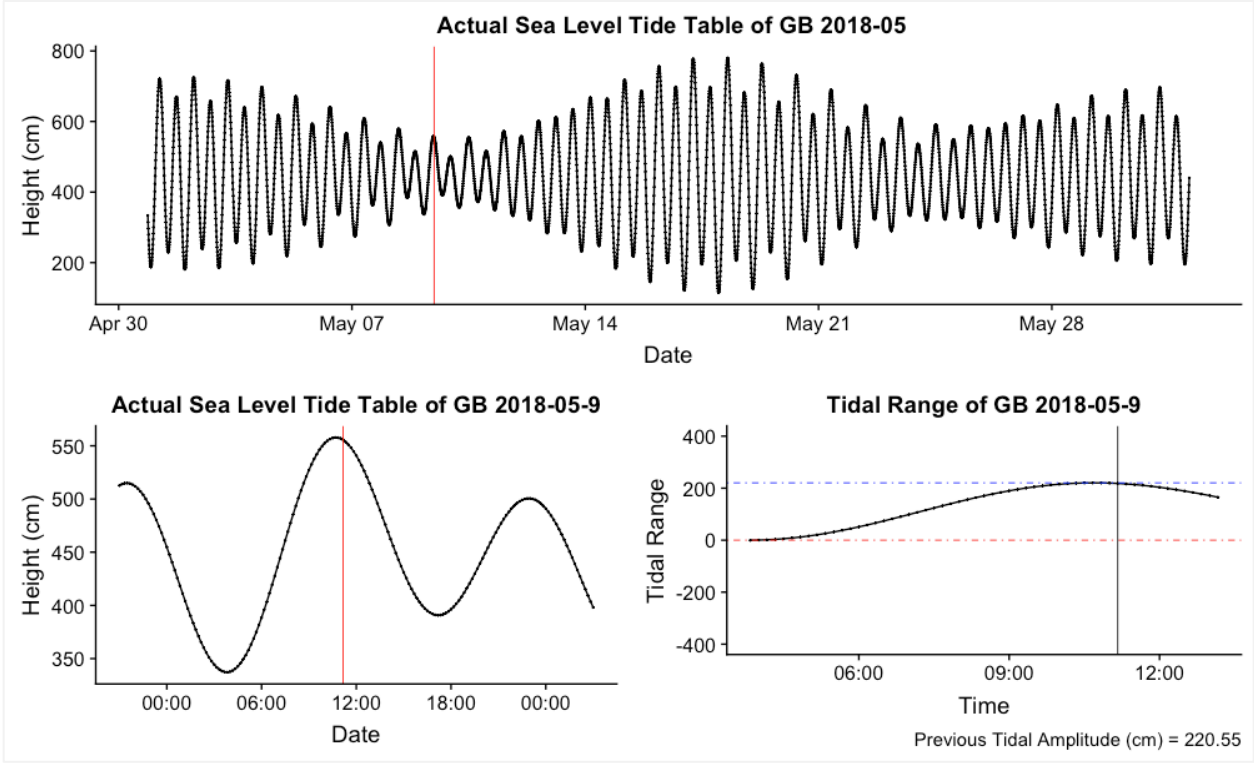
Actual Sea Level Tide Table of GB 2018-05
Height (cm)
800
600
400
200
Apr 30
May 07
May 14
May 21
May 28
Date
Actual Sea Level Tide Table of GB 2018-05-9
Height (cm)
550
500
450
400
350
00:00
06:00
12:00
18:00
00:00
Date
Tidal Range of GB 2018-05-9
Tidal Range
400
200
0
-200
-400
06:00
09:00
12:00
Time
Previous Tidal Amplitude (cm) = 220.55

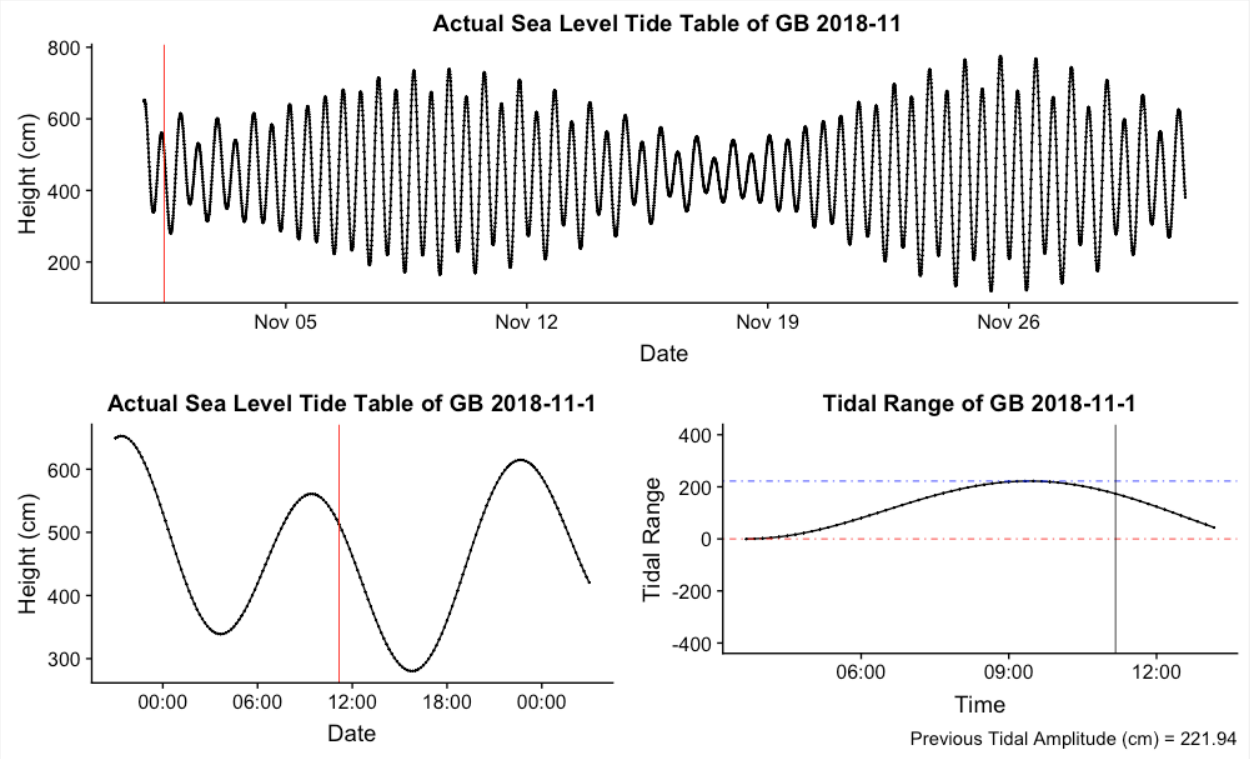
Actual Sea Level Tide Table of GB 2018-11
Height (cm)
800
600
400
200
Nov 05
Nov 12
Nov 19
Nov 26
Date
Actual Sea Level Tide Table of GB 2018-11-1
Height (cm)
600
500
400
300
00:00
06:00
12:00
18:00
00:00
Date
Tidal Range of GB 2018-11-1
Tidal Range
400
200
0
-200
-400
06:00
09:00
12:00
Time
Previous Tidal Amplitude (cm) = 221.94

Tidal Graphs: GOK

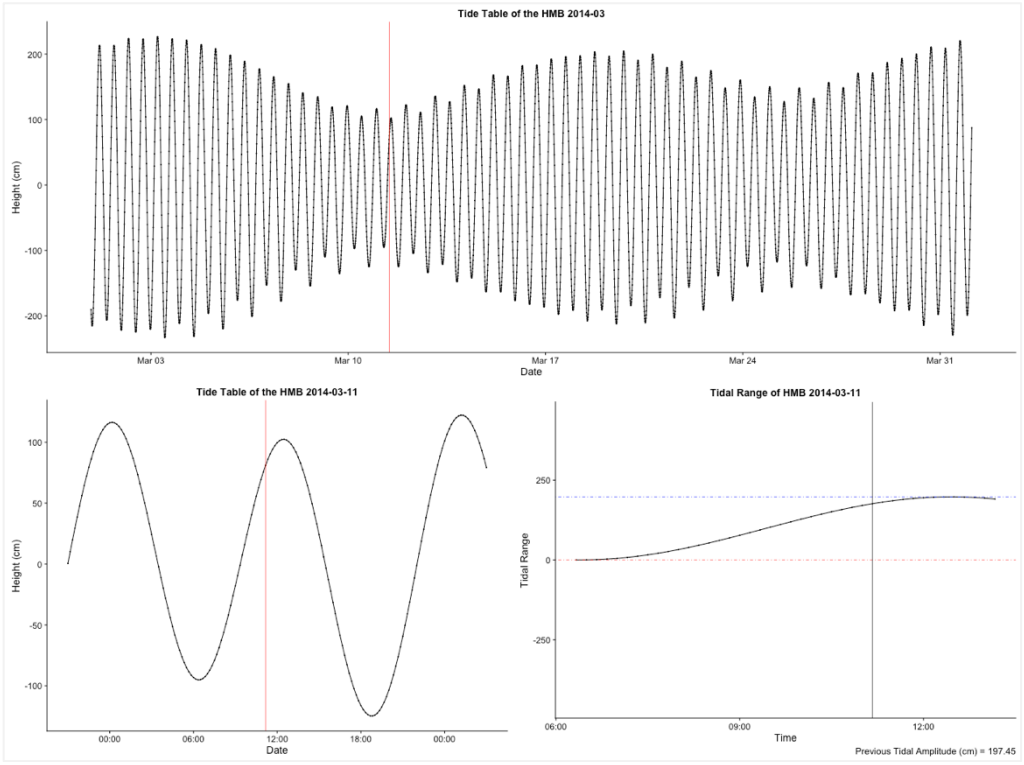

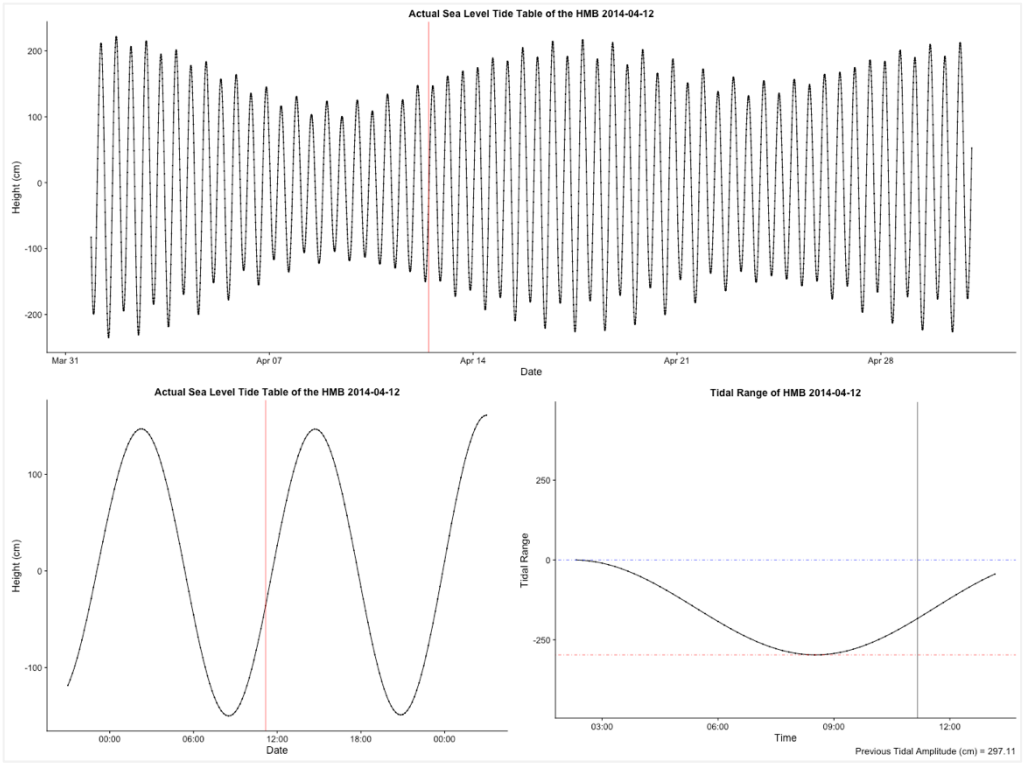
Actual Sea Level Tide Table of the HMB 2014-04-12
Height (cm)
200
100
0
-100
-200
Mar 31
Apr 07
Apr 14
Apr 21
Apr 28
Date
Actual Sea Level Tide Table of the HMB 2014-04-12
Height (cm)
100
0
-100
00:00
06:00
12:00
18:00
00:00
Date
Tidal Range of HMB 2014-04-12
Tidal Range
250
0
-250
03:00
06:00
09:00
12:00
Time
Previous Tidal Amplitude (cm) = 297.11

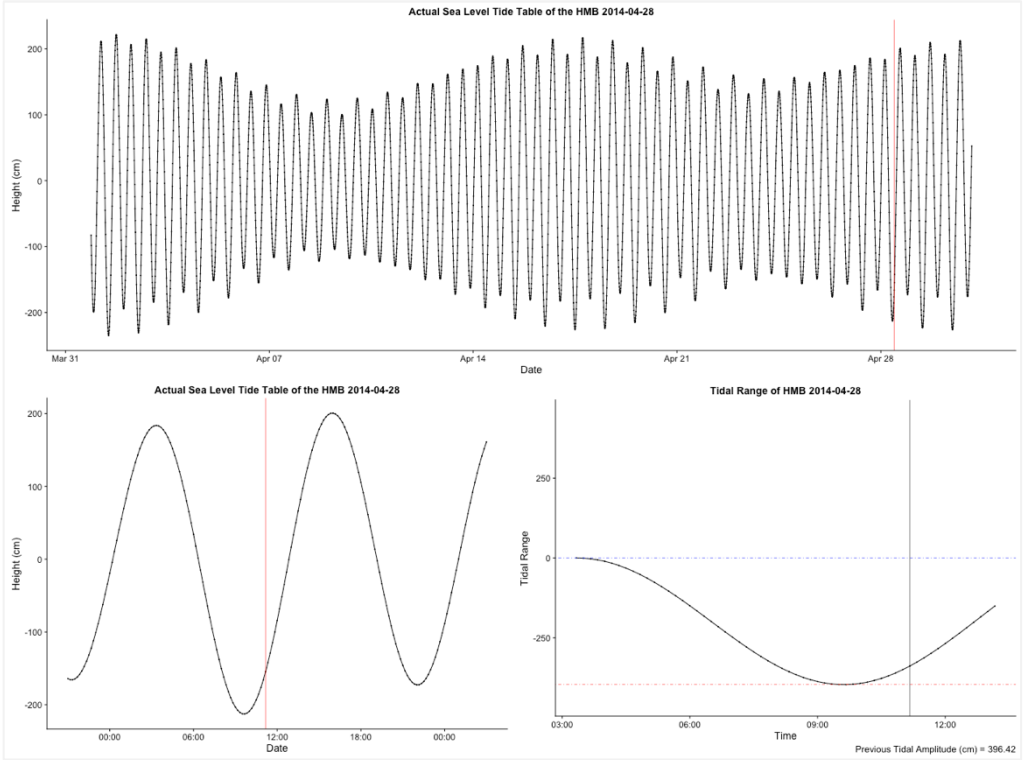
Actual Sea Level Tide Table of the HMB 2014-04-28
Height (cm)
200
100
0
-100
-200
Mar 31
Apr 07
Apr 14
Apr 21
Apr 28
Date
Actual Sea Level Tide Table of the HMB 2014-04-28
Height (cm)
200
100
0
-100
-200
00:00
06:00
12:00
18:00
00:00
Date
Tidal Range of HMB 2014-04-28
Tidal Range
250
0
-250
03:00
06:00
09:00
12:00
Time
Previous Tidal Amplitude (cm) = 396.42

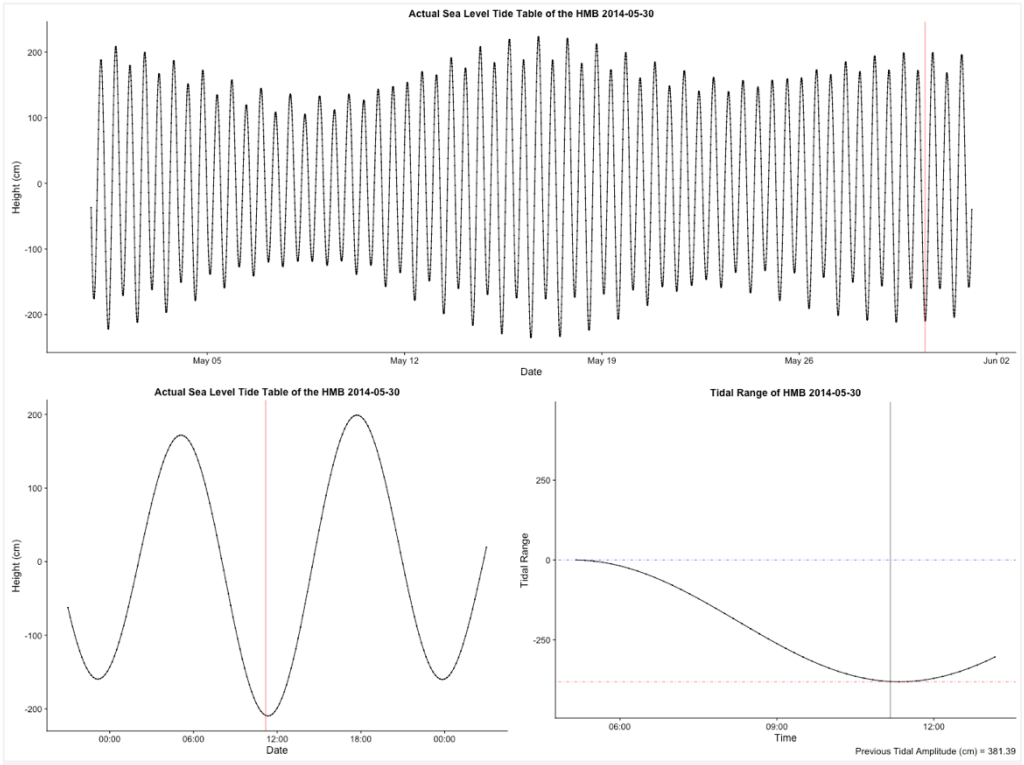
Actual Sea Level Tide Table of the HMB 2014-05-30
Height (cm)
200
100
0
-100
-200
May 05
May 12
May 19
May 26
Jun 02
Date
Actual Sea Level Tide Table of the HMB 2014-05-30
Height (cm)
200
100
0
-100
-200
00:00
06:00
12:00
18:00
00:00
Date
Tidal Range of HMB 2014-05-30
Tidal Range
250
0
-250
06:00
09:00
12:00
Time
Previous Tidal Amplitude (cm) = 381.39

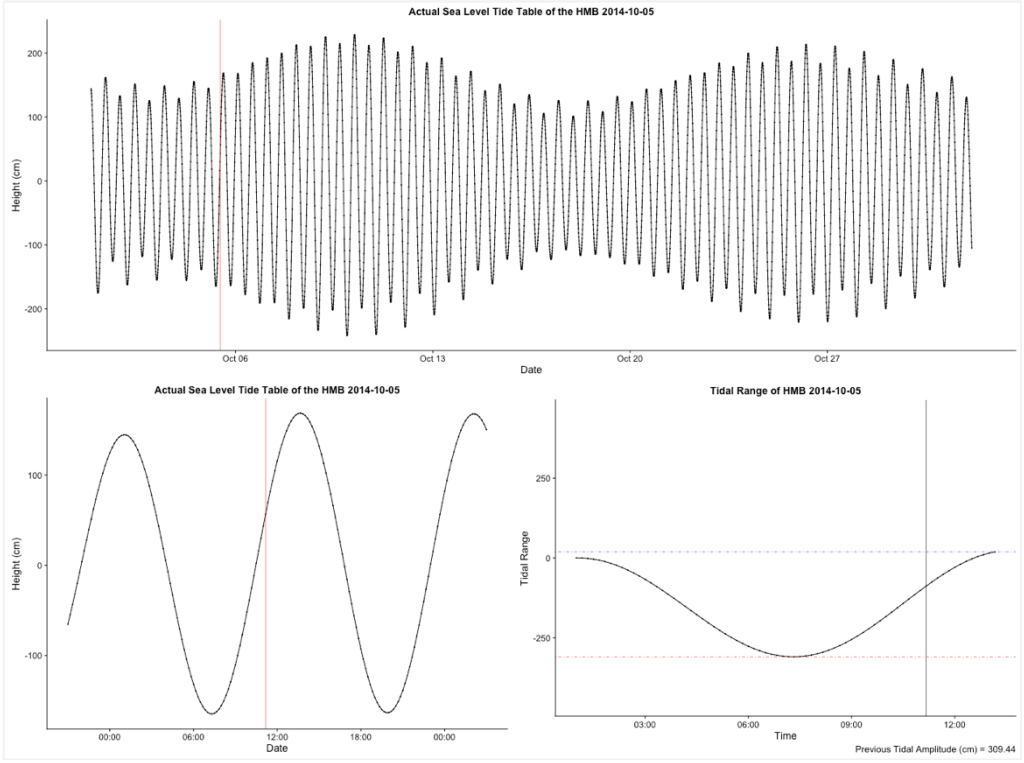
Actual Sea Level Tide Table of the HMB 2014-10-05
Height (cm)
200
100
0
-100
-200
Oct 06
Oct 13
Oct 20
Oct 27
Date
Actual Sea Level Tide Table of the HMB 2014-10-05
Height (cm)
100
0
-100
00:00
06:00
12:00
18:00
00:00
Date
Tidal Range of HMB 2014-10-05
Tidal Range
250
0
-250
03:00
06:00
09:00
12:00
Time
Previous Tidal Amplitude (cm) = 309.44

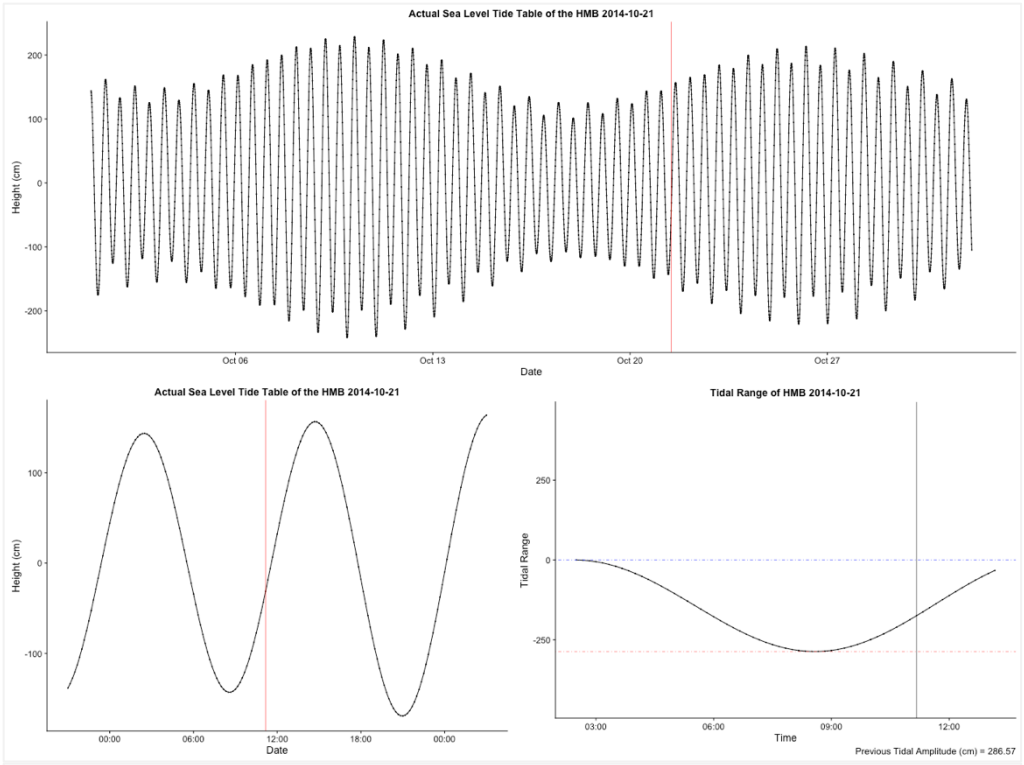
Actual Sea Level Tide Table of the HMB 2014-10-21
Height (cm)
200
100
0
-100
-200
Oct 06
Oct 13
Oct 20
Oct 27
Date
Actual Sea Level Tide Table of the HMB 2014-10-21
Height (cm)
100
0
-100
00:00
06:00
12:00
18:00
00:00
Date
Tidal Range of HMB 2014-10-21
Tidal Range
250
0
-250
03:00
06:00
09:00
12:00
Time
Previous Tidal Amplitude (cm) = 286.57

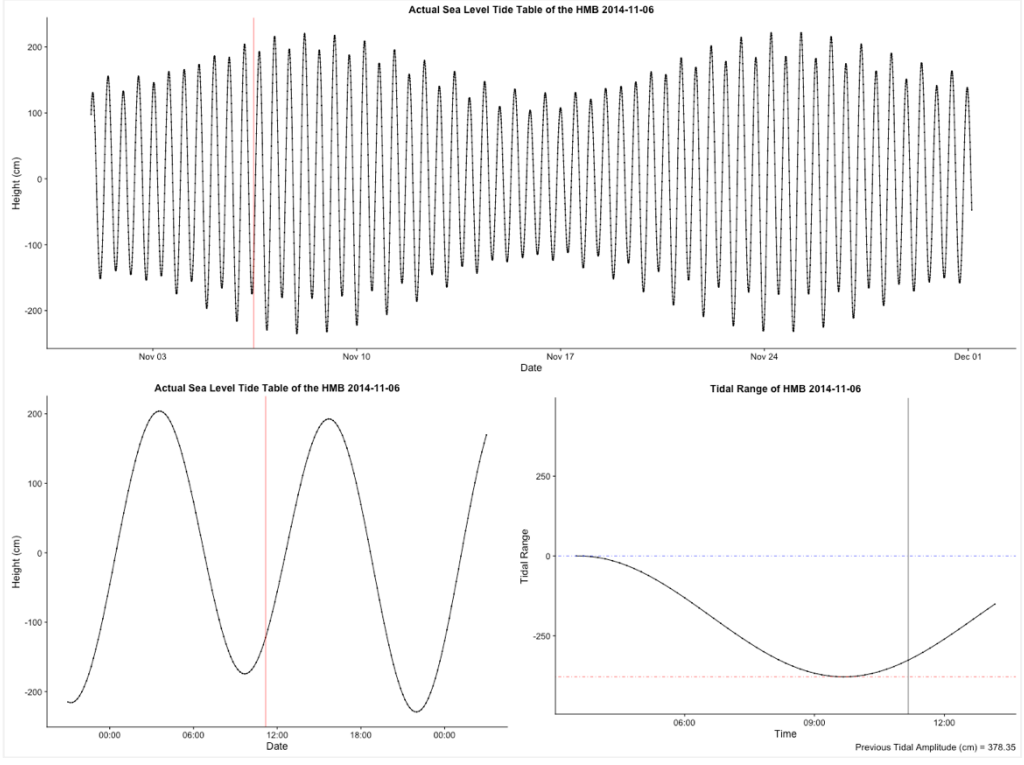
Actual Sea Level Tide Table of the HMB 2014-11-06
Height (cm)
200
100
0
-100
-200
Nov 03
Nov 10
Nov 17
Nov 24
Dec 01
Date
Actual Sea Level Tide Table of the HMB 2014-11-06
Height (cm)
200
100
0
-100
-200
00:00
06:00
12:00
18:00
00:00
Date
Tidal Range of HMB 2014-11-06
Tidal Range
250
0
-250
06:00
09:00
12:00
Time
Previous Tidal Amplitude (cm) = 378.35

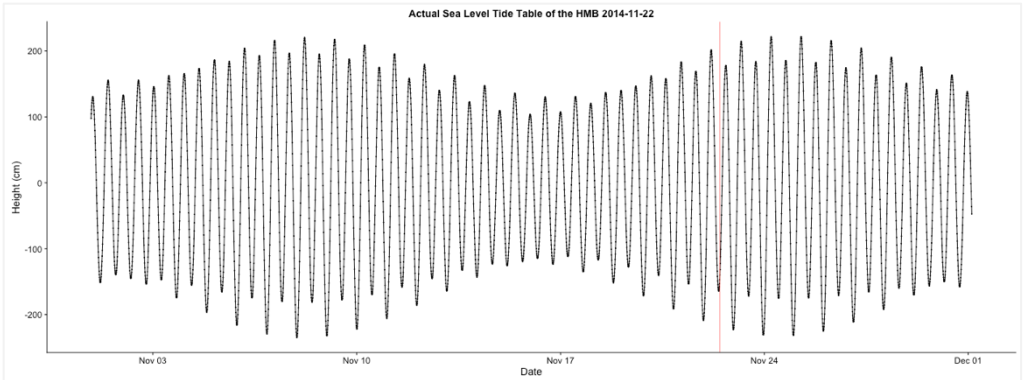
Actual Sea Level Tide Table of the HMB 2014-11-22
Height (cm)
200
100
0
-100
-200
Nov 03
Nov 10
Nov 17
Nov 24
Dec 01
Date

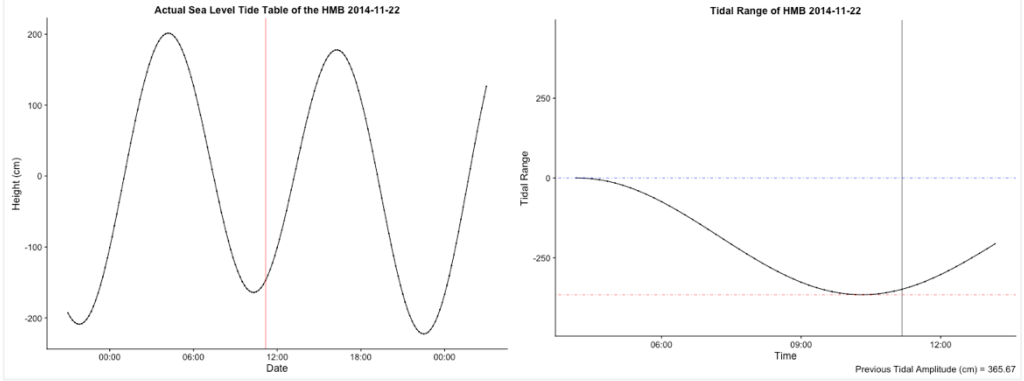
Actual Sea Level Tide Table of the HMB 2014-11-22
Height (cm)
200
100
0
-100
-200
00:00
06:00
12:00
18:00
00:00
Date

Tidal Range of HMB 2014-11-22
Tidal Range
250
0
-250
06:00
09:00
12:00
Time
Previous Tidal Amplitude (cm) = 365.67

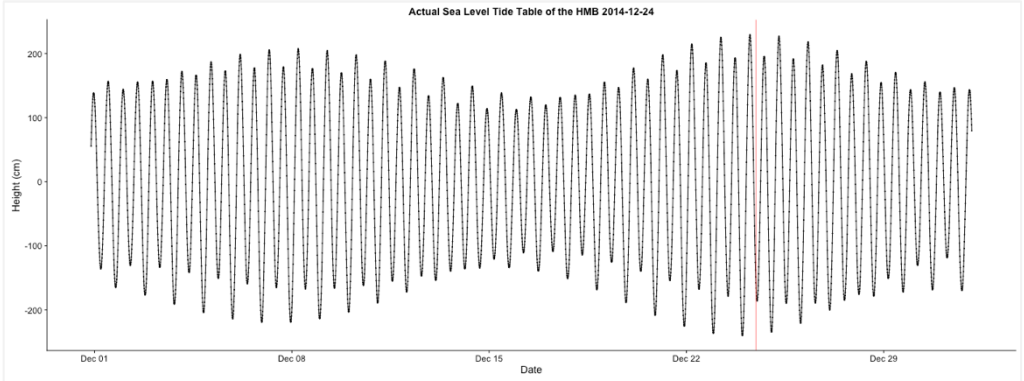
Actual Sea Level Tide Table of the HMB 2014-12-24
Height (cm)
200
100
0
-100
-200
Dec 01
Dec 08
Dec 15
Dec 22
Dec 29
Date

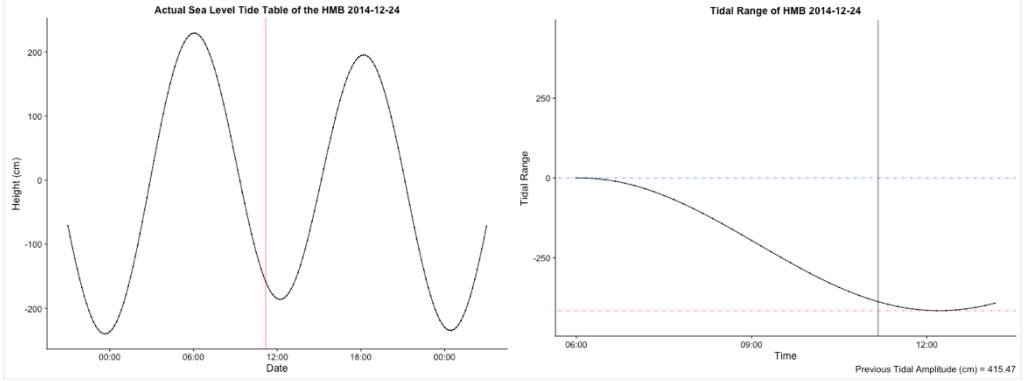
Actual Sea Level Tide Table of the HMB 2014-12-24
Height (cm)
200
100
0
-100
-200
00:00
06:00
12:00
18:00
00:00
Date

Tidal Range of HMB 2014-12-24
Tidal Range
250
0
-250
06:00
09:00
12:00
Time
Previous Tidal Amplitude (cm) = 415.47

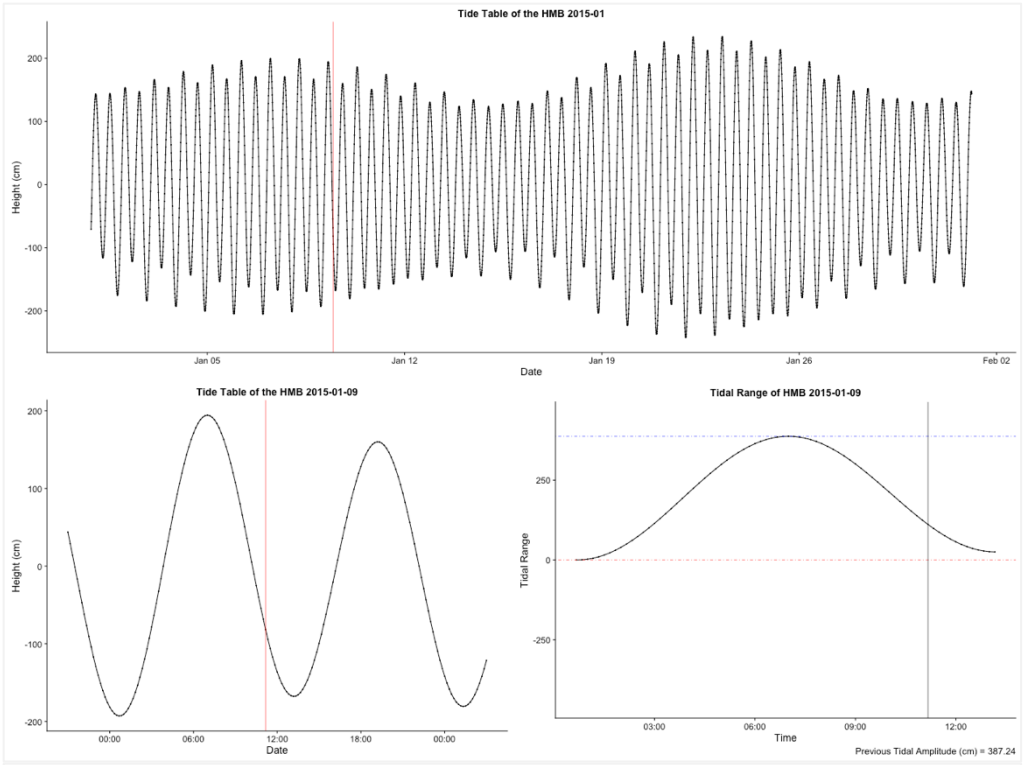
Tide Table of the HMB 2015-01
Height (cm)
200
100
0
-100
-200
Jan 05
Jan 12
Jan 19
Jan 26
Feb 02
Date
Tide Table of the HMB 2015-01-09
Height (cm)
200
100
0
-100
-200
00:00
06:00
12:00
18:00
00:00
Date
Tidal Range of HMB 2015-01-09
Tidal Range
250
0
-250
03:00
06:00
09:00
12:00
Time
Previous Tidal Amplitude (cm) = 387.24

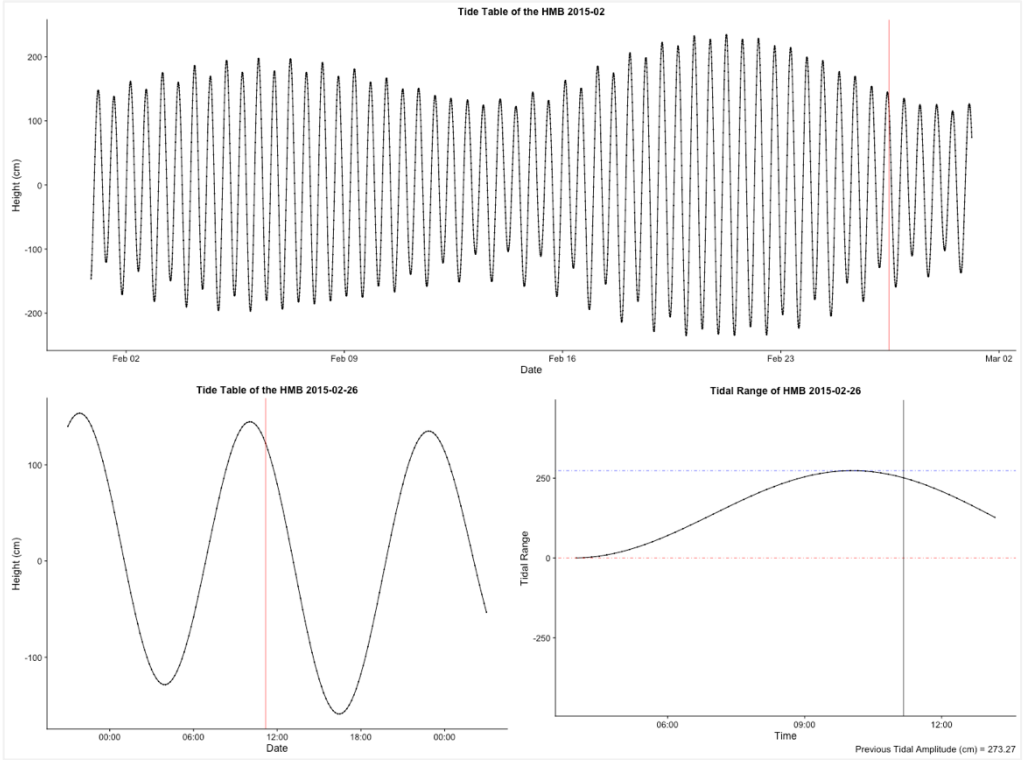
Tide Table of the HMB 2015-02
Height (cm)
200
100
0
-100
-200
Feb 02
Feb 09
Feb 16
Feb 23
Mar 02
Date
Tide Table of the HMB 2015-02-26
Height (cm)
100
0
-100
00:00
06:00
12:00
18:00
00:00
Date
Tidal Range of HMB 2015-02-26
Tidal Range
250
0
-250
06:00
09:00
12:00
Time
Previous Tidal Amplitude (cm) = 273.27

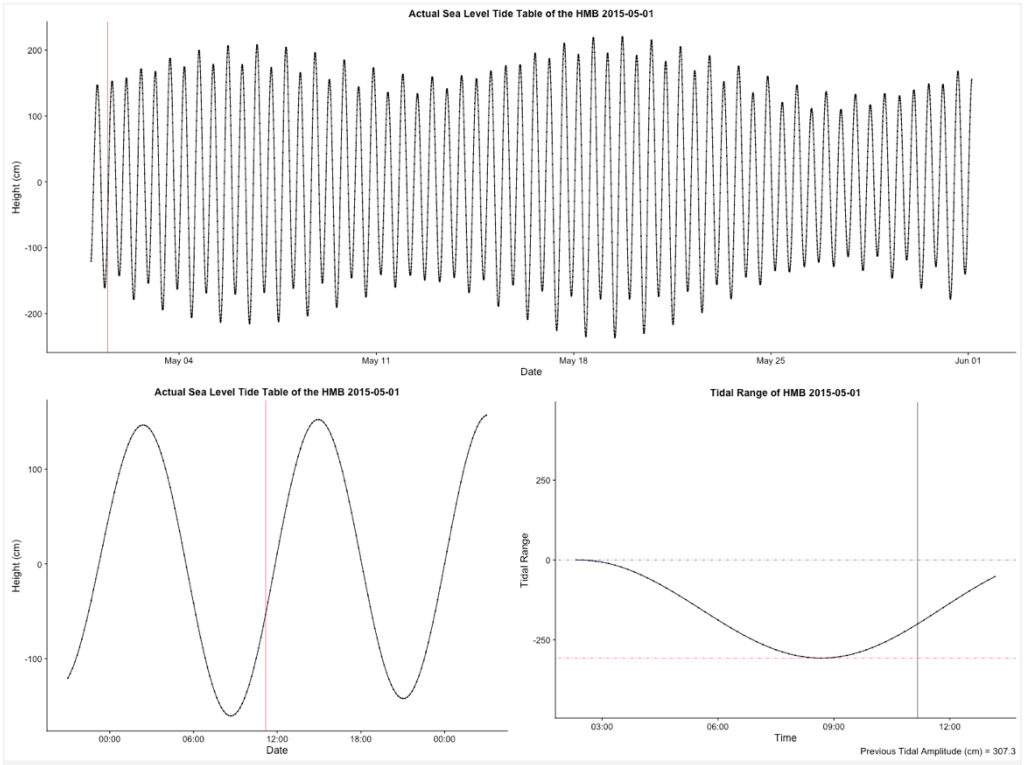
Actual Sea Level Tide Table of the HMB 2015-05-01
Height (cm)
200
100
0
-100
-200
May 04
May 11
May 18
May 25
Jun 01
Date
Actual Sea Level Tide Table of the HMB 2015-05-01
Height (cm)
100
0
-100
00:00
06:00
12:00
18:00
00:00
Date
Tidal Range of HMB 2015-05-01
Tidal Range
250
0
-250
03:00
06:00
09:00
12:00
Time
Previous Tidal Amplitude (cm) = 307.3

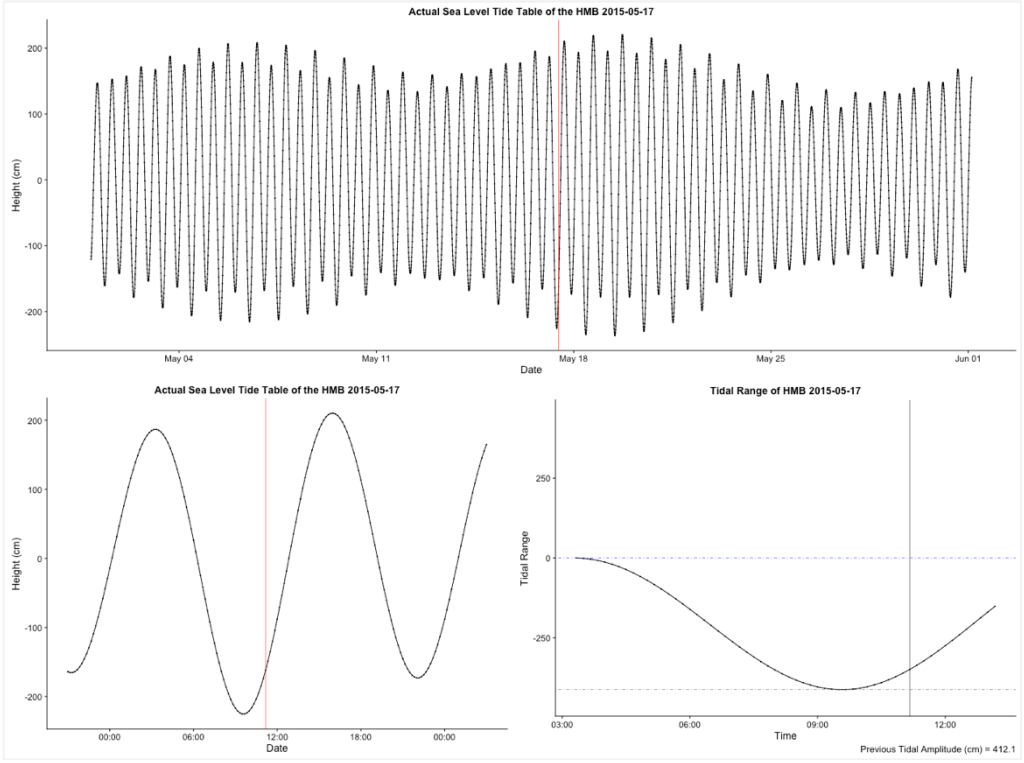
Actual Sea Level Tide Table of the HMB 2015-05-17
Height (cm)
200
100
0
-100
-200
May 04
May 11
May 18
May 25
Jun 01
Date
Actual Sea Level Tide Table of the HMB 2015-05-17
Height (cm)
200
100
0
-100
-200
00:00
06:00
12:00
18:00
00:00
Date
Tidal Range of HMB 2015-05-17
Tidal Range
250
0
-250
03:00
06:00
09:00
12:00
Time
Previous Tidal Amplitude (cm) = 412.1

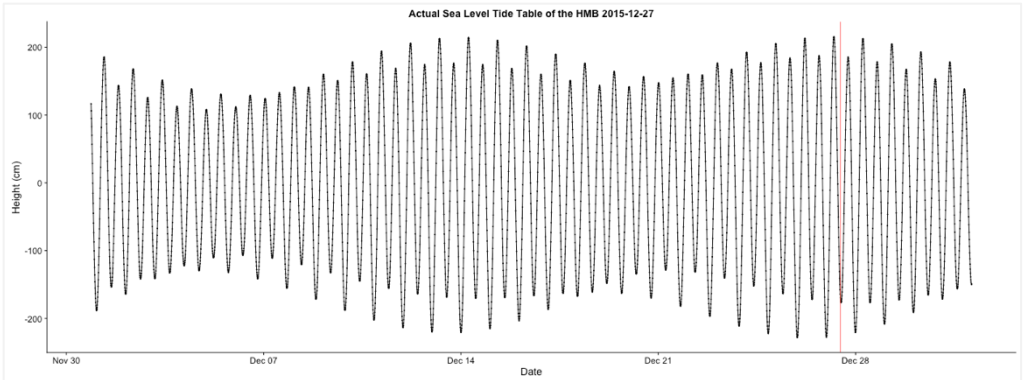
Actual Sea Level Tide Table of the HMB 2015-12-27
Height (cm)
200
100
0
-100
-200
Nov 30
Dec 07
Dec 14
Dec 21
Dec 28
Date

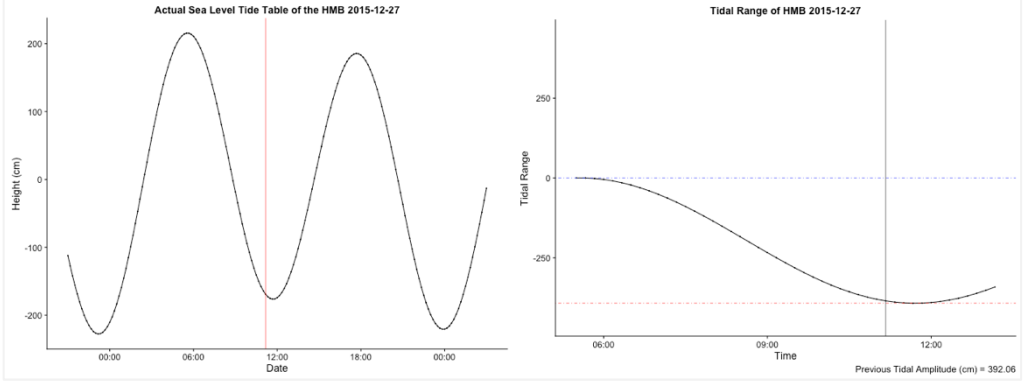
Actual Sea Level Tide Table of the HMB 2015-12-27
Height (cm)
200
100
0
-100
-200
00:00
06:00
12:00
18:00
00:00
Date

Tidal Range of HMB 2015-12-27
Tidal Range
250
0
-250
06:00
09:00
12:00
Time
Previous Tidal Amplitude (cm) = 392.06

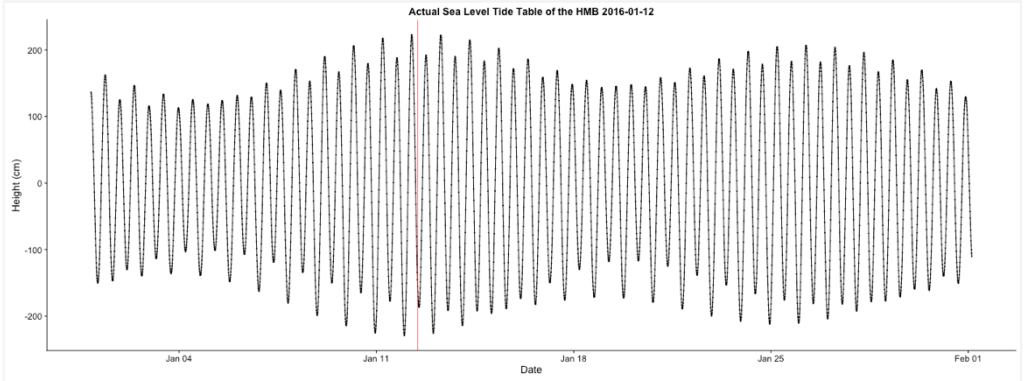
Actual Sea Level Tide Table of the HMB 2016-01-12
Height (cm)
200
100
0
-100
-200
Jan 04
Jan 11
Jan 18
Jan 25
Feb 01
Date

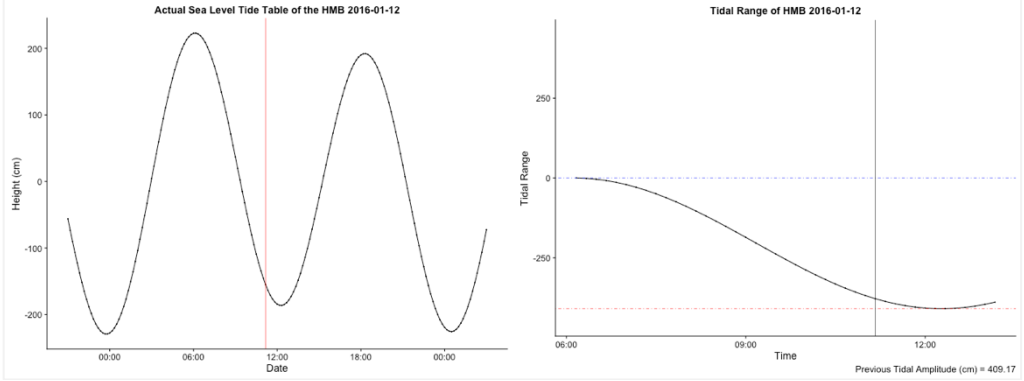
Actual Sea Level Tide Table of the HMB 2016-01-12
Height (cm)
200
100
0
-100
-200
00:00
06:00
12:00
18:00
00:00
Date

Tidal Range of HMB 2016-01-12
Tidal Range
250
0
-250
06:00
09:00
12:00
Time
Previous Tidal Amplitude (cm) = 409.17

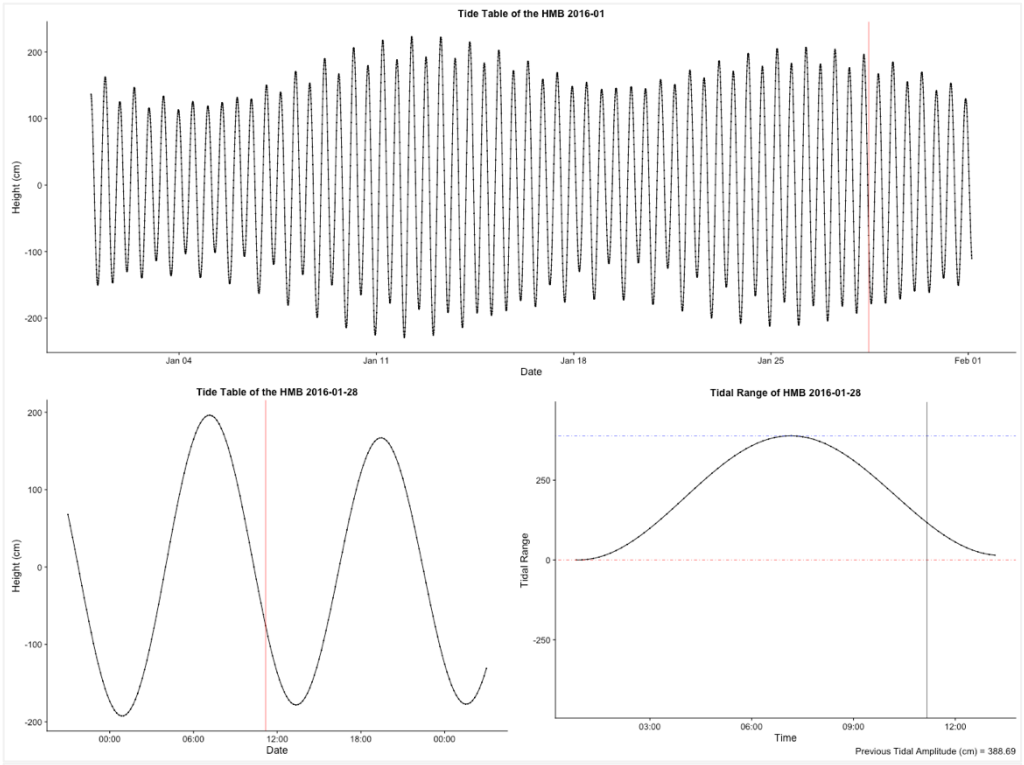
Tide Table of the HMB 2016-01
Height (cm)
200
100
0
-100
-200
Jan 04
Jan 11
Jan 18
Jan 25
Feb 01
Date
Tide Table of the HMB 2016-01-28
Height (cm)
200
100
0
-100
-200
00:00
06:00
12:00
18:00
00:00
Date
Tidal Range of HMB 2016-01-28
Tidal Range
250
0
-250
03:00
06:00
09:00
12:00
Time
Previous Tidal Amplitude (cm) = 388.69

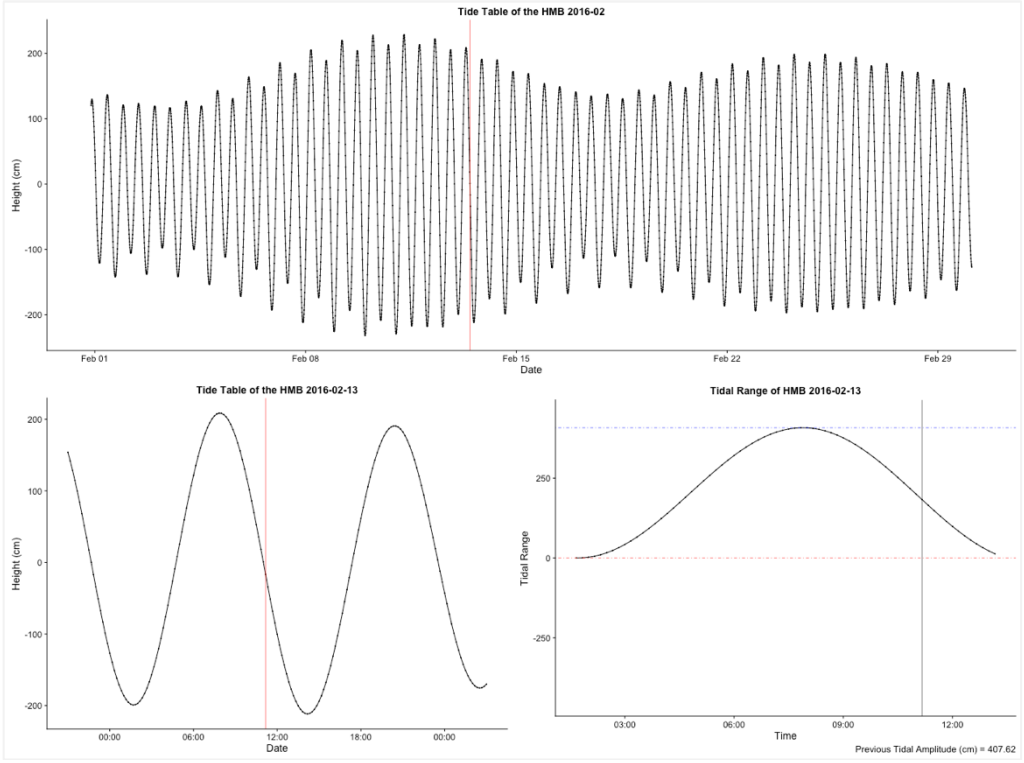
Tide Table of the HMB 2016-02
Height (cm)
200
100
0
-100
-200
Feb 01
Feb 08
Feb 15
Feb 22
Feb 29
Date
Tide Table of the HMB 2016-02-13
Height (cm)
200
100
0
-100
-200
00:00
06:00
12:00
18:00
00:00
Date
Tidal Range of HMB 2016-02-13
Tidal Range
250
0
-250
03:00
06:00
09:00
12:00
Time
Previous Tidal Amplitude (cm) = 407.62

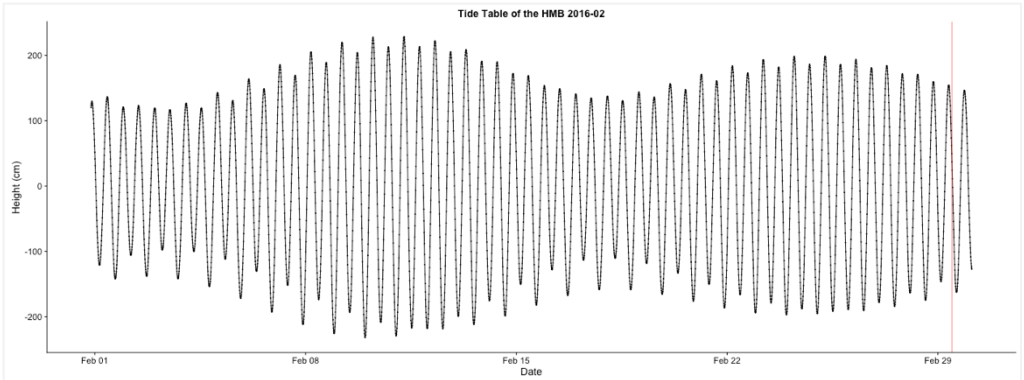
Tide Table of the HMB 2016-02
Height (cm)
200
100
0
-100
-200
Feb 01
Feb 08
Feb 15
Feb 22
Feb 29
Date

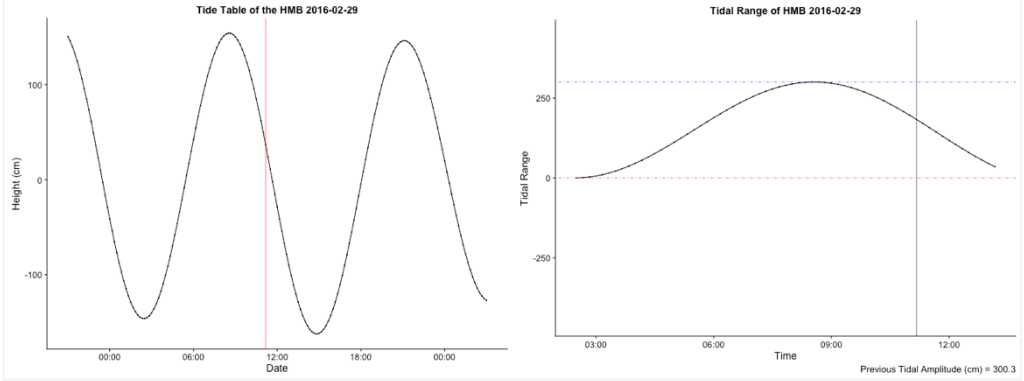
Tide Table of the HMB 2016-02-29
Height (cm)
100
0
-100
00:00
06:00
12:00
18:00
00:00
Date

Tidal Range of HMB 2016-02-29
Tidal Range
250
0
-250
03:00
06:00
09:00
12:00
Time
Previous Tidal Amplitude (cm) = 300.3

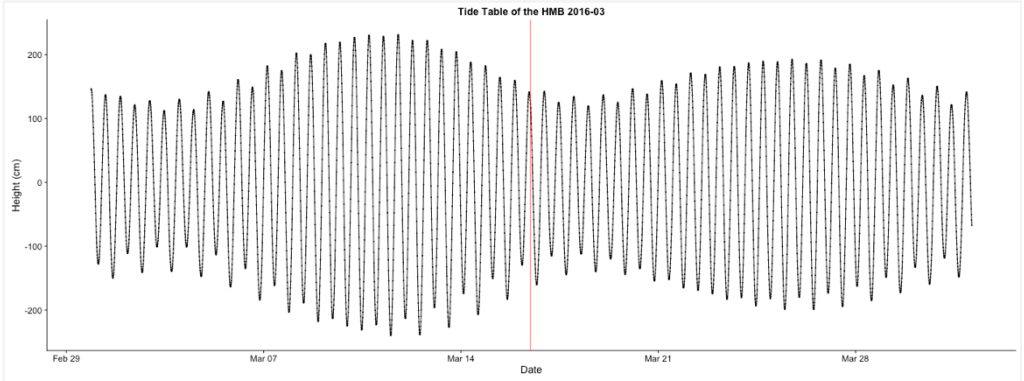
Tide Table of the HMB 2016-03
Height (cm)
200
100
0
-100
-200
Feb 29
Mar 07
Mar 14
Mar 21
Mar 28
Date

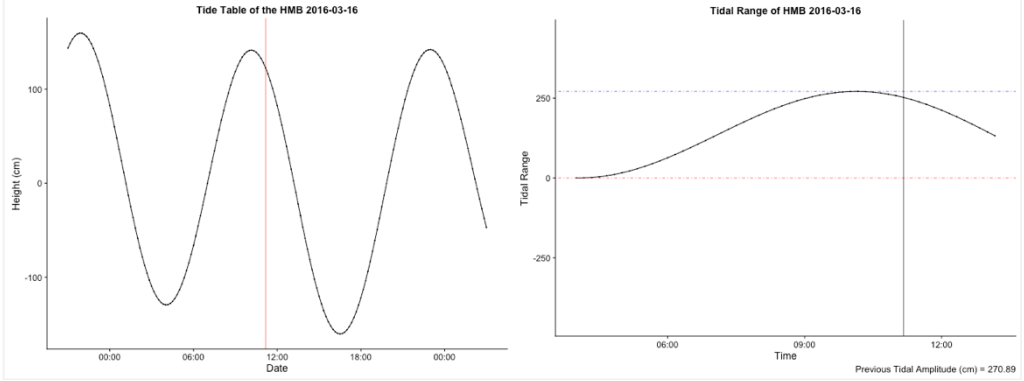
Tide Table of the HMB 2016-03-16
Height (cm)
100
0
-100
00:00
06:00
12:00
18:00
00:00
Date

Tidal Range of HMB 2016-03-16
Tidal Range
250
0
-250
06:00
09:00
12:00
Time
Previous Tidal Amplitude (cm) = 270.89

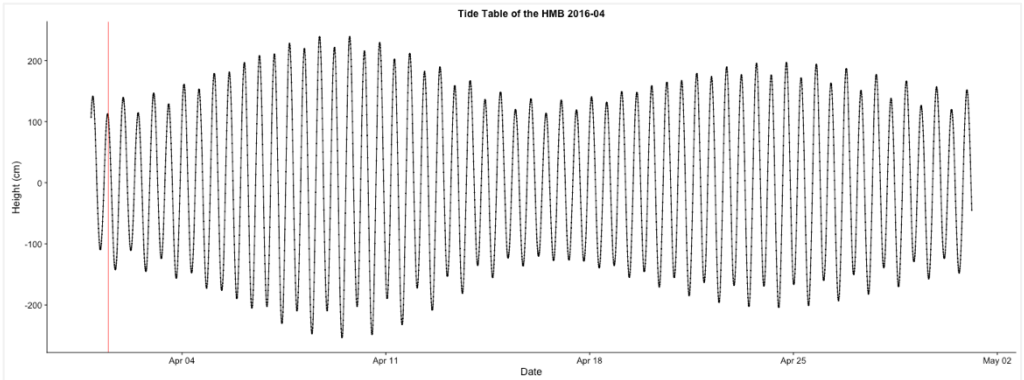
Tide Table of the HMB 2016-04
Height (cm)
200
100
0
-100
-200
Apr 04
Apr 11
Apr 18
Apr 25
May 02
Date

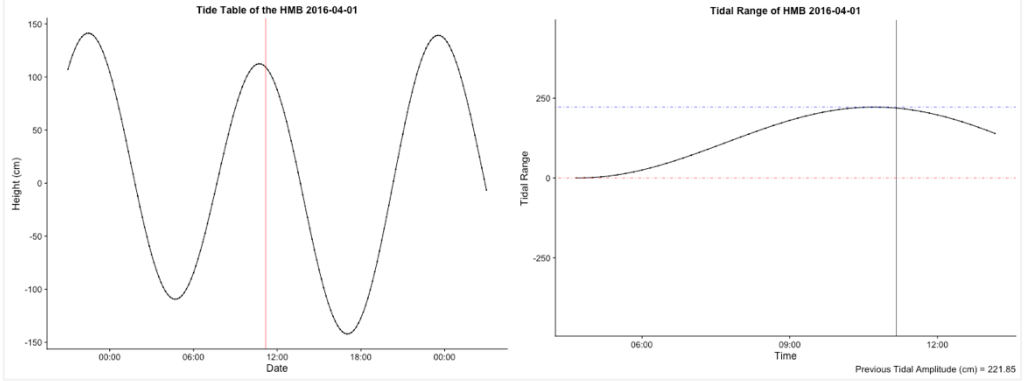
Tide Table of the HMB 2016-04-01
Height (cm)
150
100
50
0
-50
-100
-150
00:00
06:00
12:00
18:00
00:00
Date

Tidal Range of HMB 2016-04-01
Tidal Range
250
0
-250
06:00
09:00
12:00
Time
Previous Tidal Amplitude (cm) = 221.85

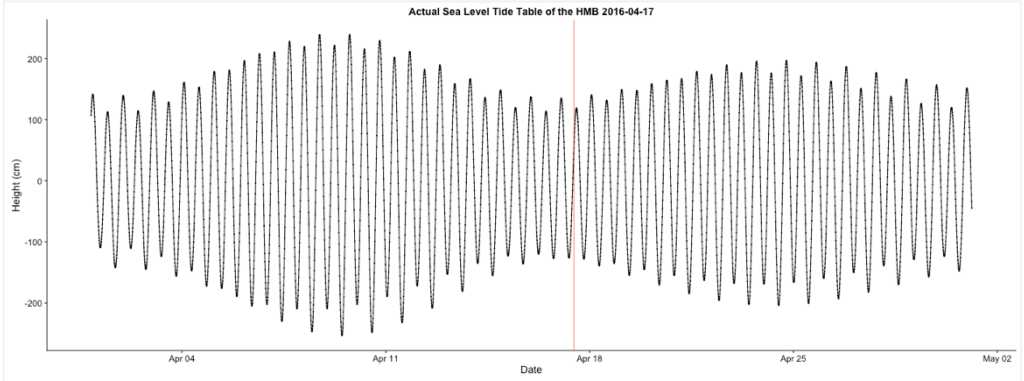
Actual Sea Level Tide Table of the HMB 2016-04-17
Height (cm)
200
100
0
-100
-200
Apr 04
Apr 11
Apr 18
Apr 25
May 02
Date

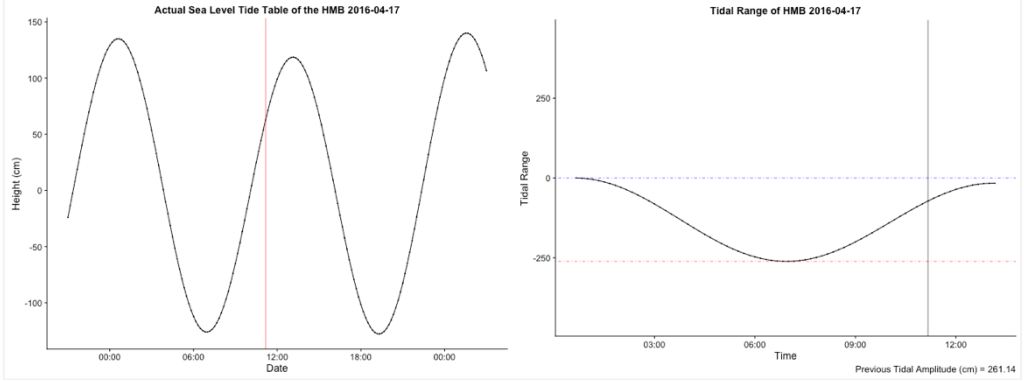
Actual Sea Level Tide Table of the HMB 2016-04-17
Height (cm)
150
100
50
0
-50
-100
00:00
06:00
12:00
18:00
00:00
Date

Tidal Range of HMB 2016-04-17
Tidal Range
250
0
-250
03:00
06:00
09:00
12:00
Time
Previous Tidal Amplitude (cm) = 261.14

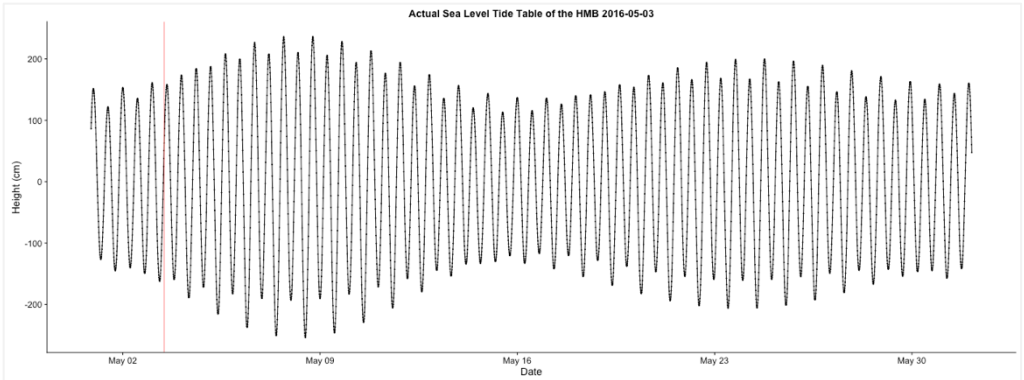
Actual Sea Level Tide Table of the HMB 2016-05-03
Height (cm)
200
100
0
-100
-200
May 02
May 09
May 16
May 23
May 30
Date

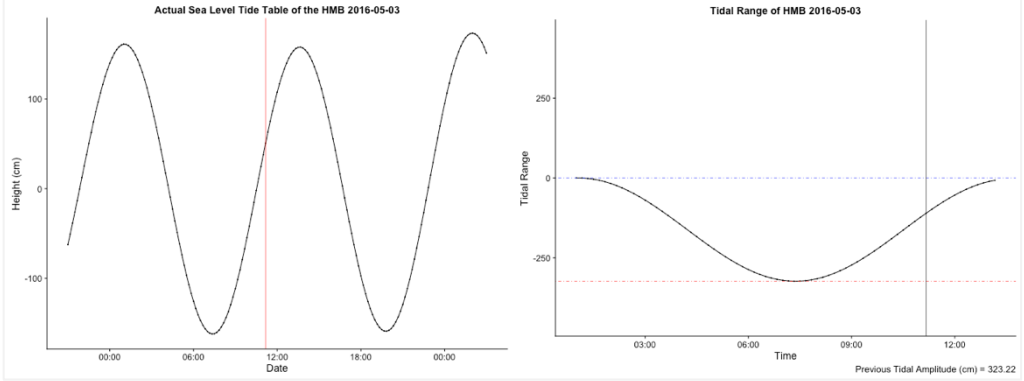
Actual Sea Level Tide Table of the HMB 2016-05-03
Height (cm)
100
0
-100
00:00
06:00
12:00
18:00
00:00
Date
Tidal Range of HMB 2016-05-03
Tidal Range
250
0
-250
03:00
06:00
09:00
12:00
Time
Previous Tidal Amplitude (cm) = 323.22

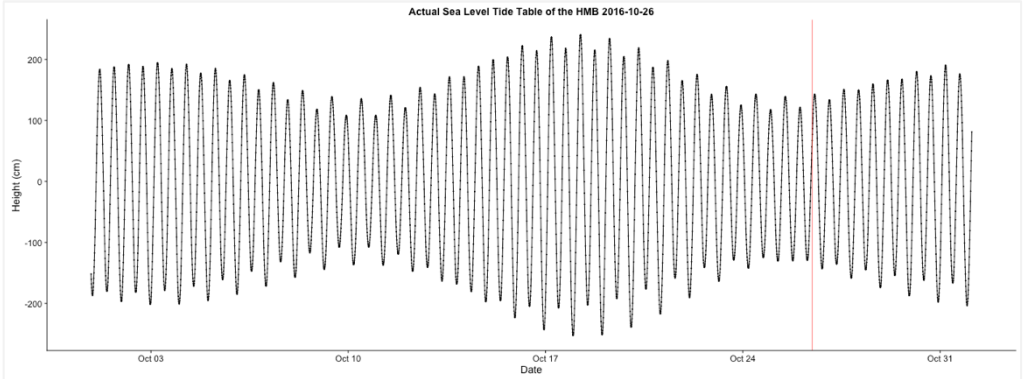
Actual Sea Level Tide Table of the HMB 2016-10-26
Height (cm)
200
100
0
-100
-200
Oct 03
Oct 10
Oct 17
Oct 24
Oct 31
Date

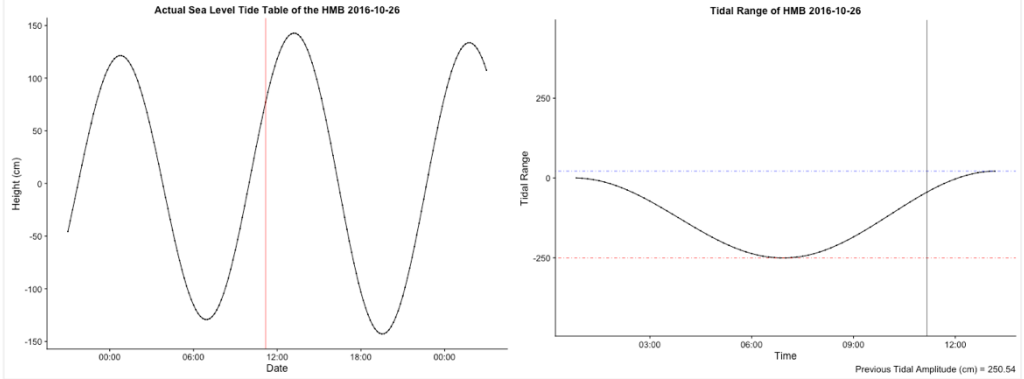
Actual Sea Level Tide Table of the HMB 2016-10-26
Height (cm)
150
100
50
0
-50
-100
-150
00:00
06:00
12:00
18:00
00:00
Date
Tidal Range of HMB 2016-10-26
Tidal Range
250
0
-250
03:00
06:00
09:00
12:00
Time
Previous Tidal Amplitude (cm) = 250.54

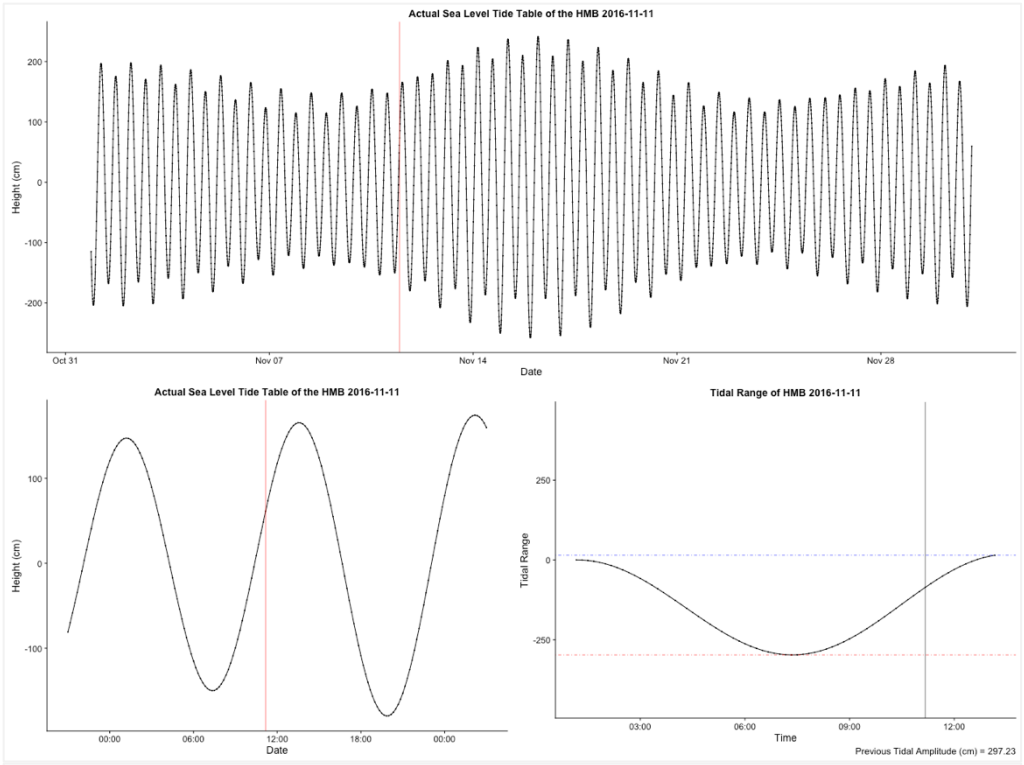
Actual Sea Level Tide Table of the HMB 2016-11-11
Height (cm)
200
100
0
-100
-200
Oct 31
Nov 07
Nov 14
Nov 21
Nov 28
Date
Actual Sea Level Tide Table of the HMB 2016-11-11
Height (cm)
100
0
-100
00:00
06:00
12:00
18:00
00:00
Date
Tidal Range of HMB 2016-11-11
Tidal Range
250
0
-250
03:00
06:00
09:00
12:00
Time
Previous Tidal Amplitude (cm) = 297.23

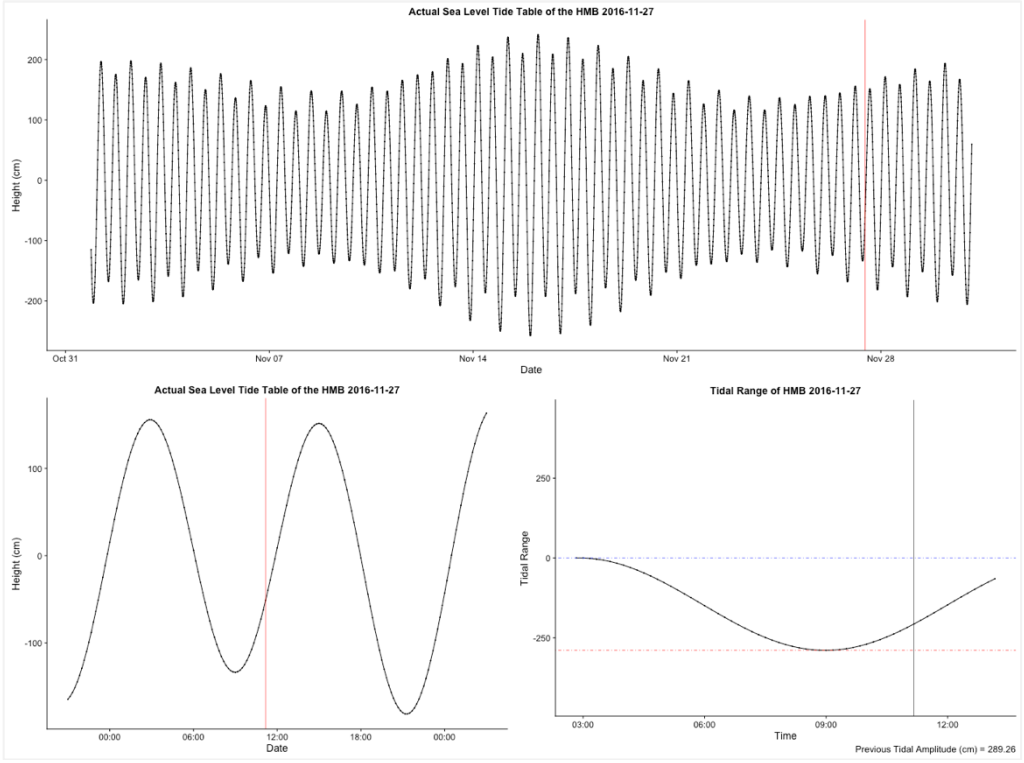
Actual Sea Level Tide Table of the HMB 2016-11-27
Height (cm)
200
100
0
-100
-200
Oct 31
Nov 07
Nov 14
Nov 21
Nov 28
Date
Actual Sea Level Tide Table of the HMB 2016-11-27
Height (cm)
100
0
-100
00:00
06:00
12:00
18:00
00:00
Date
Tidal Range of HMB 2016-11-27
Tidal Range
250
0
-250
03:00
06:00
09:00
12:00
Time
Previous Tidal Amplitude (cm) = 289.26

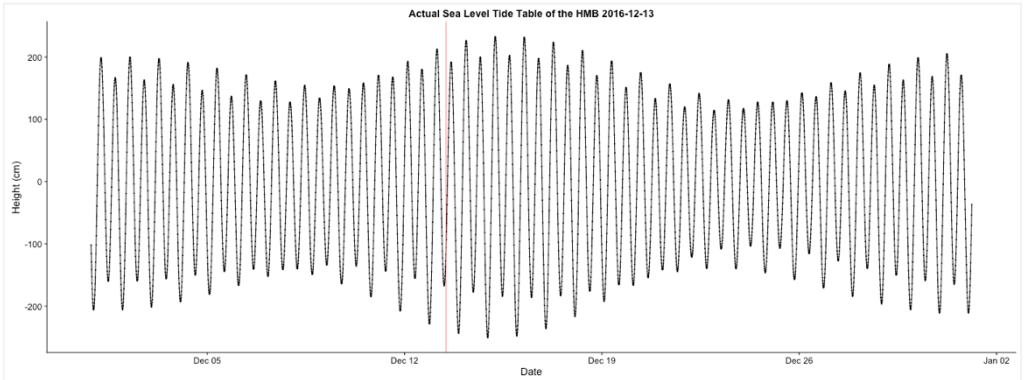
Actual Sea Level Tide Table of the HMB 2016-12-13
Height (cm)
200
100
0
-100
-200
Dec 05
Dec 12
Dec 19
Dec 26
Jan 02
Date

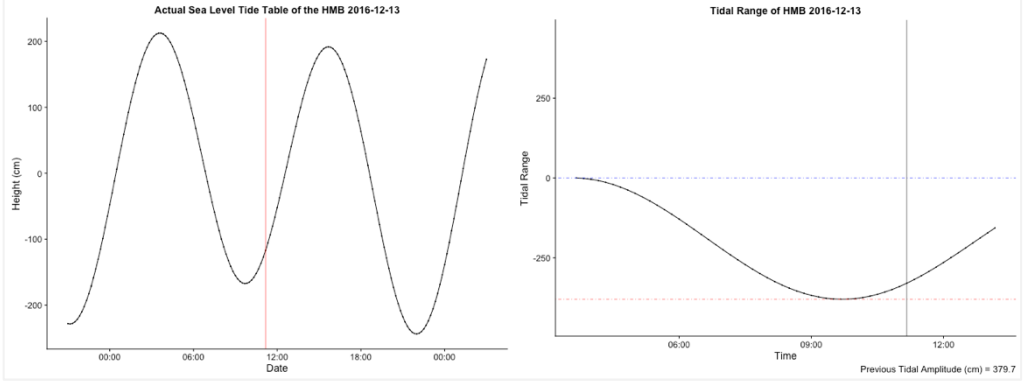
Actual Sea Level Tide Table of the HMB 2016-12-13
Height (cm)
200
100
0
-100
-200
00:00
06:00
12:00
18:00
00:00
Date

Tidal Range of HMB 2016-12-13
Tidal Range
250
0
-250
06:00
09:00
12:00
Time
Previous Tidal Amplitude (cm) = 379.7

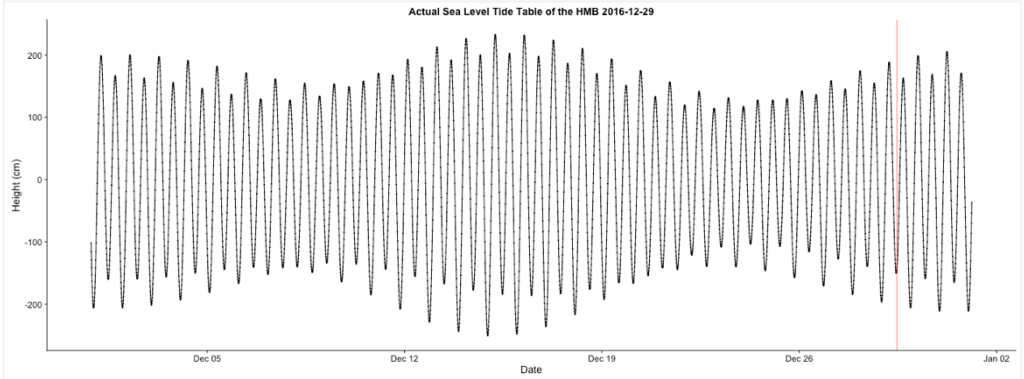
Actual Sea Level Tide Table of the HMB 2016-12-29
Height (cm)
200
100
0
-100
-200
Dec 05
Dec 12
Dec 19
Dec 26
Jan 02
Date

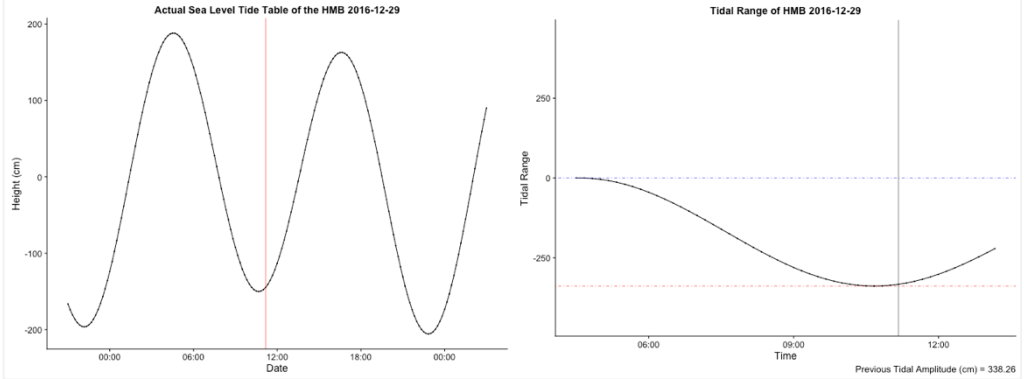
Actual Sea Level Tide Table of the HMB 2016-12-29
Height (cm)
200
100
0
-100
-200
00:00
06:00
12:00
18:00
00:00
Date

Tidal Range of HMB 2016-12-29
Tidal Range
250
0
-250
06:00
09:00
12:00
Time
Previous Tidal Amplitude (cm) = 338.26

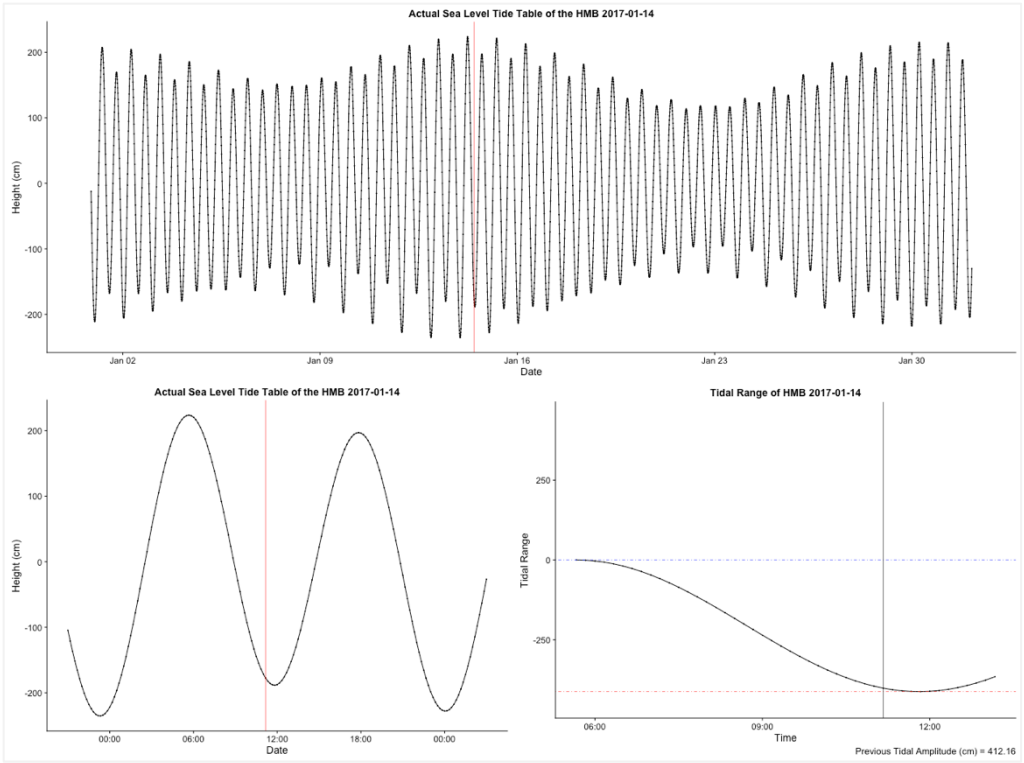
Actual Sea Level Tide Table of the HMB 2017-01-14
Height (cm)
200
100
0
-100
-200
Jan 02
Jan 09
Jan 16
Jan 23
Jan 30
Date
Actual Sea Level Tide Table of the HMB 2017-01-14
Height (cm)
200
100
0
-100
-200
00:00
06:00
12:00
18:00
00:00
Date
Tidal Range of HMB 2017-01-14
Tidal Range
250
0
-250
06:00
09:00
12:00
Time
Previous Tidal Amplitude (cm) = 412.16

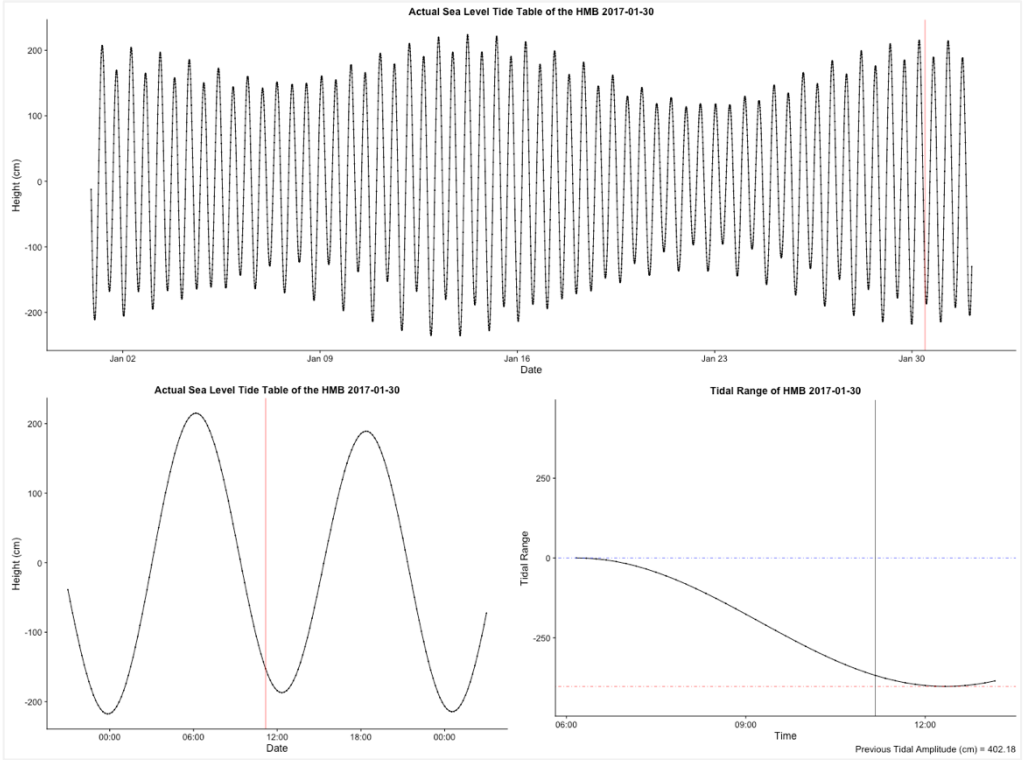
Actual Sea Level Tide Table of the HMB 2017-01-30
Height (cm)
200
100
0
-100
-200
Jan 02
Jan 09
Jan 16
Jan 23
Jan 30
Date
Actual Sea Level Tide Table of the HMB 2017-01-30
Height (cm)
200
100
0
-100
-200
00:00
06:00
12:00
18:00
00:00
Date
Tidal Range of HMB 2017-01-30
Tidal Range
250
0
-250
06:00
09:00
12:00
Time
Previous Tidal Amplitude (cm) = 402.18

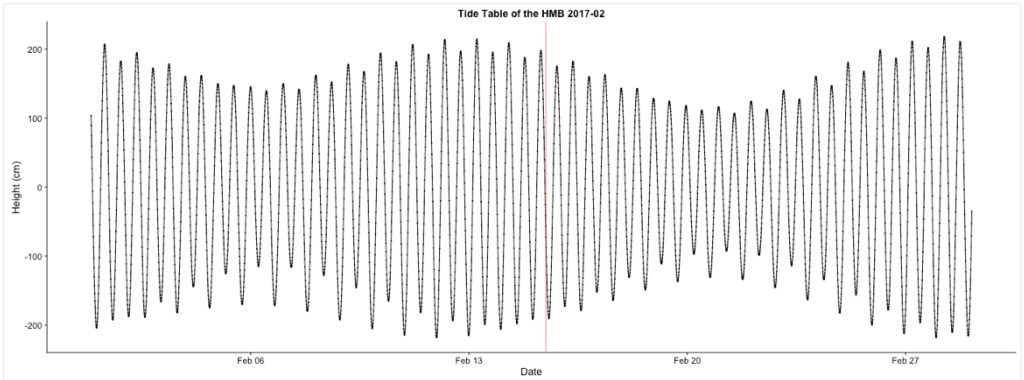

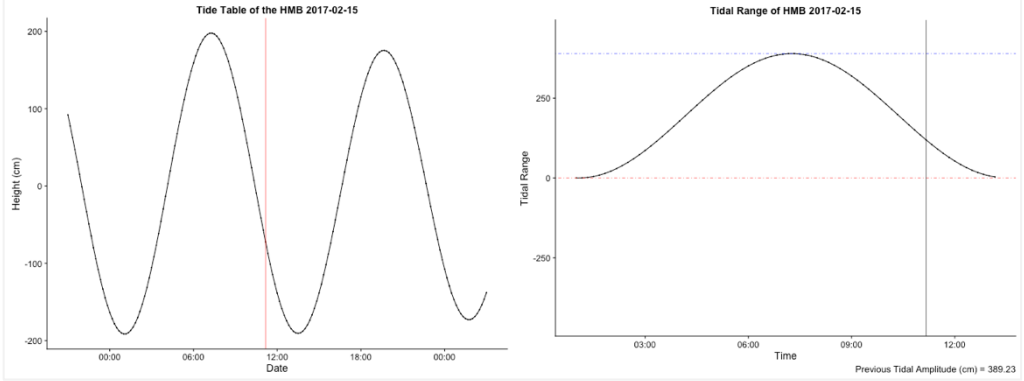

Previous Tidal Amplitude (cm) = 389.23

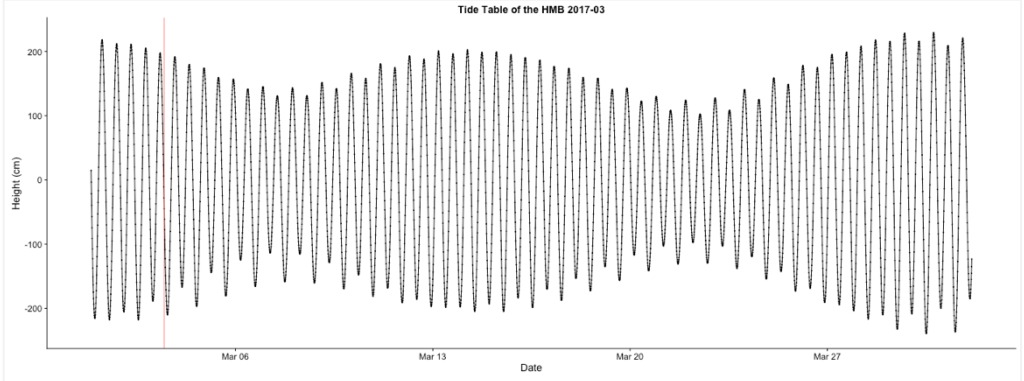

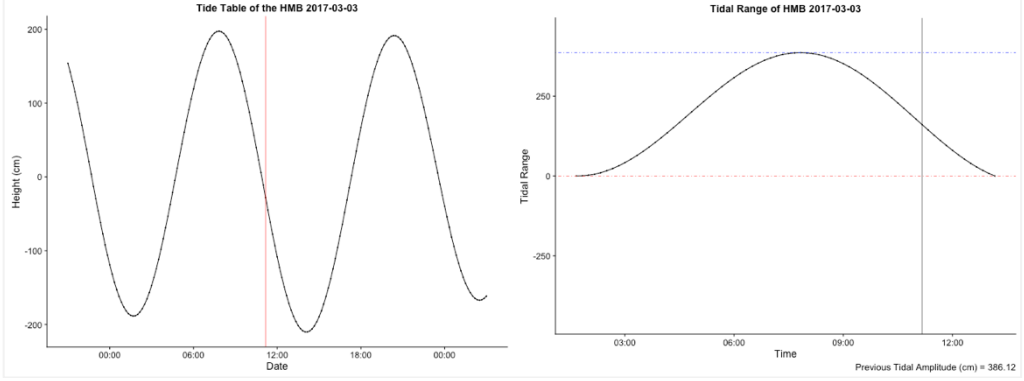

Previous Tidal Amplitude (cm) = 386.12

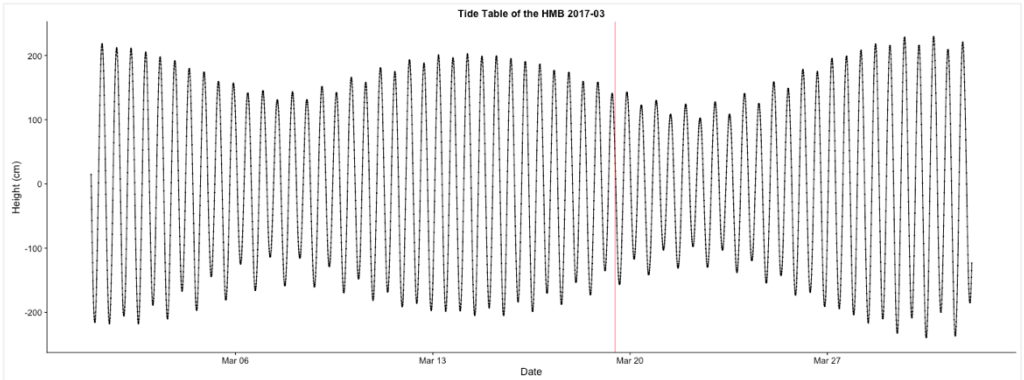
Tide Table of the HMB 2017-03
Height (cm)
200
100
0
-100
-200
Mar 06
Mar 13
Mar 20
Mar 27
Date

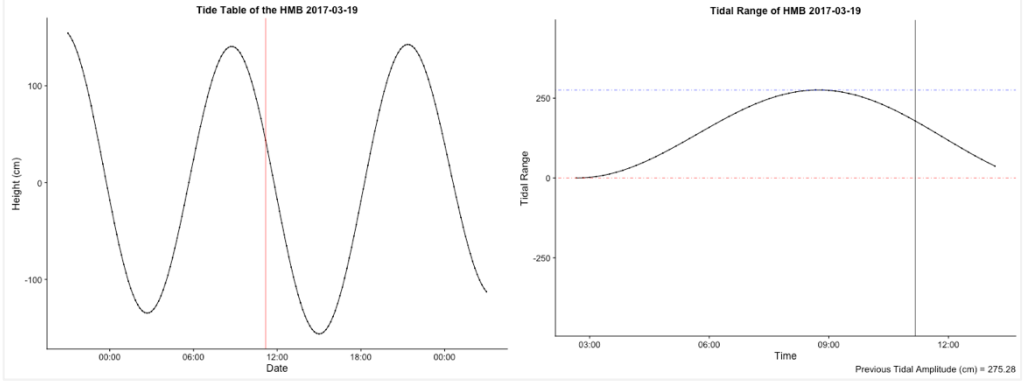
Tide Table of the HMB 2017-03-19
Height (cm)
100
0
-100
00:00
06:00
12:00
18:00
00:00
Date

Tidal Range of HMB 2017-03-19
Tidal Range
250
0
-250
03:00
06:00
09:00
12:00
Time
Previous Tidal Amplitude (cm) = 275.28

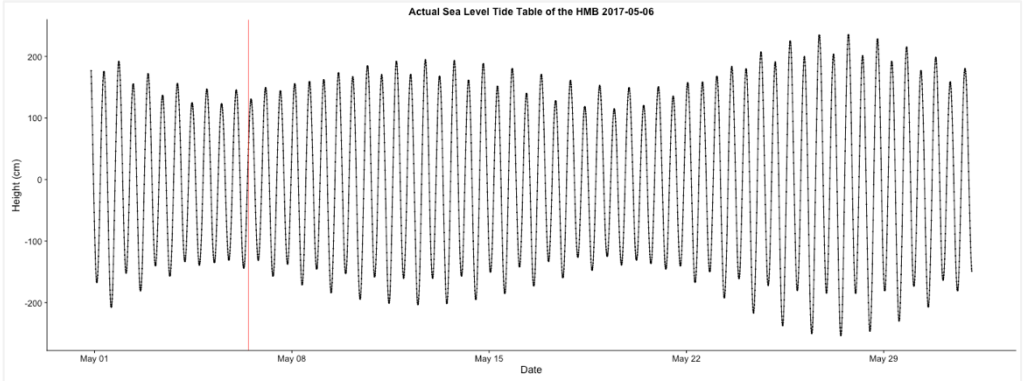
Actual Sea Level Tide Table of the HMB 2017-05-06
Height (cm)
200
100
0
-100
-200
May 01
May 08
May 15
May 22
May 29
Date

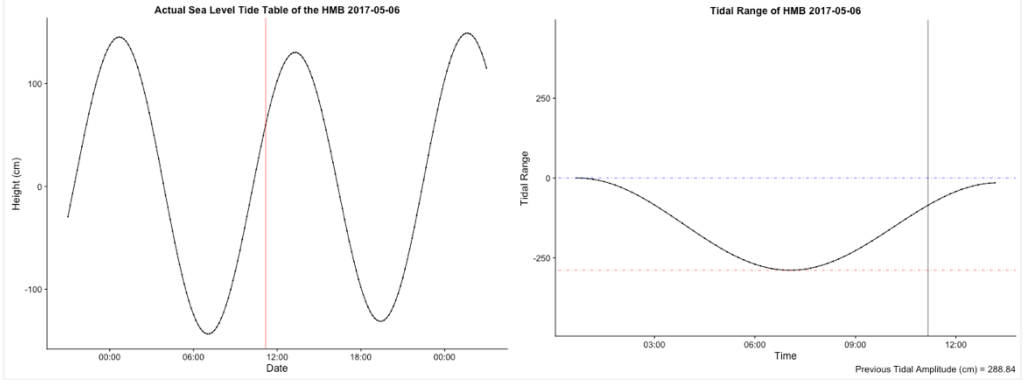
Actual Sea Level Tide Table of the HMB 2017-05-06
Height (cm)
100
0
-100
00:00
06:00
12:00
18:00
00:00
Date

Tidal Range of HMB 2017-05-06
Tidal Range
250
0
-250
03:00
06:00
09:00
12:00
Time
Previous Tidal Amplitude (cm) = 288.84

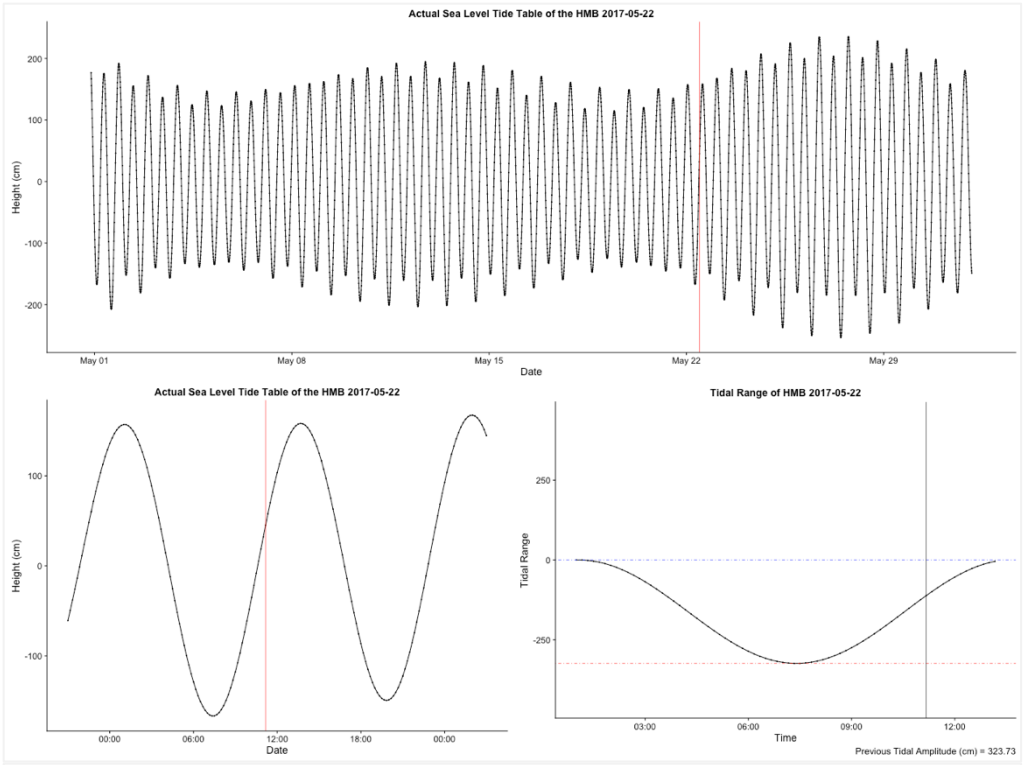
Actual Sea Level Tide Table of the HMB 2017-05-22
Height (cm)
200
100
0
-100
-200
May 01
May 08
May 15
May 22
May 29
Date
Actual Sea Level Tide Table of the HMB 2017-05-22
Height (cm)
100
0
-100
00:00
06:00
12:00
18:00
00:00
Date
Tidal Range of HMB 2017-05-22
Tidal Range
250
0
-250
03:00
06:00
09:00
12:00
Time
Previous Tidal Amplitude (cm) = 323.73

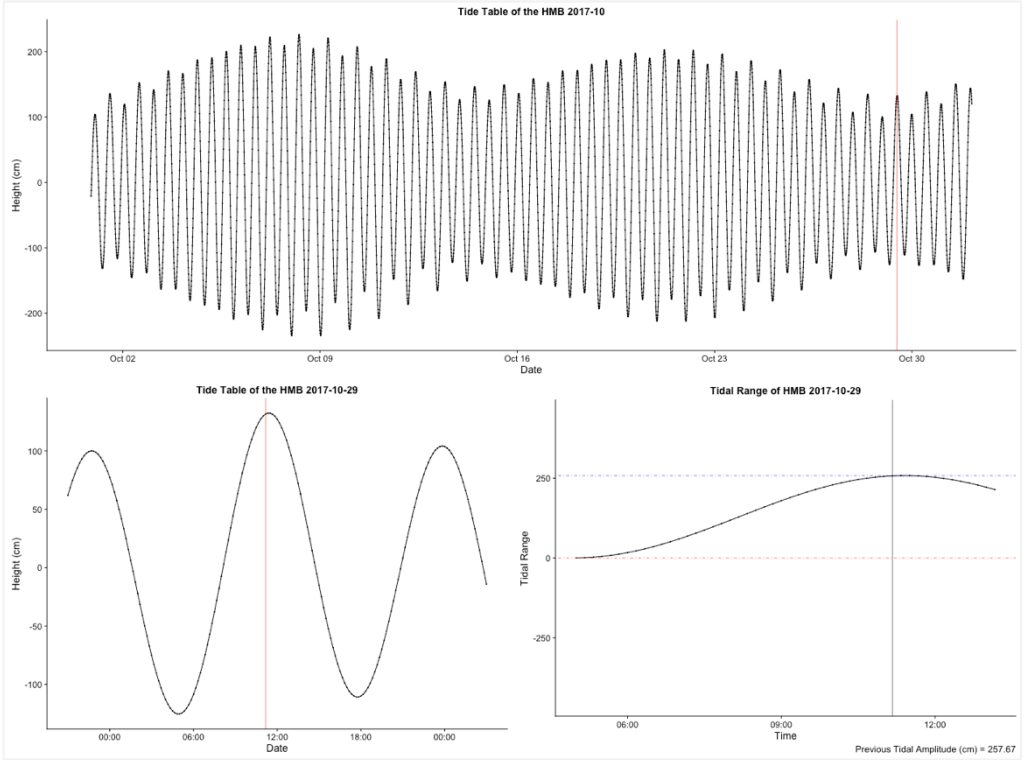
Tide Table of the HMB 2017-10
Height (cm)
200
100
0
-100
-200
Oct 02
Oct 09
Oct 16
Oct 23
Oct 30
Date
Tide Table of the HMB 2017-10-29
Height (cm)
100
50
0
-50
-100
00:00
06:00
12:00
18:00
00:00
Date
Tidal Range of HMB 2017-10-29
Tidal Range
250
0
-250
06:00
09:00
12:00
Time
Previous Tidal Amplitude (cm) = 257.67

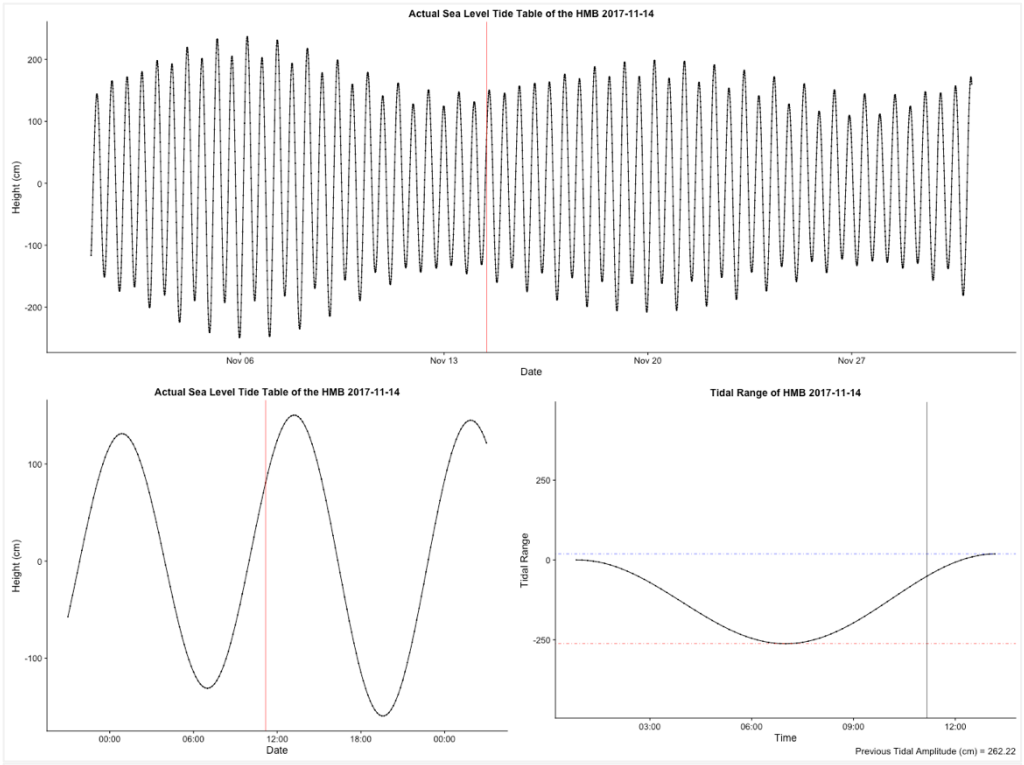
Actual Sea Level Tide Table of the HMB 2017-11-14
Height (cm)
200
100
0
-100
-200
Nov 06
Nov 13
Nov 20
Nov 27
Date
Actual Sea Level Tide Table of the HMB 2017-11-14
Height (cm)
100
0
-100
00:00
06:00
12:00
18:00
00:00
Date
Tidal Range of HMB 2017-11-14
Tidal Range
250
0
-250
03:00
06:00
09:00
12:00
Time
Previous Tidal Amplitude (cm) = 262.22

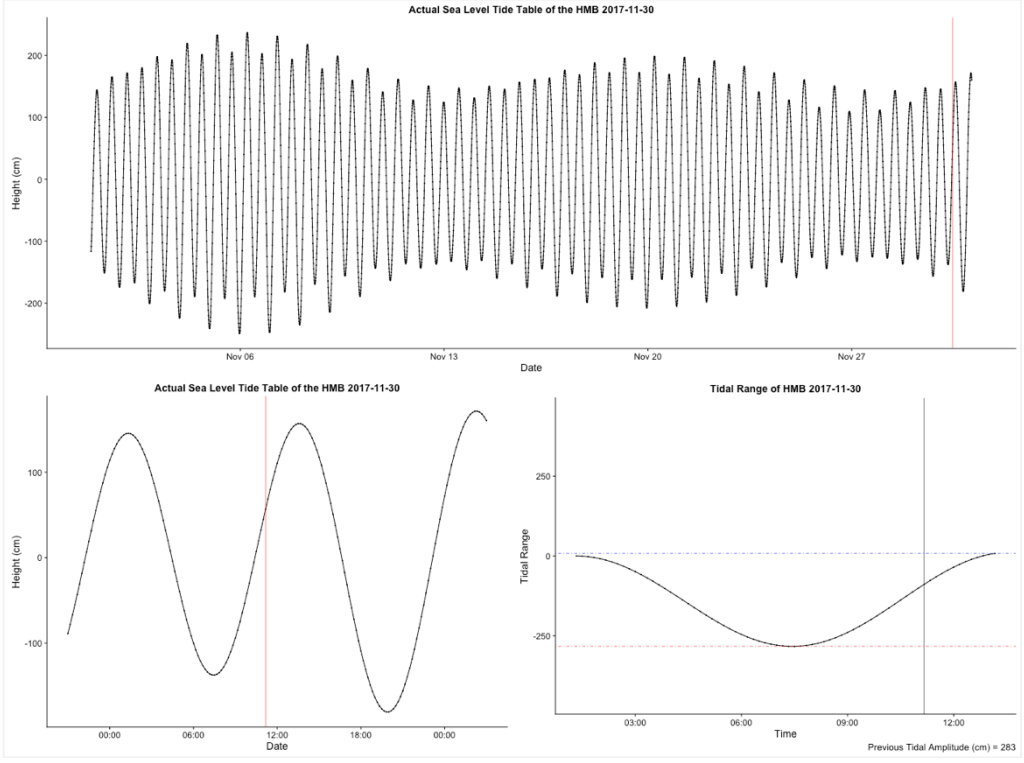
Actual Sea Level Tide Table of the HMB 2017-11-30
Height (cm)
200
100
0
-100
-200
Nov 06
Nov 13
Nov 20
Nov 27
Date
Actual Sea Level Tide Table of the HMB 2017-11-30
Height (cm)
100
0
-100
00:00
06:00
12:00
18:00
00:00
Date
Tidal Range of HMB 2017-11-30
Tidal Range
250
0
-250
03:00
06:00
09:00
12:00
Time
Previous Tidal Amplitude (cm) = 283

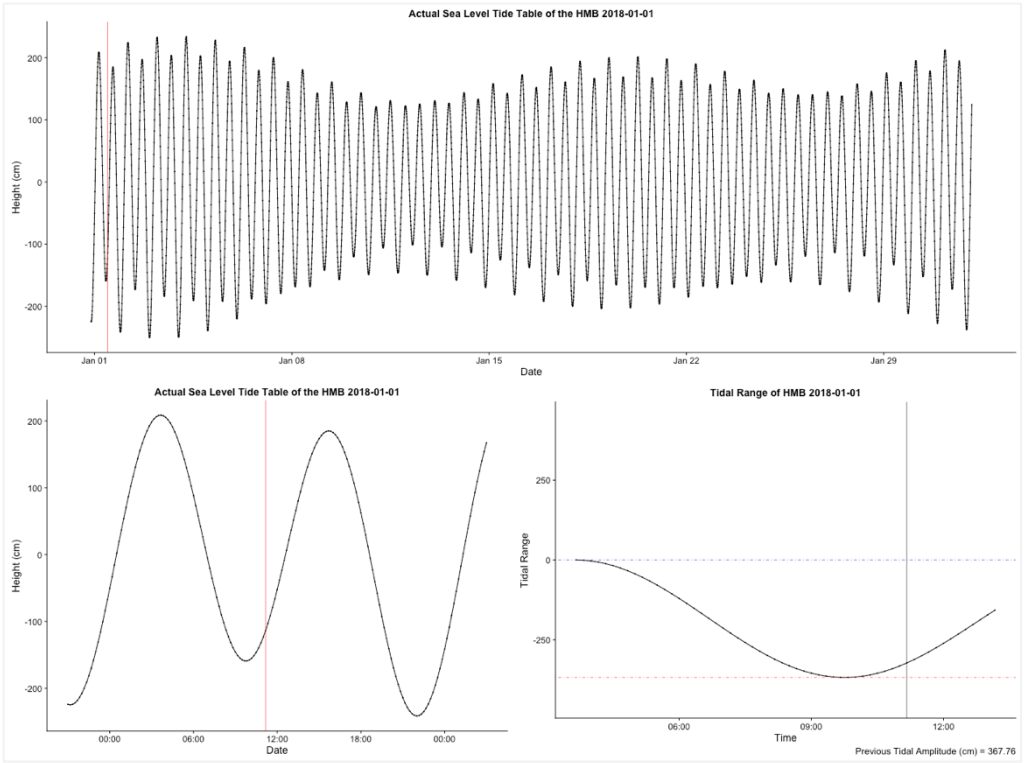
Actual Sea Level Tide Table of the HMB 2018-01-01
Height (cm)
200
100
0
-100
-200
Jan 01
Jan 08
Jan 15
Jan 22
Jan 29
Date
Actual Sea Level Tide Table of the HMB 2018-01-01
Height (cm)
200
100
0
-100
-200
00:00
06:00
12:00
18:00
00:00
Date
Tidal Range of HMB 2018-01-01
Tidal Range
250
0
-250
06:00
09:00
12:00
Time
Previous Tidal Amplitude (cm) = 367.76

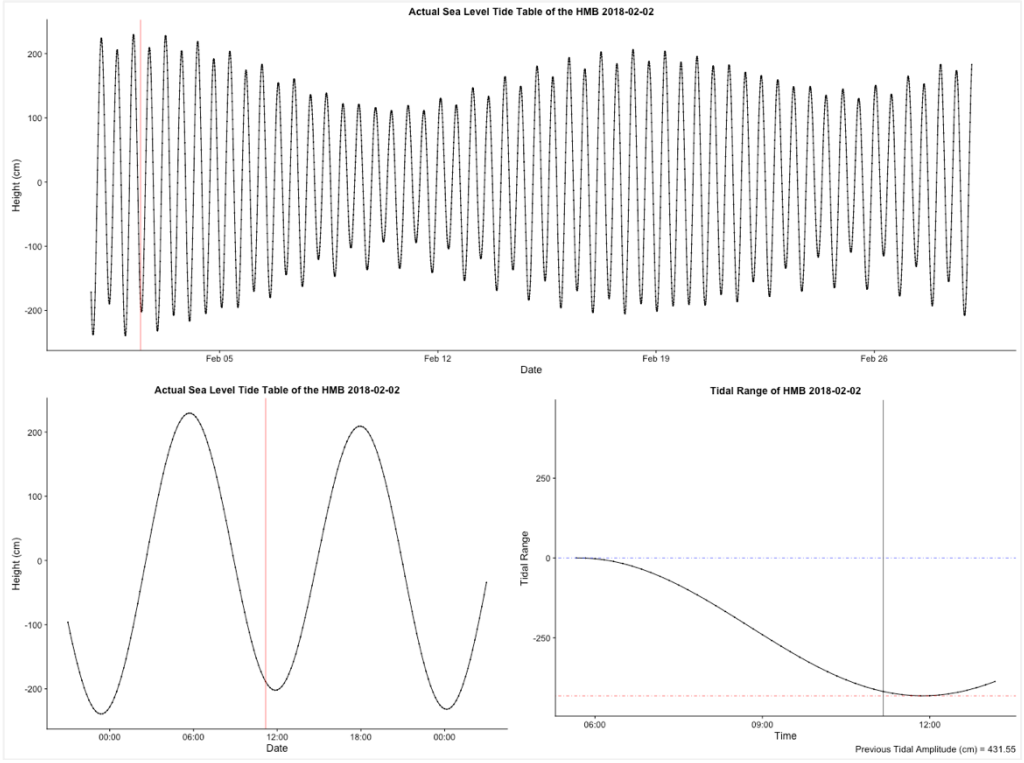
Actual Sea Level Tide Table of the HMB 2018-02-02
Height (cm)
200
100
0
-100
-200
Feb 05
Feb 12
Feb 19
Feb 26
Date
Actual Sea Level Tide Table of the HMB 2018-02-02
Height (cm)
200
100
0
-100
-200
00:00
06:00
12:00
18:00
00:00
Date
Tidal Range of HMB 2018-02-02
Tidal Range
250
0
-250
06:00
09:00
12:00
Time
Previous Tidal Amplitude (cm) = 431.55

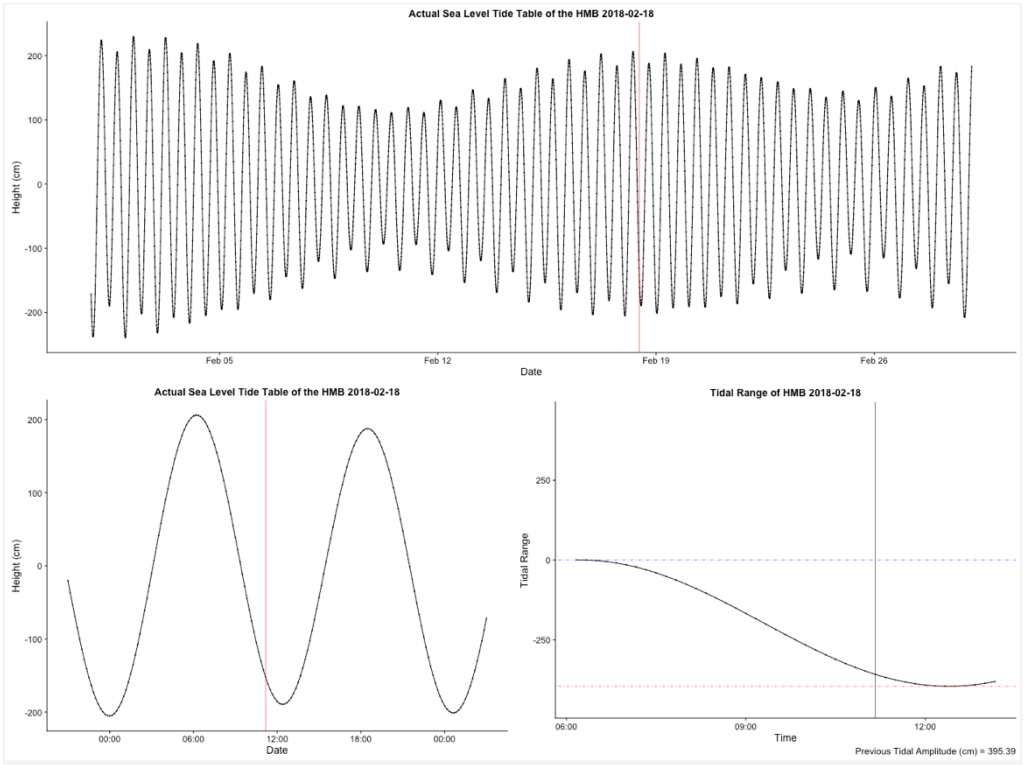
Actual Sea Level Tide Table of the HMB 2018-02-18
Height (cm)
200
100
0
-100
-200
Feb 05
Feb 12
Feb 19
Feb 26
Date
Actual Sea Level Tide Table of the HMB 2018-02-18
Height (cm)
200
100
0
-100
-200
00:00
06:00
12:00
18:00
00:00
Date
Tidal Range of HMB 2018-02-18
Tidal Range
250
0
-250
06:00
09:00
12:00
Time
Previous Tidal Amplitude (cm) = 395.39

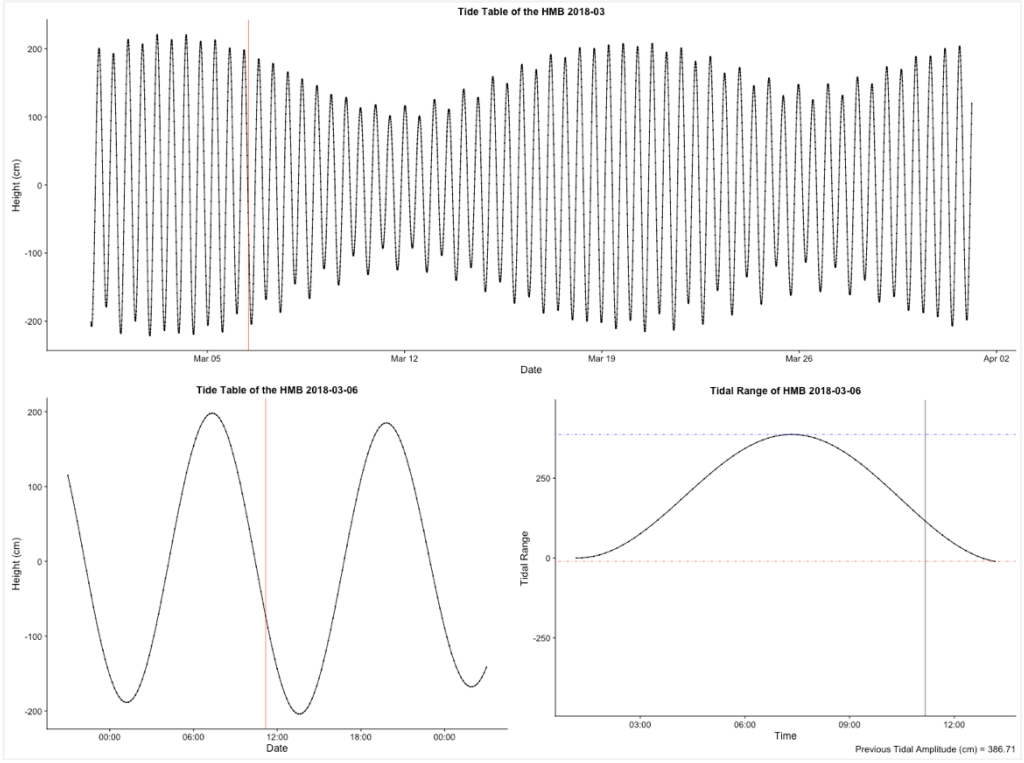
Tide Table of the HMB 2018-03
Height (cm)
200
100
0
-100
-200
Mar 05
Mar 12
Mar 19
Mar 26
Apr 02
Date
Tide Table of the HMB 2018-03-06
Height (cm)
200
100
0
-100
-200
00:00
06:00
12:00
18:00
00:00
Date
Tidal Range of HMB 2018-03-06
Tidal Range
250
0
-250
03:00
06:00
09:00
12:00
Time
Previous Tidal Amplitude (cm) = 386.71

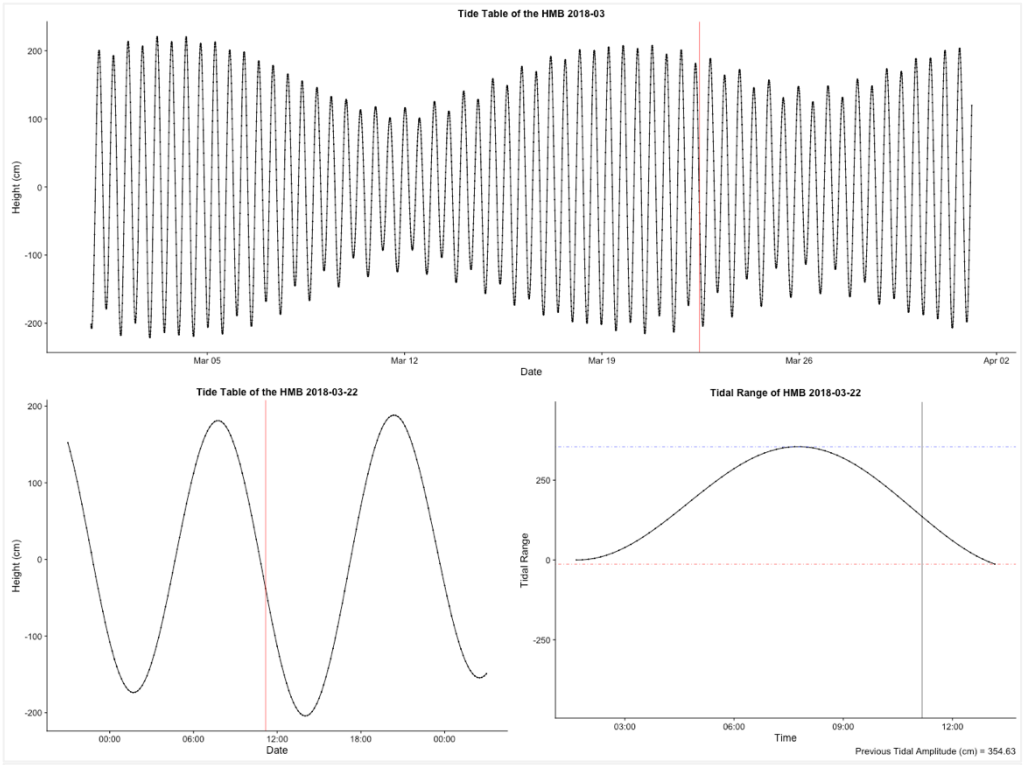
Tide Table of the HMB 2018-03
Height (cm)
200
100
0
-100
-200
Mar 05
Mar 12
Mar 19
Mar 26
Apr 02
Date
Tide Table of the HMB 2018-03-22
Height (cm)
200
100
0
-100
-200
00:00
06:00
12:00
18:00
00:00
Date
Tidal Range of HMB 2018-03-22
Tidal Range
250
0
-250
03:00
06:00
09:00
12:00
Time
Previous Tidal Amplitude (cm) = 354.63

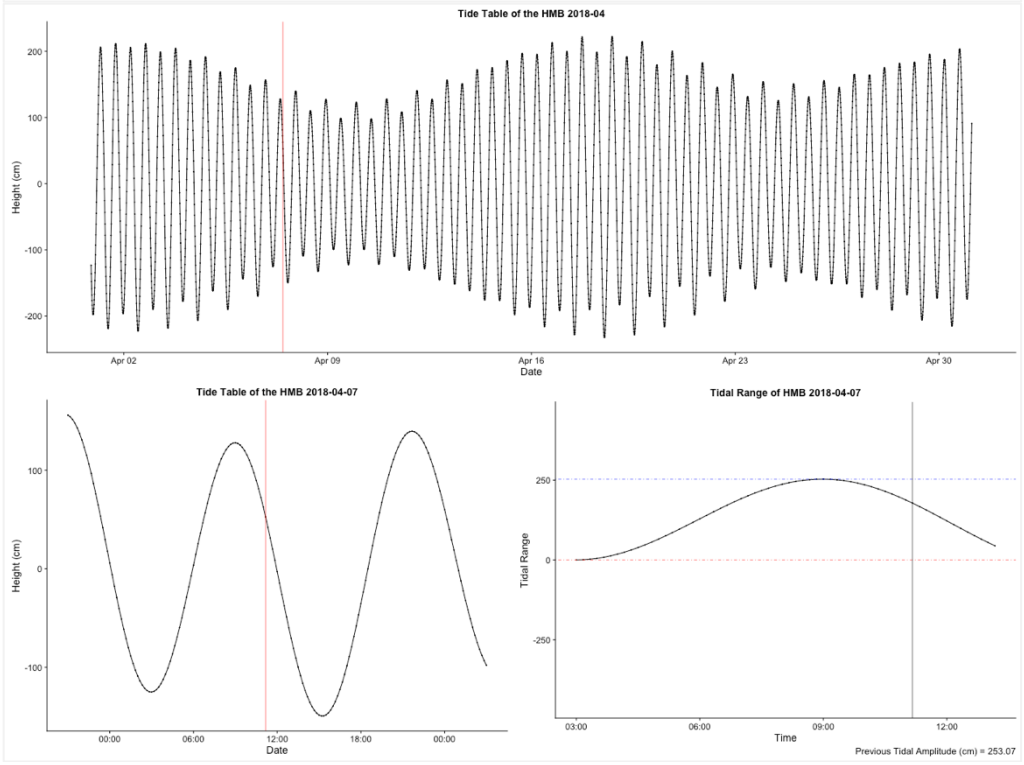
Tide Table of the HMB 2018-04
Height (cm)
200
100
0
-100
-200
Apr 02
Apr 09
Apr 16
Apr 23
Apr 30
Date
Tide Table of the HMB 2018-04-07
Height (cm)
100
0
-100
00:00
06:00
12:00
18:00
00:00
Date
Tidal Range of HMB 2018-04-07
Tidal Range
250
0
-250
03:00
06:00
09:00
12:00
Time
Previous Tidal Amplitude (cm) = 253.07

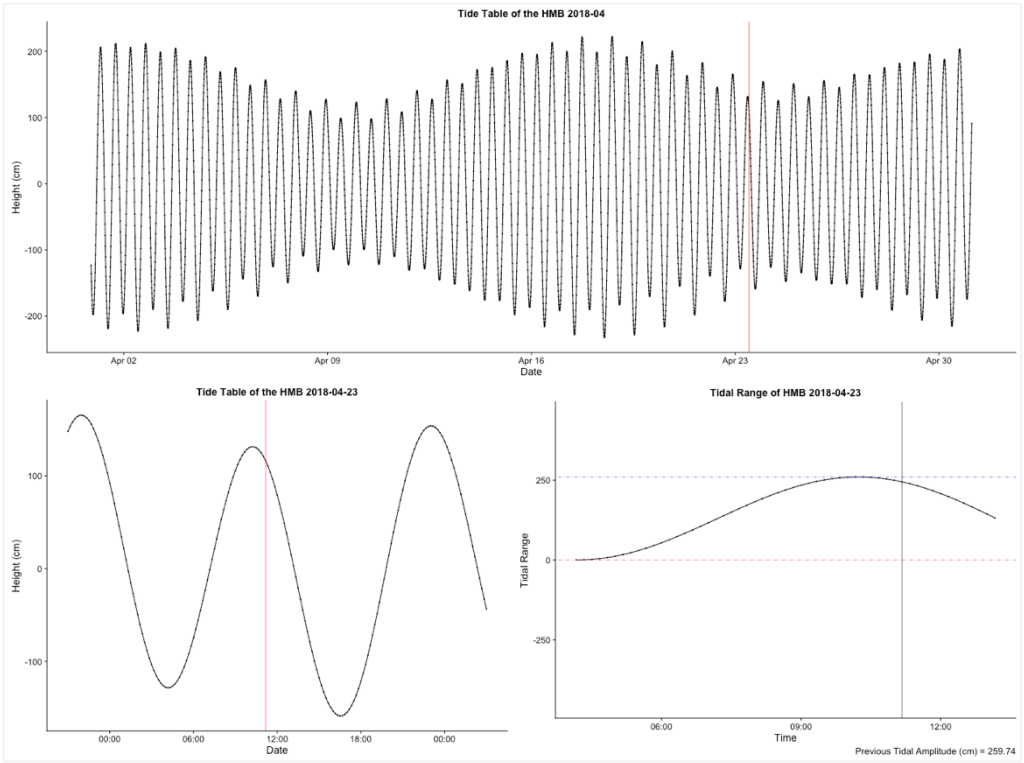
Tide Table of the HMB 2018-04
Height (cm)
200
100
0
-100
-200
Apr 02
Apr 09
Apr 16
Apr 23
Apr 30
Date
Tide Table of the HMB 2018-04-23
Height (cm)
100
0
-100
00:00
06:00
12:00
18:00
00:00
Date
Tidal Range of HMB 2018-04-23
Tidal Range
250
0
-250
06:00
09:00
12:00
Time
Previous Tidal Amplitude (cm) = 259.74

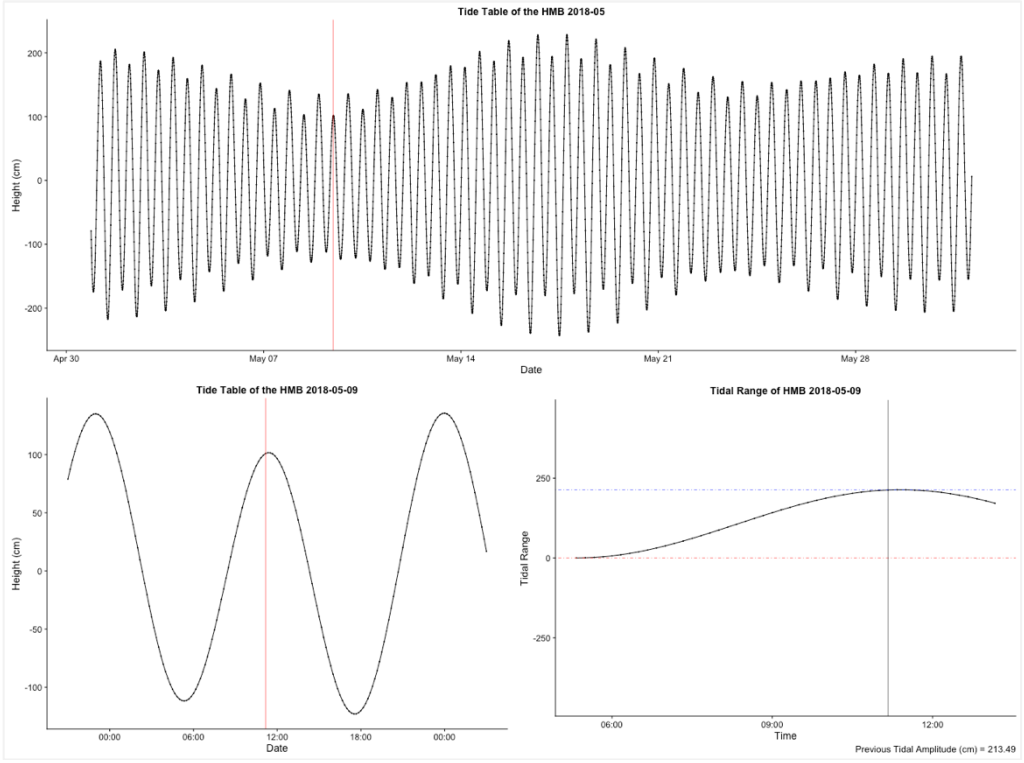
Tide Table of the HMB 2018-05
Height (cm)
200
100
0
-100
-200
Apr 30
May 07
May 14
May 21
May 28
Date
Tide Table of the HMB 2018-05-09
Height (cm)
100
50
0
-50
-100
00:00
06:00
12:00
18:00
00:00
Date
Tidal Range of HMB 2018-05-09
Tidal Range
250
0
-250
06:00
09:00
12:00
Time
Previous Tidal Amplitude (cm) = 213.49

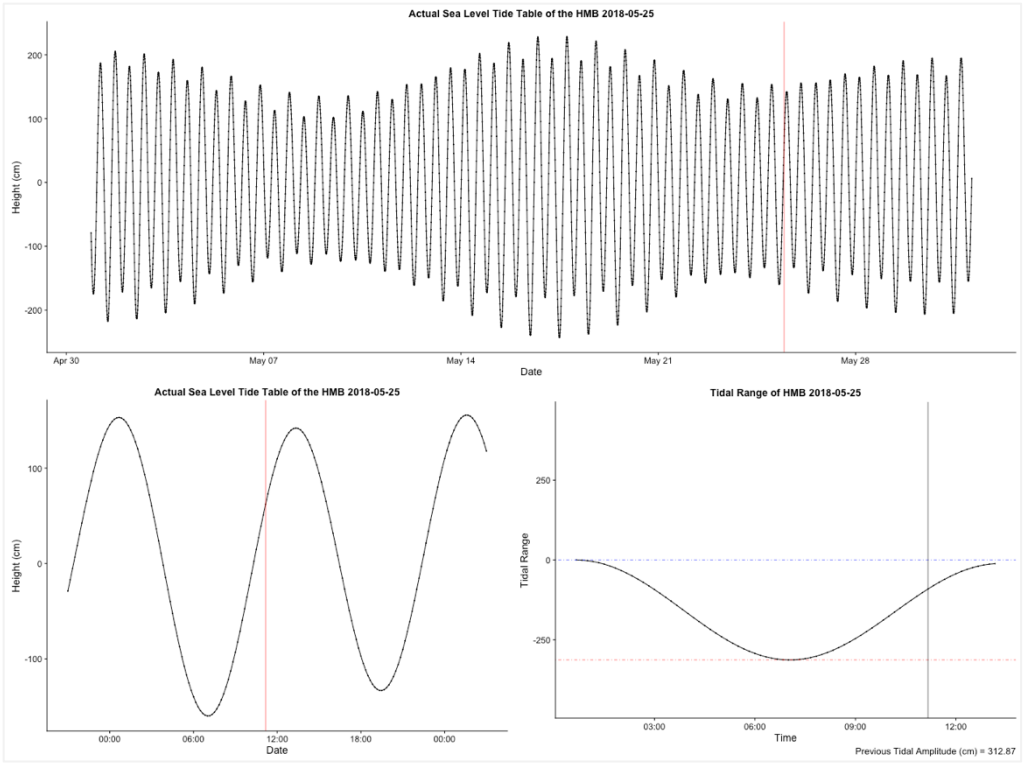
Actual Sea Level Tide Table of the HMB 2018-05-25
Height (cm)
200
100
0
-100
-200
Apr 30
May 07
May 14
May 21
May 28
Date
Actual Sea Level Tide Table of the HMB 2018-05-25
Height (cm)
100
0
-100
00:00
06:00
12:00
18:00
00:00
Date
Tidal Range of HMB 2018-05-25
Tidal Range
250
0
-250
03:00
06:00
09:00
12:00
Time
Previous Tidal Amplitude (cm) = 312.87